Titre: Title:	Dynamics of Cylindrical Particles in a Rotating Drum Using Multiple Radioactive Particle Tracking
Auteur: Author:	Majid Rasouli
Date:	2015
Type:	Mémoire ou thèse / Dissertation or Thesis
Référence: Citation:	Rasouli, M. (2015). Dynamics of Cylindrical Particles in a Rotating Drum Using Multiple Radioactive Particle Tracking [Thèse de doctorat, École Polytechnique de Montréal]. PolyPublie. https://publications.polymtl.ca/1848/

Document en libre accès dans PolyPublie
Open Access document in PolyPublie

URL de PolyPublie: PolyPublie URL:	https://publications.polymtl.ca/1848/
Directeurs de recherche: Advisors:	Jamal Chaouki, & François Bertrand
Programme: Program:	Génie chimique

UNIVERSITÉ DE MONTRÉAL

DYNAMICS OF CYLINDRICAL PARTICLES IN A ROTATING DRUM USING MULTIPLE
RADIOACTIVE PARTICLE TRACKING

MAJID RASOULI

DÉPARTEMENT DE GÉNIE CHIMIQUE

ÉCOLE POLYTECHNIQUE DE MONTRÉAL

THÈSE PRÉSENTÉE EN VUE DE L'OBTENTION

DU DIPLÔME DE PHILOSOPHIAE DOCTOR

(GÉNIE CHIMIQUE)

AOÛT 2015

UNIVERSITÉ DE MONTRÉAL

ÉCOLE POLYTECHNIQUE DE MONTRÉAL

Cette thèse intitulée:

DYNAMICS OF CYLINDRICAL PARTICLES IN A ROTATING DRUM USING MULTIPLE
RADIOACTIVE PARTICLE TRACKING

présentée par : RASOULI Majid

en vue de l'obtention du diplôme de : Philosophiae Doctor

a été dûment acceptée par le jury d'examen constitué de :

M. PATIENCE Gregory S., Ph. D., président

M. CHAOUKI Jamal, Ph. D., membre et directeur de recherche

M. BERTRAND François, Ph. D., membre et codirecteur de recherche

M. LEGROS Robert, Ph. D., membre

M. AL-DAHHAN Muthanna H., Ph. D., membre

DEDICATION

To my beloved family

ACKNOWLEDGEMENTS

I could not continue through this long journey without the support of my true friends. I have a list of great people to include here: Amin, Mohammad, Smaira, Jaber, Hamed, Sepehr, Ali, Kiana, Mohsen, Milad, Mahsa, Jaber, Laleh, Rouzbeh, Manian, Ata, Ebrahim, Atefeh, Touraj, Maryam, Hesam, Richard, Philippe, Ebrahim J., Sepehr R., Babak, Reza, Saman, Mohammad Gol., Hamed, Meghdad, Alireza, Iman, Majid and...

The last but not the least, I would like to express my endless gratefulness to my lovely Myriam and Dhiya, who have always been there for me in happy and sad moments. Words are incapable to express what I feel in my heart towards them.

RÉSUMÉ

Les écoulements granulaires sont d'une grande importance par rapport à plusieurs domaines allant des sciences planétaires à la géophysique ainsi qu'à plusieurs industries telles que l'industrie métallurgique, des céramiques, chimique, alimentaire, des cosmétiques, du charbon et pharmaceutique. La fabrication, l'analyse des procédés et le contrôle des produits granulaires dépendent fortement d'une maitrise fondamentale des écoulements granulaires. Les régimes d'écoulements granulaires englobent les classes générales suivantes : quasi-statique, dense (écoulements liquides) et rapide (écoulements gazeux). Le régime dense est considéré comme le plus compliqué des trois classes et aussi le moins étudié dans la littérature comparé aux deux autres régimes.

Le tambour rotatif représente l'équipement expérimental standard utilisé pour étudier l'écoulement granulaire dense. De plus, les tambours rotatifs possèdent plusieurs applications industrielles et sont utilisés dans plusieurs procédés (le mélangeage, la réduction de taille, le frittage, le chauffage, le refroidissement, le séchage ainsi que les réactions chimiques). Afin de réaliser le dimensionnement approprié des tambours rotatifs et d'ajuster les conditions opératoires optimales, il est essentiel d'étudier la phénoménologie intrinsèque à ce type d'équipement de manière fondamentale. Dans les procédés industriels, les tambours rotatifs fonctionnent dans le régime de roulement étant donné que ce régime assure un fort mélangeage des particules et un bon transfert de chaleur. Plusieurs études expérimentales ont été menées pour déterminer le régime d'écoulement régnant dans le tambour rotatif. Néanmoins, la majeure partie de ces recherches ont considéré des particules sphériques ou quasi-sphériques. Pourtant, l'étude des particules non sphériques est d'une très grande importance vu que les particules trouvées dans la nature et celles provenant des procédés de broyage sont de forme irrégulière. Aussi, les particules non sphériques ayant une forme spécifique (ellipsoïdale par exemple) ont plusieurs utilités. En outre, il est très important de mentionner que la forme des particules possède une influence majeure sur le régime d'écoulement.

Ainsi, le présent travail a pour objectif d'étudier l'effet de la forme des particules sur la dynamique des écoulements granulaires. Afin d'y parvenir, des particules cylindriques ont été considérées pour deux principales raisons. Premièrement, il existe plusieurs applications industrielles qui utilisent des particules cylindriques comme les capsules et les pastilles.

Deuxièmement, la forme des particules étudiées doit être facilement identifiable et distincte d'une sphère pour pouvoir tirer une bonne conclusion sur l'effet de la forme des particules sur le régime d'écoulement granulaire. À ce titre, le cylindre représente l'une des formes curvilignes les plus basiques. Ainsi, plusieurs autres formes comprenant celles ayant un facteur de forme élevé, peuvent être approchées par la forme cylindrique.

Plusieurs techniques de mesure non intrusives comme les méthodes optiques et radioactives ont été utilisées pour étudier l'écoulement granulaire dans un tambour rotatif. Comme la matière particulaire est opaque, les techniques optiques sont limitées à l'observation au niveau des écoulements surfaciques. Par contre, les techniques de mesure radioactives sont plus adaptées pour fournir des informations sur l'intérieur du lit de particules. En effet, les rayons gamma ont la particularité de traverser la matière avec une grande facilité. La technique de suivi de particules radioactives (RPT) est l'une des techniques appropriées pour cette étude. Cependant, la RPT est limitée au suivi de la position d'un seul traceur à la fois. Étant donné que des particules de forme cylindrique présentent le cas d'étude, il est essentiel de trouver une technique de mesure permettant de repérer la position ainsi que l'orientation d'une particule de manière simultanée.

Ainsi, la première partie de cette thèse introduit une technique de suivi d'une multitude de particules radioactives (MRPT) qui permet de déterminer la trajectoire de deux traceurs en mouvement dans le système. Ces derniers peuvent être libres ou attachés à la même particule. L'exactitude (<5 mm) et la précision (<5 mm) des mesures obtenues par la technique proposée ont été évalués en suivant deux traceurs immobiles et deux traceurs en mouvement. Les résultats obtenus démontrent la fiabilité et la validité de la MRPT lorsque les deux traceurs possèdent le même isotope et lorsque la distance entre ces deux traceurs n'est pas très petite (>2 cm). Le suivi de deux traceurs fixés aux deux extrémités d'une particule cylindrique dans un tambour rotatif est également étudié afin d'illustrer le potentiel de cette méthode de caractérisation.

La deuxième partie de cette thèse présente la comparaison entre l'écoulement de particules cylindriques (2 cm de longueur et 6 mm de diamètre) et l'écoulement de particules sphériques (6 mm de diamètre). Cette comparaison est réalisée à l'aide de la MRPT afin de détecter la position et l'orientation des particules cylindriques de manière simultanée. Deux composantes principales de la dynamique de l'écoulement transversal ont été analysées. La première est la frontière entre

la couche active et la couche passive. La deuxième est le profil de vitesse sur la surface libre en régime de roulement (7,5 à 15 tours/min pour les particules cylindriques dans les conditions de cette étude). La dynamique de l'écoulement des particules cylindriques est différente de manière significative de celle des particules sphériques. Pour la première fois, l'orientation des particules cylindriques à l'intérieur du lit a été mesurée. Les résultats confirment l'existence d'une orientation spatiale préférentielle pour les particules cylindriques dans la couche active (elle correspond à une déviation d'environ 25° de l'angle de repos dynamique). Il a également été démontré que cette orientation spatiale préférentielle n'est pas sensible à la vitesse de rotation du tambour. Ainsi, pour les particules cylindriques, la dilatation du lit de particules était constante (environ 25%) pour toutes les vitesses de rotation, alors qu'elle était d'environ 1% pour les particules sphériques. Aussi, les profils de vitesse obtenus pour la surface libre des particules cylindriques montrent une forme asymétrique (le pic du profil de vitesse est situé à 70% de la longueur de la surface libre). En ce qui concerne les particules sphériques, les profils de vitesse démontrent une forme symétrique (le pic du profil de vitesse est situé à 50% de la longueur de la surface libre). Pour la première fois pour des particules cylindriques, deux modèles généraux ont été proposés pour calculer le profil de vitesse à la surface libre ainsi que la taille effective des particules dans les couches active et passive.

Finalement, la troisième partie de ce projet doctoral présente une analyse plus poussée des données obtenues dans les deux parties précédentes à l'aide de la MRPT et de la RPT. Les équations de mouvement pour les particules sphériques et cylindriques dans les couches active et passive ont été obtenues. En outre, les équations des lignes de courbe représentant le point d'inflexion de la vitesse ainsi que les équations du yield ont été développées. L'utilisation potentielle de ces équations de mouvement a été illustrée à l'aide des simulations numériques considérant l'effet de l'advection sur la qualité de mélangeage des particules sphériques et cylindriques.

ABSTRACT

Granular flows are important in a wide range of fields, ranging from planetary science to geophysics, and industries such as metallurgy, ceramics, chemicals, food, cosmetics, coal and pharmaceuticals. The manufacturing, processing, and control of granular products depend on a fundamental understanding of the granular flows. The quasi-static, dense (liquid) and fast (gaseous) flow regimes are general granular flow regimes. Of these, the dense granular flow regime is the most complicated, and the one with the least investigation.

The rotating drum is one of the standard experimental systems for studying the dense granular flow regime. In addition, rotating drums have many industrial applications, and are used in a great variety of processes (mixing, size reduction, sintering, coating, heating, cooling, drying, and reaction). To design and operate rotating drums optimally, it is essential to study the phenomena that occur inside such devices on a fundamental level. In industrial operations, rotating drums mainly use the rolling regime, which provides superior solid mixing and heat transfer. Many experimental studies have been conducted to obtain the flow behavior of particles inside a rotating drum, though a majority of them used spherical or nearly spherical particles. However, an investigation of non-spherical particles is very important because natural or crushed particles usually have an irregular shape, non-spherical particles with certain shapes have many usages, and more importantly, particle shape greatly affects the flow behaviour.

Therefore, this work aims to study of the effect of particle shape on flow dynamics. To do so, the cylinder was chosen as the particle shape for two main reasons. Firstly, there are lots of industrial applications for cylindrical particles, such as capsules, candies, biomass pellets, etc. Secondly, to be able to identify the effect of particle shape on flow behaviour, the shape should be readily identified, and distinct from a sphere. The cylinder is one the most basic curvilinear geometric shapes, and many other curvilinear shapes, especially those with a high aspect ratio, can be approximated as a cylinder.

Many nonintrusive techniques have been used to study granular flow in a rotating drum, including optical methods and radioactive techniques. Since particulate matter is principally opaque, optical methods are essentially limited to surface flow. Conversely, radioactive

techniques are well suited for providing information about inside the bed in such systems, because gamma rays can penetrate relatively easily through materials. Radioactive particle tracking (RPT) is one suitable measurement techniques for this investigation. However, RPT is limited to tracking the position of a single tracer. As cylindrical particles are used for this study, it is essential to employ a measurement technique capable of simultaneously tracking the position and orientation of a cylindrical particle.

The first part of this thesis introduces a multiple radioactive particle tracking technique (MRPT) that can determine the trajectory of two free or restricted moving tracers in a system (attached to the same particle). The accuracy (<5 mm) and precision (<5 mm) of the proposed technique is evaluated by tracking two stationary tracers and two moving tracers. The results confirm the reliability and validity of the MRPT technique when the two tracers have the same isotope and the distance between them is not too small (>2 cm). The tracking of two sticking tracers at the two ends of a cylindrical particle in a rotating drum is also considered to illustrate the potential of this characterization method.

In the second part of this thesis, we compare the flow behavior of cylindrical (2 cm long and 6 mm in diameter) and spherical (6 mm in diameter) particles using the multiple radioactive particle tracking (MRPT) technique to capture the positions and orientations of cylindrical particles simultaneously. We analyzed two important components of the transverse flow dynamic, namely, the boundary between the active and passive layers and the velocity profile on the free surface, in the rolling regime (7.5-15 RPM for cylindrical particles under the conditions of this study). For the first time, we measured the orientation of cylindrical particles inside the bed. The results confirm the existence of a preferred spatial orientation (about a 25-degree deviation from the dynamic repose angle) for cylindrical particles in the active layer. The results show that the spatial orientation of cylindrical particles within the bed are insensitive to the rotational speed of the drum. Therefore, for cylindrical particles at all rotational speeds, bed dilation was constant (about 25%), while the bed dilation of spherical particles is about 1%. Velocity profiles on the free surface for cylindrical particles show an asymmetrical shape (the peak of velocity profile is located at 70% of the free surface length) while that of spherical particles is symmetrical; (the peak of velocity profile is located at 50% of the free surface length). For the first time, two general models are proposed to calculate the velocity profiles for

cylindrical particles on the free surface and the effective particle sizes in the active and passive layers.

Finally, the third part of this thesis presents a further analysis of the data obtained by the MRPT and RPT techniques in the previous part. We obtain the equations of motion for cylindrical and spherical particles in the active and passive layers, as well as equations of the yield and turning point curve lines. Using numerical simulation, the effect of advection on the quality of mixing for both cylindrical and spherical particles is also considered to illustrate the potential use of these equations of motion.

TABLE OF CONTENTS

LIST OF TABLES

LIST OF FIGURES

LIST OF SYMBOLS AND ABBREVIATIONS

^{198}Au	Gold-198
^{137}Cs	Caesium-137
DEM	Discrete element method
^{18}F	Flourine-18
MRI	Magnetic resonance imaging
MRPT	Multiple radioactive particle tracking
^{24}Na	Sodium-24
NaI-Tl	Sodium Iodide
PEPT	Positron emission particle tracking
PET	Positron emission tomography
PIV	Particle image velocimetry
PTV	Particle tracking velocimetry
RPM	Revolutions per minute
RPT	Radioactive particle tracking
^{46}Sc	Scandium-46

CHAPTER 1   INTRODUCTION AND MOTIVATION

The 125th anniversary issue of *Science* determined one of the 125 big scientific questions is the flow of particulate materials (also called granular materials) (Meier, Lueptow, & Ottino, 2007). Granular flows are important in a wide range of fields, from the planetary science to geophysics to industrial processing, and it brings into play topics such as mixing and segregation, granular mechanics, solid-gas flows, solid-fluid flows, solid-solid flows, etc. (Bertrand, Leclaire, & Levecque, 2005; Paul, Atiemo-Obeng, & Kresta, 2004). Solid mixing is one of the main processes in many industries such as metallurgy, ceramics, chemicals, food, cosmetics, coal, advanced materials and pharmaceuticals (Bertrand et al., 2005; Paul et al., 2004). It can exist in many different process phases, from the blending of raw materials such as ceramics to final production as in the case of the cosmetics industry (Paul et al., 2004). To give an idea of the magnitude of applications involving powder processes, worldwide production exceeds a trillion kilograms (equalling about one trillion dollars) of powder and granular products (Scott, 2003). The manufacture, processing, and control of granular products depend on a fundamental understanding of granular flows, which is extremely complex and often obtained after years of tedious trial-and-error experimentations (Paul et al., 2004).

The complex nature of granular materials and their multifaceted flow behaviour are the two main reasons for the complexities of such materials (Bertrand et al., 2005). More specifically, for granular materials, the relationships between microscopic properties (i.e. at the level of the particle) and macroscopic properties (i.e. for a bulk of particles) have not yet been completely established. In addition, based on the boundary conditions, particulate materials may show characteristics that are specific to gases (e.g. compression), solids (e.g. deformation) or liquids (e.g. flow). Furthermore, study of the behaviour of a single particle and its interaction with other particles does not reveal the macroscopic behavior of a bulk of the particles because segregation patterns are only obtained within a particulate system consisting of different types of particles. Consequently, mathematical models are significantly complicated since all the elements of particle system must be included in the models (Doucet, 2008). In addition, there are few reliable measurement techniques suitable for granular materials as a consequence of their opaqueness.

According to the Media Research Group Divided (MiDi, 2004), based on the flow velocity, particulate flows can be classified into three regimes: quasi-static, dense (liquid), and fast (gaseous). In the first case, as the particle inertia is negligible, the flow is dominated by friction stresses resulting from prolonged contact between particles. These flows are described using soil mechanics and plasticity models (Dube, 2013; Herminghaus, 2005; MiDi, 2004; Savage, 1984). In the case of the gaseous regime, the system is strongly agitated and the particles drift far apart one from another, for instance, in a turbulent fluidized bed. In addition, in this regime particles interact through short binary collisions. Thus, to describe this regime a kinetic theory has been developed by analogy with the kinetic theory of gases (Campbell, 2006; Dube, 2013; Savage, 1984). The quasi-static and fast particulate regimes have been studied most often (Dube, 2013; Meier et al., 2007). The flow regime in between these two is called a dense flow regime, where particle inertia is considerable; as well, there are friction stresses due to the existing of the contact network between the particles (MiDi, 2004). Therefore, the study of dense particulate flows regime is more complicated since this regime includes the relative contribution of stresses due to friction and collision at the same time. For that reason, this work focuses on the dense granular flow regime.

A rotating drum is one of the standard experimental systems for studying the dense granular flow regime (MiDi, 2004). In addition, rotating drums, also called rotary kilns, have an important role in processing granular materials in a wide range of industries, such as chemical, pharmaceutical, metallurgical, food, polymer, waste treatments, etc. They are used in a variety of processes, such as mixing, size reduction, sintering, coating, heating, cooling, drying, and reaction. This wide range of applications is a result of the drums' ability to handle heterogeneous feedstock, as well as provide satisfactory mixing and heat transfer during the solid phase (Boateng, 1998; Descoins, Dirion, & Howes, 2005; Dube, Alizadeh, Chaouki, & Bertrand, 2013). Since the flow dynamics of particles imposes mass and heat transfer rate, it plays a critical role in controlling and/or limiting the above-mentioned processes (Heydenrych, Greeff, Heesink, & Versteeg, 2002; Liu, Specht, Gonzalez, & Walzel, 2006; Mellmann, Specht, & Liu, 2004). Therefore, to optimally design and operate rotating drums, it is essential to study the phenomena occurring inside such devices on a fundamental level. Although the concept of rotating drums is simple, the solid motion in these devices is rather complex (Ding, Forster, Seville, & Parker, 2002; Meier et al., 2007). In addition, if particle properties (e.g. size, shape, surface roughness, etc.) change over the

course of a process, as in the case of pyrolysis, sintering, combustion, and incineration, the characterization becomes much more difficult because flow dynamics may be affected by new phenomena.

Many experimental studies have been conducted to reveal the flow behaviour of particles inside a rotating drum. In fact, a majority of these studies have used spherical or nearly spherical particles. However, the investigation of non-spherical particles is very important because particles in nature usually have an irregular shape (e.g. sand, ore grains, lime stone grains etc.), non-spherical particles with certain shapes have many usages (e.g. biomass pellets, capsules, rice grains, candy, etc.), and more importantly, particle shape greatly affects flow behaviour (Dube et al., 2013; Ridgway & Rupp, 1971; Woodle & Munro, 1993). Particle shape could change the flow behaviour in terms of resistance to shear, dilation under shear, compaction efficiency, transfer of momentum between translational and rotational motions, as well as the ability to form arches and block the flow (Cleary, 2010; Dube et al., 2013).

Therefore, this work aims to study the effect of particle shape on flow dynamics. To do so, the cylinder was chosen as the particle shape for two main reasons. Firstly, there are lots of industrial applications for cylindrical particles, such as capsules, candies, biomass pellets, etc. Secondly, to be able to make solid conclusions about the effect of particle shape on flow behaviour, the shape should be readily identified, and distinct from a sphere. The cylinder is one the most basic curvilinear geometric shapes, and many other curvilinear shapes, especially those with a high aspect ratio, can be approximated as a cylinder, such an ovoid, bottle-shape candies, etc.

As the aim of this study is related to characterising flow behaviour, the non-intrusiveness of the employed measurement technique is crucial. Many non-intrusive techniques have been used to study granular flow in a rotating drum, including optical methods such as laser Doppler velocimetry (LDV) (Longo & Lamberti, 2002) and particle image velocimetry (PIV/PTV) (Alexander, Shinbrot, & Muzzio, 2002; Ashish V Orpe & Khakhar, 2007), and radioactive techniques such as radioactive particle tracking (RPT) (Larachi, Chaouki, & Kennedy, 1995), magnetic resonance imaging (MRI) (Nakagawa, Altobelli, Caprihan, Fukushima, & Jeong, 1993) and positron emission particle tracking (PEPT) (Parker, Broadbent, Fowles, Hawkesworth, & McNeil, 1993). Since particulate matter is principally opaque, optical methods are essentially limited to surface flow, while radioactive techniques are well suited to provide information about

inside the beds of such systems, because gamma rays can penetrate relatively easily through materials. RPT setups have the advantage of being compact, flexible and cheap compared to PEPT and MRI. Therefore, RPT is the most suitable measurement technique in terms of reliability, validity and cost to be applied in the rotating drum.

Considering these facts, the general objective of this thesis is to characterize cylindrical particle flow dynamics inside a rotating drum using multiple radioactive particle tracking.

CHAPTER 2   LITERATURE REVIEW

This chapter provides a brief review of the literature concerning particle flows, rotating drums and relevant experimental characterization techniques.

2.1   Dense particulate flows

According to Groupement De Recherche Milieux Divises (MiDi, 2004), the studies on the dynamics of granular flow in dense granular flow regimes has been principally conducted in six different configurations, where rheological properties can be measured by applying a simple shear force. These six configurations are presented in Figure 2.1 and include: 1) plane shear (Figure 2.1a), where the motion of one wall applies a shear, 2) annular shear (Figure 2.1b), where the material confined between two coaxial cylinders and a shear is applied by the rotation of the inner cylinder, 3) vertical chute flow (Figure 2.1c), where gravity forces material to flow vertically in between two rough vertical walls, 4) inclined plane (Figure 2.1d), where gravity forces granular material to flow on a rough inclined plane, 5) heap flow (Figure 2.1e), where gravity forces material to flow on the surface of a pile, and 6) rotating drum (Figure 2.1f), where gravity and rotation make material to flow inside a drum. The first three and last three configurations are considered confined and free-surface flows, respectively.
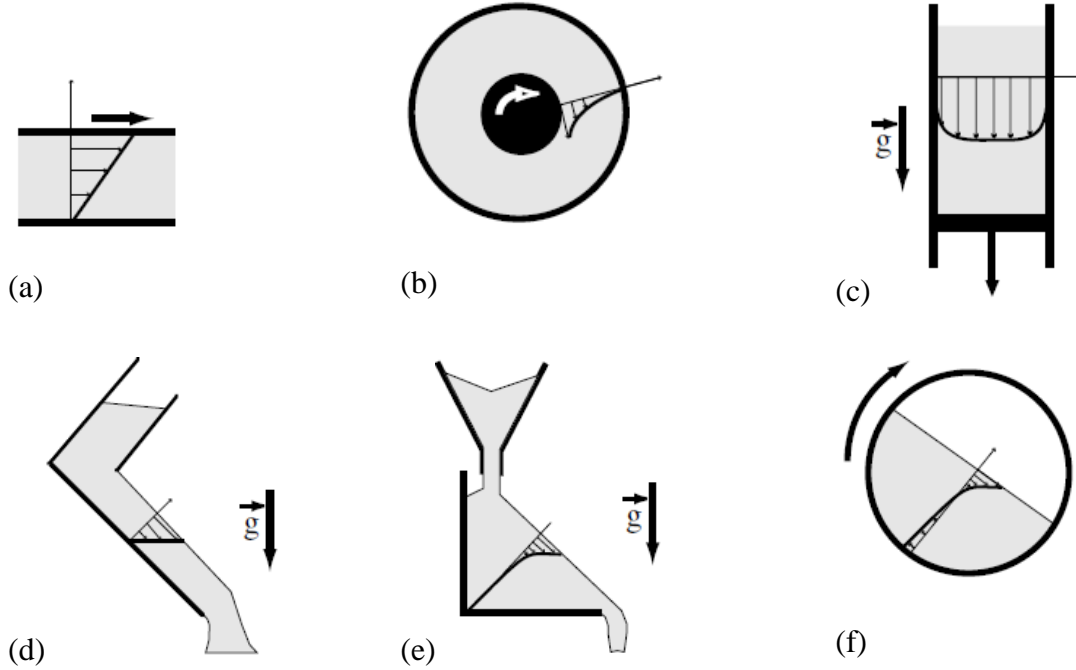
Figure 2.1: The six common configurations of granular flows: (a) plane shear, (b) annular shear, (c) vertical chute flows, (d) inclined plane, (e) heap flow, and (f) rotating drum. Adapted from MiDi GDR (2004).

For all these configurations, based on the operational conditions as well as particles properties, particles could be mixed or segregated. Three main mechanisms for mixing a particulate mixture were identified by Lacey (1954), namely convection, dispersion (diffusion) and shear (Lacey, 1954). Mixing by convection is when a bulk of particles move from one place to another. This is the fastest mixing mechanism. Dispersion (diffusion) is related to the rearrangement of the position of particles at the scale of a few particles. Finally, shear mixing is the exchange of particles between two layers of moving particles (Alizadeh, 2013; Dube, 2013; Lacey, 1954). It is widely accepted that in a horizontal rotating drum mixing along the axis of rotation is purely dispersive (i.e. axial), while on the cross section of the drum (radial) mixing occurs through a combination of convection and dispersion (Alizadeh, 2013; Dube, 2013; Elperin & Vikhansky, 1998; Gray, 2001; Khakhar, 2011; Khakhar, McCarthy, Shinbrot, & Ottino, 1997; Rao, Bhatia, & Khakhar, 1991).

Handling a mixture that contains particles with different physical properties generally leads to some degree of segregation (Ottino & Khakhar, 2000). The extent and structure of segregation

depend on many parameters, including particle properties, the geometry of the system and the origin of the particle motion (e.g. vibrations, flow) (Khakhar, 2011). As the operating condition and system properties can affect segregation at the same time, it is very difficult to establish a reliable rule to predict the occurrence of segregation, if not impossible (Dube, 2013). However, Harnby et al. (1992) claimed that segregation happens mainly due to differences in particle properties, namely, in order of importance: size, morphology and density (Harnby, Edwards, & Nienow, 1992). Segregation due to size and density have been most frequently studied (Jain, Ottino, & Lueptow, 2005). The study of the effect of particle shape on segregation is extremely complicated since it is difficult to develop an experimental setup where the effect of the shape is single out from other factors that may affect segregation (Dube, 2013).

2.2 Rotating drum

Rotating drums have an important role to play in processing granular materials in a wide range of industries, such as chemicals, pharmaceuticals, metallurgy, food, polymers, waste treatment, etc. They are used in a great variety of processes such as mixing, size reduction, sintering, coating, heating, cooling, drying, and reaction. This wide range of applications result from the ability of these devices to handle heterogeneous feedstock, as well as provide a satisfactory mixing and heat transfer for the solid phase (Boateng, 1998; Descoins et al., 2005; Dube et al., 2013). Such variety of applications have caused this system to be extensively investigated for practical interest, and it has served as the experimental model for many fundamental studies (Bonamy, Daviaud, & Laurent, 2002; Dube, 2013; MiDi, 2004; A. V. Orpe & Khakhar, 2001; Yamane, Nakagawa, Altobelli, Tanaka, & Tsuji, 1998).

Although the concept of rotating drums is simple, the solid motion in these devices is rather complex, for in a given system different flow regimes occur based on different rotational speeds (Ding et al., 2002; Meier et al., 2007). Based on Mellman (2001), increasing the rotational speed of the drum, these flow regimes are: sliding, avalanching (surging), slumping (continuous avalanching), rolling, cascading, cataracting and centrifuging (Table 2.1).

Table 2.1: Granular flow regimes inside a rotating drum (Mellmann, 2001).
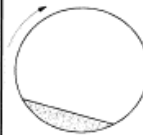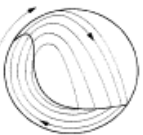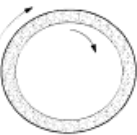
Basic form	Slipping motion		Cascading ("tumbling") motion			Cataracting motion	
Subtype	Sliding	Surging	Slumping	Rolling	Cascading	Cataracting	Centrifuging
Schematic							
Physical process	Slipping		Mixing			Crushing	Centrifuging
Froude number Fr [-]	$0 < Fr < 10^{-4}$		$10^{-5} < Fr < 10^{-3}$	$10^{-4} < Fr < 10^{-2}$	$10^{-3} < Fr < 10^{-1}$	$0.1 < Fr < 1$	$Fr \geq 1$
Filling degree f [-]	f < 0.1	f > 0.1	f < 0.1	f > 0.1		f > 0.2	
Wall friction coeff. μ_w [−]	$\mu_w < \mu_{w,c}$	$\mu_w \geq \mu_{w,c}$	$\mu_w > \mu_{w,c}$			$\mu_w > \mu_{w,c}$	
Application	no use		Rotary kilns and reactors; rotary dryers and coolers; mixing drums			Ball mills	no use

Table 2.1 shows these flow regimes, their conditions and applications, as well as the Froude number (Fr), which is the ratio of the inertia over gravitational forces, and calculated by:

$$Fr = \frac{R\omega^2}{g} \qquad\qquad 2.1$$

where ω, R and g are the rotational speed, radius of the drum and gravitational acceleration, respectively. However, it is recognized that the obtained flow regime not only depends on the Froude number, but also on the level of filling, the ratio of particle size to drum size, and particle properties such as size, roughness, shape, and friction coefficient (Alizadeh, 2013; H Henein, Brimacombe, & Watkinson, 1983; Mellmann, 2001). In industrial operations, rotating drums are mainly employed in a rolling regime since this provides superior solid mixing and results in enhanced heat transfer (Dube et al., 2013; Fantozzi, Colantoni, Bartocci, & Desideri, 2007; Li, Yan, Li, Chi, & Cen, 2002; Liu et al., 2006; Meier et al., 2007).

A rolling regime is characterized by two regions: a thin, rapidly flowing layer – the so-called active layer with a flat surface that flows in a dynamic repose angle (β_d) with respect to the horizontal line – and a thick layer underneath the active layer, the so-called passive layer that undergoes a solid body rotation with the drum (Figure 2.2). On the upstream end, particles leave

the passive layer and enter the active layer, and on the downstream end the opposite takes place (Alizadeh, Bertrand, & Chaouki, 2014; Meier et al., 2007). As passive layer particles undergo a solid body rotation, mixing and segregation mostly occurs in the active layer where particles can have different speeds with respect to each other (Cheng, Zhou, Keat Tan, & Zhao, 2011; Ingram, Seville, Parker, Fan, & Forster, 2005). Hence, characterizing the active layer is of primary importance. In particular, the dynamic repose angle is a distinct aspect of the active layer, which depends on the rotating drum properties, including dimension, end-wall effects and rotation speed, as well as particles properties such as size, surface roughness and shape (Meier et al., 2007). Therefore, if particles properties (e.g. size, shape, surface roughness) change over the course of a process, as in the case of pyrolysis, sintering, combustion and incineration, the characterization becomes much more difficult because flow dynamics may be affected by new phenomena. Thus, the particle shape is one of the most important parameters that affects the flow dynamic of granular materials.
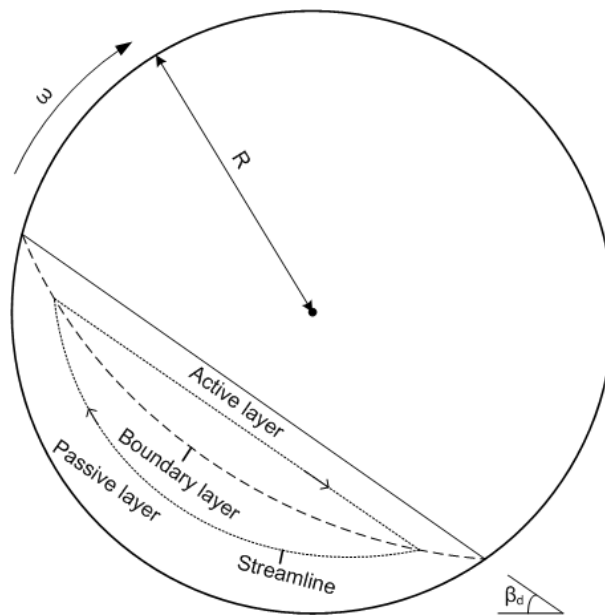
Figure 2.2: Typical schematic of the cross-section view of a rotating drum operating in a rolling regime.

In general, the investigation of particulate systems inside a rotating drum can be performed by numerical simulation and experimental methods. In the next two sections, short descriptions are provide of these two methods with respect to the flow motion of granular materials inside a rotating drum.

2.3 Modeling particulate flows

The numerical models to simulate particulate flows are classified into two groups: 1) continuum and 2) discrete approaches. The first approach considers the bulk of granular materials as a fluid, and works in a Eulerian framework (Khakhar, Orpe, & Ottino, 2001; Meier et al., 2007). The second approach treats particles as discrete, and works in Lagrangian frameworks, for instance, Monte Carlo, cellular automata and discrete element method (DEM) (Meier et al., 2007; Zhu, Zhou, Yang, & Yu, 2007). Based on the case study either of these approaches is suitable, and often a complementary use of the two approaches is required to reach a complete understanding of the flow dynamics (McCarthy, Khakhar, & Ottino, 2000; Meier et al., 2007). For example, Meier et al. (2007) specifies that a discrete approach is appropriate when the flow is significantly affected by particle properties (e.g. cohesive particles, roughness of particle surface) and the flow layers are not singly connected (e.g. the continuity of the bulk of particles break with the blades or paddles of a mixer). Conversely, a continuum model is more suitable when the interaction between particles is less important, for example when the effect of the geometry of a system on the particle flow is being studied.

2.3.1 Continuum-based approaches

Continuum-based descriptions, analogous to Navier-Stokes equations, are derived from solving a balance equation of key quantities such as mass, momentum and energy with assumed boundary conditions (Ding, Seville, Forster, & Parker, 2001; Meier et al., 2007). For given particles, the obtained constitutive laws depend considerably on flow regimes. This is due to fact that the transportation of mass, momentum and energy is related to how the particles are in contact. For example, the frictional stress dominates in the quasi-static regime, where each particle has contact with multiple particles for long durations, while collisional stress controls in the rapid flow regime, where particles only interact through short binary collisions (Meier et al., 2007). Subsequently, for these two extreme regimes, constitutive equations have been proposed based on soil mechanics (Jackson, 1983) and the kinetic theory of gases (Campbell, 1990, 2006; Goldhirsch, 2003; Savage, 1984), respectively. Between the extremes of quasi-static and rapid flow lies a broad range of flows, so the difficulty of developing a constitutive law for the dense granular flow regime arises. In this regime, constitutive laws are far from well established due to the difficulty of identifying the relative contributions of frictional and collisional stresses.

Therefore, in developing the continuum models, many assumptions (e.g. constant bulk density, constant shear rate, symmetry flow, etc.) have been made that are true for some cases and wrong in others. Consequently, the models are dependent on fitting parameters, which are obtained by experimentation (Ding et al., 2001; Khakhar et al., 2001; Meier et al., 2007). However, for this method, the required computational time is much less compared to discrete approaches.

2.3.2 Discrete approaches

The discrete framework of numerical simulation is appropriate for this field due to the discrete nature of particulate systems. The discrete element method (DEM) was introduced by Cundall and Strack (1979) and is one of the most powerful numerical simulation methods, and has been used in granular systems (Cundall & Strack, 1979). In DEM, the translational and rotational motions of each particle are based on Newton's second law of motion and angular momentum balance, respectively. DEM offers a complete set of information about position, acting forces and motion for each particle at any time within the case study, which is impossible to obtain from other experimental methods (Alizadeh et al., 2014; Bertrand et al., 2005; Cleary, 2010; Cundall & Strack, 1979; Kuo, Knight, Parker, Adams, & Seville, 2004; Suzzi et al., 2012; Zhu et al., 2007). However, such a degree of reliable results comes at a price of choosing between accurate contact force models and precise physical properties (e.g. Young's modulus, restitution coefficients, etc.). In addition, DEM has other limitations, such as a limitation on the number of particles within the case study (less than 10^6) even when applying a parallel computational technique, while the number of particles on the industrial scale is often in the order of 10^9. This expensive computation is mostly due, firstly, to the small time interval (about 10^{-6}s), and secondly, to the contact detection step. Even for the most simply shaped particles (i.e. a sphere), detection takes up to about two-thirds of the computational time. Consequently, using non-spherical particles will significantly increase the computational time. In addition, there are some other difficulties that arise when applying DEM for irregular shaped particles − and most particles used in industry have an irregular shape (Bertrand et al., 2005). Thus, continuum models should be considered in non-spherical particle applications. In addition, experimental methods should be considered due to these limitations, as well as the fact that the results of numerical simulation methods must be validated by experimental methods.

2.4   Experimental techniques for characterizing particulate flows

There are various measurement techniques for the characterization of granular flows. The ease (or difficulty) of their utilization varies from one method to another, as do the quality and quantity of the results they deliver. The choice of method mainly depends on the objectives of the study, material properties and particulate system to be characterized. In general, measurement techniques are classified into two groups: intrusive and nonintrusive measurement techniques, which are the topics of two next sections.

2.4.1   Intrusive experimental techniques

Experimental methods that cause any disturbance to the normal flow dynamic are called intrusive techniques. For instance, the presence of a probe will disturb the normal flow due to the interaction of the probe and the flow. Consequently, the flow motion measured by these techniques cannot accurately represent the actual flow. However, these methods can be easily employed and are inexpensive since they generally require less sophisticated instrumentation. Some examples of intrusive techniques that have been used in rotating drums are optical fibers (Boateng & Barr, 1997; Pugsley et al., 2003), in situ bed freeze (solidification) techniques (Brone, Alexander, & Muzzio, 1998; Wightman & Muzzio, 1998a) and the thieves sampling probe (Alizadeh, Hajhashemi, Bertrand, & Chaouki, 2013; Lemieux, Bertrand, Chaouki, & Gosselin, 2007; Muzzio, Robinson, Wightman, & Brone, 1997; Perrault, Bertrand, & Chaouki, 2010).

2.4.2   Nonintrusive experimental techniques

As the object of this study is the characterization of flow behaviour, a nonintrusive measurement technique is crucial. New and interesting studies of the hydrodynamic behavior of systems are feasible with the introduction of advanced experimental techniques. These techniques attempt to reduce the probe volume to obtain more local information about the structure of systems and/or reduce intrusiveness, by eliminating the interaction between the probe and the medium. The second type is so called non-invasive or nonintrusive methods. These methods use materials that pass through systems without disturbing the flow, such as radioactive rays, visible light (for transparent systems), sonic energy, etc.

The opaque nature of granular materials means that almost any experimental study related to such materials becomes tedious and cumbersome. However, a wide selection of non-invasive experimental techniques have been employed to carried out these investigations, such as particle image/tracking velocimetry (PIV/PTV) (Alexander et al., 2002; Chung, Hsiau, Liao, & Ooi, 2010; Felix, Falk, & D'Ortona, 2002, 2007; Jain, Ottino, & Lueptow, 2002, 2004; Jain et al., 2005; Kalbag, Wassgren, Sumana Penumetcha, & Pérez-Ramos, 2008; Ashish V Orpe & Khakhar, 2007; Santomaso et al., 2003), Laser Doppler velocimetry (LDV) (Longo & Lamberti, 2002), magnetic resonance imaging (MRI) (Hill, Caprihan, & Kakalios, 1997; Kawaguchi, 2010; Nakagawa et al., 1993), positron emission particle tracking (PEPT) (Ding et al., 2001; Ingram et al., 2005; Parker, Dijkstra, Martin, & K. Seville, 1997; Santomaso et al., 2003; R. Yang, Zou, & Yu, 2003) and radioactive particle tracking (RPT) (Alizadeh et al., 2014; Alizadeh, Dube, Bertrand, & Chaouki, 2013; Dube et al., 2013; Sheritt, Chaouki, Mehrotra, & Behie, 2003).

As mentioned above, nonintrusive techniques that have been used to study granular flow in rotating drums include optical methods such as LDV and PIV/PTV, and radioactive techniques such as RPT, MRI and PEPT. Optical methods have been most often used to investigate the flow behaviour of granular materials because they have the advantage in being easier and cheaper to use compared to radioactive techniques. Since particulate matter is principally opaque, optical methods are essentially limited to surface flow. Therefore, in a rotating drum, the optical methods can measure either the bed surface flow or the surface flow on the side-wall of the drum, which are limited to two-dimensional systems and/or biased with the end-wall effect, respectively. Conversely, radioactive techniques are well suited to provide information about inside the bed in such systems, because gamma rays can penetrate relatively easily through various materials. RPT setups have the advantage in being compact, flexible and cheap compared to PEPT and MRI. On the other hand, it is not easy to extend RPT to systems with irregular and/or moving boundaries (Doucet, Bertrand, & Chaouki, 2008b). RPT was chosen for the current work since rotating drums have simple moving boundaries. These radioactive based techniques are briefly described as follows.

But first, it is worth mentioning that in fact a majority of these experimental studies (using both intrusive and nonintrusive techniques) investigated spherical or nearly spherical particles. While investigation of non-spherical particles is very important because crushed particles or particles in nature usually have an irregular shape (e.g. sand, ore grains, limestone grains etc.), non-spherical

particles with certain shapes have many usages (e.g. biomass pellet, capsule, rice grains, candy, etc.) and more importantly particle shape affects flow behaviour (Dube et al., 2013; Ridgway & Rupp, 1971; Woodle & Munro, 1993). Particles shape can change flow behaviour in terms of resistance to shear, dilation under shear, compaction efficiency, transfer of momentum between translational and rotational motions, as well as forming arches and blocking the flow (Cleary, 2010; Dube et al., 2013). A few experimental investigations on flow behaviour in a rotating drum have used non-spherical particles such as limestone grains (Boateng & Barr, 1997; H. Henein, Brimacombe, & Watkinson, 1985), sand (H. Henein et al., 1985; Ingram et al., 2005), rice grains (Boateng & Barr, 1997), gravel (H. Henein et al., 1985), shale (Van Puyvelde, Young, Wilson, & Schmidt, 2000), and tablet (Tobiska & Kleinebudde, 2003; Wilson & Crossman, 1997), as well as wooden ovoid, shell and tube particles (Woodle & Munro, 1993). These studies have revealed useful information about the flow behaviour of non-spherical particles. However, the results are restricted by either the objectives of their study, the inability to single out the effect of the particle shape, or the experimental technique used. For instance, Dube, Alizadeh et al. (Dube et al., 2013) used RPT to capture the flow dynamics of non-spherical tablets in a rotating drum. They concluded that the tablets with an aspect ratio over 2 had a significantly different flow behaviour than spherical particles. They also found that the axial dispersion coefficient for non-spherical tablets was lower than spherical particles, due to the higher degree of spatial orientation in the active layer. However, their chosen measurement method (RPT) was unable to capture the orientation of the particles. Therefore, employing an experimental technique which is non-invasive and able to capture the spatial position and orientation of cylindrical particles is of great interest.

2.4.2.1 MRI technique

To carry out a study, the system (i.e. rotating drum) is positioned within an MRI scanner. A strong oscillating magnetic field with a proper resonance frequency is temporarily applied to the system, which excites hydrogen atoms. The excited hydrogenated molecules emit a radio frequency signal which is measured by the scanner, which can encode velocity and concentration profiles. However, the sophisticated instrumentation for this method and the operation equipment can be very expensive. In addition, the size and the type of particulate systems that can be studied by this method are greatly limited (Kawaguchi, 2010).

2.4.2.2   Positron Emission Particle Tracking (PEPT)

PEPT has been developed at University of Birmingham since 1987 as an alternative to Positron Emission Tomography (PET) to track a single particle trajectory. In PEPT, a positron is emitted by the tracer particle labelled with a radionuclide, usually fluorine-18 (^{18}F). A pair of back-to-back gamma rays are then emitted by interaction of each positron with a nearby electron. The tracer position can be determined by triangulating the detected gamma-rays pairs. PEPT is a powerful method for dense solid systems, since gamma rays is able to penetrate through considerably thick materials. For example, 50% of the beam can pass through steel and aluminum with thickness of 11 mm and 30 mm, respectively (Waters, Rowson, Fan, Parker, & Cilliers, 2008).
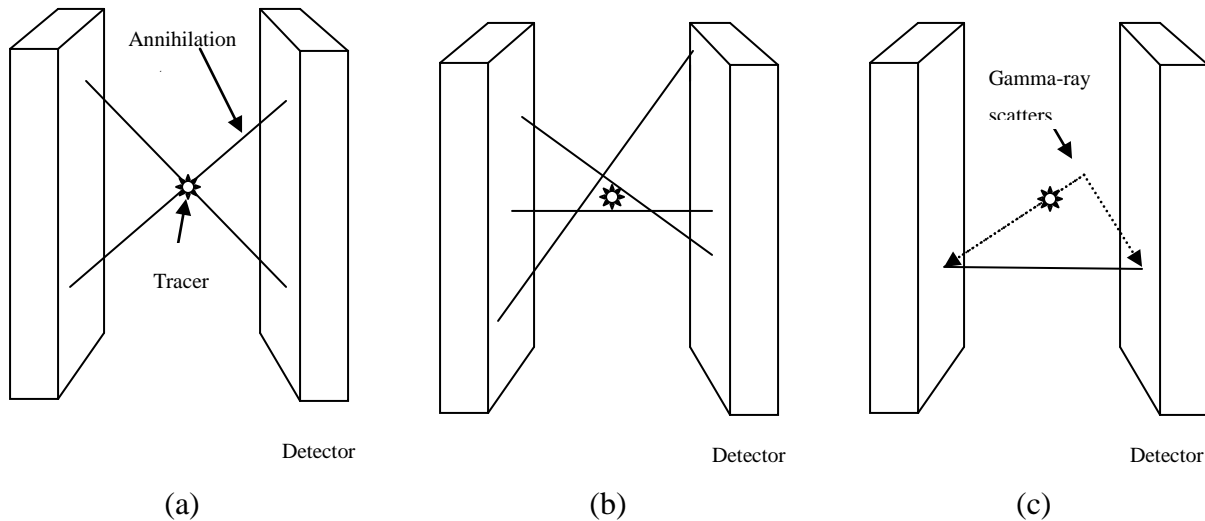
Figure 2.3: Schematic of PEPT

Theoretically, the tracer position can be determined by finding the location of the intersection of two successive annihilation vectors (see Figure 2.3a). However, in practice, the position of the intersections of successive annihilation vectors are distributed around the true position of tracer (see Figure 2.3b) as a consequence of physical factors, such as the positron range, finite spatial resolution of the detectors, etc. Other effects, which make extra difficulties on the calculation of tracer position are gamma-ray scattering and random coincidence. In Figure 2.3c, a corrupt annihilation vector that passes too far from the true tracer position can occur. In order to address this problem, a large enough set of annihilation vectors is selected. An iterative algorithm is then

used to get the rid of corrupt annihilation. The principle of the algorithm is based on rejecting the annihilation vector, which has the largest perpendicular distance from a point that has a minimum total perpendicular distance to all set of annihilation vectors. Therefore, a new set of vectors is produced by rejecting the annihilation vector in the previous step. The algorithm is then repeated for this new set and so on.

During the last decade, PEPT has been applied to many mixers such as the ploughshares mixer (Broadbent, Bridgwater, Parker, Keningley, & Knight, 1993; Forrest, Bridgwater, Mort, Litster, & Parker, 2003; Jones & Bridgwater, 1998), the planetary mixer (Hiseman et al., 2002), the single blade mixer (Laurent, Bridgwater, & Parker, 2000), the shear mixer (Kuo et al., 2004), the V-blender with various levels of filling (Kuo, Knight, Parker, & Seville, 2005) and the rotating drum (Ding et al., 2002; Ding et al., 2001; Parker et al., 1997; Santomaso et al., 2003; R. Yang et al., 2003). Yang et al. (2008) studied the transitional and rotational motion of particles in a cylindrical blender using three tracers simultaneously (Z. Yang, Fan, Bakalis, Parker, & Fryer, 2008). PEPT is one of the most powerful non-invasive methods, especially for use in solid systems. However, this technique is quite expensive because of the high price of detectors, and it can only be used for relatively small systems because its detector size is limited. In addition, it suffers from the RPT limitations that will be described in the next section.

2.4.2.3 Radioactive Particle Tracking (RPT)

The modus operandi of the RPT is relatively simple. The system detection is a network of 8 to 16 sodium iodide (NaI-Tl) detectors, which count the number of gamma-rays from a source (tracer) within the case study and completely decay during a specific sampling time (typically 5 to 10 ms). This system has the main advantage of being relatively affordable in addition to being compact compared to the PEPT system, which uses large and expensive cameras. Thus, the investigation of relatively large systems is possible, since the detectors can be arranged around the equipment individually. This method was developed by Lin et al. (1985) and applied by Larachi et al. (1994) (Larachi, Kennedy, & Chaouki, 1994; Lin, Chen, & Chao, 1985). Recently, several studies have focused on improving the resolution and sensitivity of the RPT by improving the experimental plan (Roy, Larachi, Al-Dahhan, & Dudukovic, 2002), modifying certain parameters of the experiment such as the choice of isotope for the tracer (Godfroy, Larachi, Kennedy, Grandjean, & Chaouki, 1997; Roy et al., 2002) and optimizing the detector positions

(Dube, Dube, Chaouki, & Bertrand, 2014). In order to apply RPT to a relatively high-velocity system, an investigation was done by decreasing sampling time and increasing the tracer activity (Mostoufi, Kennedy, & Chaouki, 2003). In the past, RPT was limited to systems with stationary boundaries or regular moving boundaries, such as cylindrical blender and fluidized bed. The reconstruction of the Lagrangian trajectory of a tracer was carried out on cylindrical forms, which allows for a consideration of anisotropy induced by known geometric borders or kinematics (Larachi et al., 1994). The quality of inversion depends primarily on the accuracy of the calculated anisotropy and solid angle of each detector. For irregular geometries that do not have an analytical expression to represent the boundaries and subject to an unknown kinematic a priori, Doucet et al. (2008b) proposed an extended RPT method, which was successfully applied on a V-blender (Doucet et al., 2008b).

2.4.2.3.1   Theoretical model

The algorithm of the RPT finds the position, $X(x, y, z)$, of a tracer in a closed space, $V \in R^3$, by all the measured events, $\Phi = \{\Phi_i\}_{i=1..N}$, which are obtained by N detectors at time t. The latest generation of reconstruction algorithm that is based on solving a problem of minimizing between measured events and a rigorous phenomenological model was proposed by Beam et al. (1978) and then applied by Larachi et al. (1994). This model is based on the relation between the tracer position and the number of events recorded by the detectors. A typical set up of the RPT is depicted in Figure 2.4 (Beam, Wielopolski, Gardner, & Verghese, 1978; Doucet, 2008).
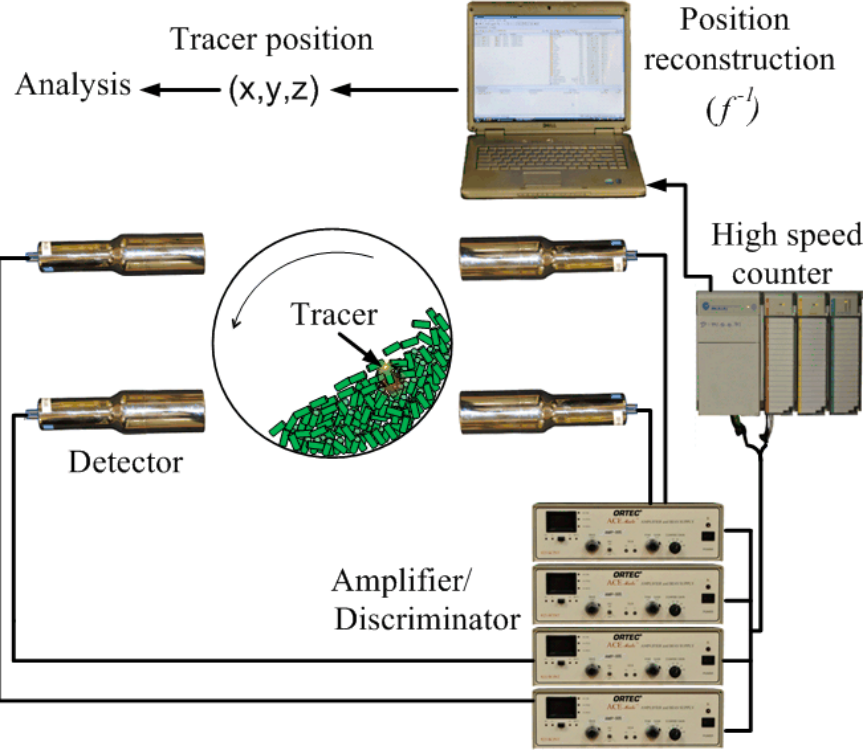
Figure 2.4: Typical set up of RPT applied to a rotating drum.

The detectors measure radiation levels according to their positions related to the tracer position. The exact position of the tracer can be obtained by using an appropriate model, which will be introduced in detail in the next section. The complexity of the model has been the subject of many discussions, but its estimation is made simply by using the Monte Carlo method (Beam et al., 1978; Doucet, 2008).

2.4.2.3.2 *The phenomenological model*

The position of the tracer in Cartesian coordinates, $X(x, y, z) \in V$, is obtained by finding the reconstruction function, $f^{-1}: R^{N+1} \to V$ such as $f^{-1}(\Phi_1, \Phi_2, .., \Phi_N, t) = X(t)$. The function that relates the number of registered events by detector i to the tracer position in the field is given by (Glenn F. Knoll, 2000):

$$\Phi_i(X, t) = \frac{T v R \phi \xi_i(X, t)}{1 + \tau v R \phi \xi_i(X, t)} \qquad 2.2$$

where T is the sampling time (s), τ is the dead time of the detector (s), R is the activity of the tracer (Beq), v is the number of photons emitted by each disintegration, ϕ is the peak-to-total (photo peak) ratio, and $\xi_i(X, t)$ is the efficiency of the ith detector related to the position X. With moving boundaries, the area of borders moves over time (i.e. the efficiency is time dependent), while in fixed boundaries efficiency is time independent.

2.4.2.3.3 *Efficiency calculation*

The major challenge in this method is to obtain the exact efficiency value for Eq. 2.2. The efficiency of the ith detector, encountered with the tracer at position X, is calculated as follows (Doucet, 2008; Doucet et al., 2008b):

$$\xi_i(X, t) = \oiint_\Omega \rho_d(r, t)\rho_s(r, t)\left(\frac{r.\,dA}{\|r\|^3}\right) \qquad 2.3$$

where r is a vector from X to the surface of the ith detector, dA is the normal vector to an element of area on the surface of the detector, and Ω is the solid angle subtended by the radiation. The functions $\rho_d(r, t)$ and $\rho_s(r, t)$ are the probability functions of the interaction between gamma-rays and the detector and the solid phase, respectively, which are obtained from the Beer-Lambert law (Doucet, 2008):

$$\int_0^{\sigma(t)} -\mu_d(s)ds = \ln(1 - \rho_d(r, t)) \qquad 2.4$$

$$\int_0^{l(t)} -\mu_s(s)ds = \ln(1 - \rho_s(r, t)) \qquad 2.5$$

where $\sigma(t)$ and $l(t)$ are the distances that the gamma ray travels in the detector and solid phase, respectively. These distances are time dependent in the irregular moving boundary cases. The parameters μ_d and μ_s are the linear attenuation coefficient of the NaI crystal and solid phase, respectively. The attenuation coefficient of a homogenous material is only a function of photonic energy. Therefore, the attenuation coefficient of a detector is a specific property of detector. A correlation for calculating the attenuation coefficient of a NaI crystal (Doucet, 2008; Snyder & Gyorey, 1965; Tsoulfanidis & Landsberger, 2011) can be found in Snyder and Gyorey (1965). In

order to calculate the efficiency, a numerical approach based on the Mont Carlo method was proposed by Beam et al. (1978). This method generates a finite number of random directions, from tracer to detector surface, within the solid angle, and calculates the exact value of $\sigma(t)$ and $l(t)$ by considering a weight function Ω_i for each solid angle. The solid angle can be calculated according to (Doucet, 2008):

$$\Omega = \frac{\alpha_{max}}{2\pi}(\cos\beta_{min} - \cos\beta_{max}) \qquad 2.6$$

where α_{max} is the maximum angle subtended by a cylinder of radius r and the tracer, which is located at the perpendicular distance d; β_{min} and β_{max} are the minimum and maximum angles that the tracer subtends along the cylinder axis, respectively.

In the Mont Carlo method, N number of random trajectories is generated by determining $\{\alpha^{(i)}, \beta^{(i)}\} \in [\alpha_{min}, \alpha_{max}] \times [\beta_{min}^{(i)}, \beta_{max}^{(i)}]$. A set of random vector, $\{\chi, \omega : \chi^{(i)}, \omega^{(i)} \in [0,1], i = 1..N\}$, is produced and $\{\alpha^{(i)}, \beta^{(i)}\}$ calculated according to (Doucet, 2008):

$$\alpha^{(i)} = \alpha_{max}(2\chi^{(i)} - 1) \qquad 2.7$$

$$\beta^{(i)} = \arccos\left(\cos\beta_{min}^{(i)} - \omega^{(i)}\left(\cos\beta_{min}^{(i)} - \cos\beta_{max}^{(i)}\right)\right) \qquad 2.8$$

The value of $\beta_{min}^{(i)}$ and $\beta_{max}^{(i)}$ are obtained geometrically. The random trajectory vectors, $\lambda^{(i)}$, can be calculated as follows:

$$\lambda^{(i)} = \left(\sin\beta^{(i)}\sin\alpha^{(i)}, \sin\beta^{(i)}\cos\alpha^{(i)}, -\cos\beta^{(i)}\right) \qquad 2.9$$

More details can be found in Beam et al. (1978). After determining $\{\alpha^{(i)}, \beta^{(i)}\} \in [\alpha_{min}, \alpha_{max}] \times [\beta_{min}^{(i)}, \beta_{max}^{(i)}]$, the ith solid angle for $\lambda^{(i)}$ is calculated from:

$$\Omega_i = \frac{\alpha_{max}}{2\pi}\left(\cos\beta_{min}^{(i)} - \cos\beta_{max}^{(i)}\right) \qquad 2.10$$

The efficiency of the kth detector is calculated as follow:

$$\xi_k(\boldsymbol{X}, t) = \lim_{N \to \infty} \frac{1}{\Omega N} \sum_{i=1}^{N} \Omega_i\, e^{-\mu_s l_i}(1 - e^{-\mu_d \sigma_i}) \qquad\qquad 2.11$$

This represents the probability of detection by a weighted solid angle in the emission direction. In practice, the value of N is finite. According to previous studies, the number of directions required to achieve sufficient accuracy is about 1,000 (Doucet, 2008; Godfroy et al., 1997; Larachi et al., 1994).

2.4.2.3.4 *Calibration*

Before starting the experiment, the tracer is located in n known positions ($\{\boldsymbol{X}_k\}_{k=1..n}$) within the bed to calibrate the signal received by the Discriminator (see Figure 2.4). The activity of tracer (R), detector dead time (τ) and attenuation coefficient of solid phase (μ_s) are obtained through a non-linear regression for the jth detector, according to (Doucet, 2008):

$$\min_{R,\tau,\mu_s} \sum_{k=1}^{n} \left(\frac{\Phi_j(\boldsymbol{X}_k) - \Phi_j^m}{\Phi_j(\boldsymbol{X}_k) + \Phi_j^m} \right)^2 \qquad\qquad 2.12$$

where $\Phi_j(\boldsymbol{X}_k)$ is the number of events calculated for the jth detector associated with position $\boldsymbol{X}_k$, and Φ_j^m is the measured value. Differences in the values of these parameters (R, τ, μ_s) are due to the specific setting of the Amplifier/Discriminator whereas for μ_s is attributed to anisotropy of solid phase (Doucet, 2008).

2.4.2.3.5 *Reconstruction step*

For a system, a count dictionary, which is a set of the counts of detectors related to each node within the system, is calculated from Eq. 2.2. For a given set of measurements, the nearest node ($P_i \in V$) to the tracer position is found using the following algorithm (Doucet, 2008):

$$\min_{P_i \in V} \sum_{j=1}^{N} \left(\frac{\Phi_j^m - \Phi_j(P_i)}{\Phi_j^m + \Phi_j(P_i)} \right)^2 \qquad\qquad 2.13$$

After finding the nearest node, the position of the tracer (X_P) is determined by refining the mesh (T_P) around the node (Doucet, 2008):

$$\min_{X_P \in T_P} \sum_{j=1}^{N} \left(\frac{\Phi_j^m - \Phi_j(X_P)}{\Phi_j^m + \Phi_j(X_P)} \right)^2 \qquad\qquad 2.14$$

The count value of X_P is obtained from a linear interpolation in the nearest nodes to X_P.

2.4.2.3.6 Isotope used for tracer

To have a reliable and valid RPT measurement, the tracer should have the same physical properties (e.g. size, shape, weight, etc.) as the particles under study. As an RPT experiment usually takes about 3 to 5 hours, a valid dictionary at the beginning of such an experiment may become inaccurate due to the decay of the used isotope. Therefore, in a RPT experiment, isotopes with a long half-life (e.g. ^{64}Sc (83.79 days), ^{137}Cs (30.17 years)) are generally preferred to isotopes with a short half-life (e.g. ^{24}Na (14.9 hrs), ^{198}Au (2.7 days)). In practice, it is sometimes too difficult to introduce a desirable isotope (e.g. ^{64}Sc) into a tracer in such way that its physical properties (e.g. density, shape, etc.) remain unchanged. In this case, the isotopes that already exist in the structure of the particles are preferred, even with short half-lives; for instance, glass beads contain sodium. However, for this type of tracer (e.g. sodium-24 tracer), the values of the dictionary should be updated due to its relatively short half-life. To overcome this difficulty, similar to Dube et al. (2013), the equation for the isotope half-life is introduced to Eq. 2.2 to take into account the decrease of tracer activity due to decay, as follows (Dube et al., 2013):

$$R = R(t) = R_0 exp \left(-\frac{t \, ln(2)}{t_{1/2}} \right) \qquad\qquad 2.15$$

where t is the time since the beginning of the experiment, $t_{1/2}$ the half-life of the isotope and R_0 the activity of the tracer at the beginning of the experiment.

2.4.2.3.7 RPT limitation

RPT is one of the most powerful methods for use with dense granular systems due to the penetrability of gamma rays. Furthermore, it is non-intrusive and precise enough to obtain the flow pattern, which is representative of actual phenomena. However, there are some limitations

in this method. First of all, there is a lower limit for the tracer size. The required time for obtaining a certain activity (activation time) of a tracer is proportional to the tracer mass. The tracer mass is proportional to the cubic size of a tracer. Therefore, a finer tracer requires more activation time. Practically, as the tracer size becomes less than $400 \, \mu m$, it could not be sufficiently activated. Consequently, RPT cannot be used for fine particles, which are very important in pharmaceutical applications. In addition, the density, size, shape and roughness of a tracer should be identical with other particles. To obtain the actual flow pattern, the tracer should be able to exactly mimic movement of other particles, which is very sensitive to the particle physical properties. Therefore, the tracer needs to be built in such way to have as much as similar physical properties with other particles that is impossible in some cases. Moreover, particles have size distribution whereas the tracer has only one particle size. Therefore, RPT can only capture trajectory of the particles that have the same size as the tracer. Due to segregation phenomena, a certain size of particles tends to appear in specific regions of the bed. Consequently, only the flow pattern of that specific region will be obtained, not the entire domain. In order to overcome this problem, one can attempt to use different tracer sizes for different experiments.

In addition, RPT is still limited to the tracking of only one tracer at a time. Tracking more than one particle simultaneously is of interest because it could yield direct information about both the translational and rotational motions of particles. In particular, the rotational motion of particles may play a significant role, for instance, on the lift force exerted on them, as well as their distribution (Duchanoy & Jongen, 2003). In systems where heat transfer is involved, the rotational motion of solid particles may change the rate of heating or cooling by increasing the interphase heat transfer coefficient (Mankad & Fryer, 1997; Z. Yang et al., 2008). In addition, by tracking more than one particle at the same time, the effect of the spatial orientation of non-spherical particles when they hit the wall of a system or bubbles in a fluidized bed, can be studied, as well as the relative motion of two freely moving particles. Furthermore, the validation of discrete element-based models is another reason why the tracking of multiple particles is of interest.

CHAPTER 3   COHERENCE OF THE CHAPTERS (ARTICLES)

It was shown in previous two chapters that studies on the granular flow could potentially benefit many industries. Among the particulate flow regimes, dense granular flow is the most complex and the one with the least investigation. A rotating drum is one of the standard experimental systems for studying of the dense granular flow regime, as it has widespread industrial applications, and mainly employed in the rolling regime. Many experimental studies have been conducted to reveal the flow behaviour of particles inside a rotating drum. However, a majority of these studies used spherical or nearly spherical particles. Thus an investigation of non-spherical particles is very important because natural or crushed particles usually have an irregular shape, non-spherical particles with certain shapes have many usages, and more importantly, particles shape greatly affects flow behaviour.

To do so, the cylinder was chosen as the particle shape for two main reasons. Firstly, there are many industrial applications for cylindrical particles, such as capsules, candies, biomass pellets, etc. Secondly, to be able to make solid conclusions about the effect of particle shape on flow behaviour, the shape should be readily identified, and distinct from a sphere. The cylinder is one the most basic curvilinear geometric shapes, and many other curvilinear shapes, especially those with a high aspect ratio, can be approximated as a cylinder.

The reliability and validity of results depend on the experimental technique used. As the object of this study is related to characterizing flow behaviour, a non-intrusive measurement technique is crucial. Among the available nonintrusive radioactive based techniques, RPT setups have the advantage of being compact, flexible and inexpensive. Although RPT has demonstrated its capability to track the position of particles, it is unable to provide information about the orientation of non-spherical particles, which is crucial in a study of cylindrical particles.

Thus, the specific objectives of this thesis are:

1. To develop a multiple radioactive particle tracking (MRPT) technique to investigate particulate flows;

2. To compare the dynamics of cylindrical and spherical particles in a rotating drum using MRPT; and

3. To obtain a model for the flow dynamic of cylindrical particles inside a rotating drum.

The achievement of each of these specific objectives is presented in Chapters 4, 5 and 6, corresponding to the two scientific articles and a complementary chapter from this thesis.

Chapter 4 introduces a multiple radioactive particle tracking technique (MRPT) that can determine the trajectory of two free or restricted (attached to the same particle) moving tracers in a system. The accuracy and precision of the proposed technique is evaluated by tracking two stationary tracers and two moving tracers. The results confirm the reliability and validity of the MRPT technique when the two tracers have the same isotope and the distance between them is not too small (>2 cm). The tracking of two sticking tracers at the two ends of a cylindrical particle in a rotating drum is also considered to illustrate the potential of this characterization method. It is worth mentioning that the proposed idea can be theoretically applied for more than two tracers.

Chapter 5 presents a comparative study between the flow motions of cylindrical and spherical particles inside a rotating drum. We used RPT to determine the positions of the spherical particles over time. We used MRPT to determine the positions and orientations of the cylindrical particles at any time and to calculate the essential components of the transverse flow dynamics of particles in a rotating drum, that is, the boundary between the active and passive layers and the velocity profile on the free surface. We then developed two general models to calculate these components.

Chapter 6 discusses the dynamics of cylindrical particles within a rotating drum. More specifically, this chapter deals with the modeling of the passive layer, boundary layer, active layer, and velocity profile on the free surface. Throughout this chapter, the behaviour of the non-spherical particles tested is compared with that of spherical particles.

The thesis concludes with a general discussion (Chapter 7) of the main advances resulting from this research and makes recommendations for work future (Chapter 8).

CHAPTER 4   ARTICLE 1: A MULTIPLE RADIOACTIVE PARTICLE TRACKING TECHNIQUE TO INVESTIGATE PARTICULATE FLOWS

Majid Rasouli, Francois Bertrand, Jamal Chaouki[1]

Department of Chemical Engineering, École Polytechnique de Montréal, c.p. 6079, Succ. Centre-ville, Montréal, Québec, H3C 3A7, Canada

4.1 Abstract

Radioactive particle tracking is a nonintrusive technique that has been successfully employed to study the flow dynamics in a wide range of reactors and blenders. However, it is still limited to the tracking of only one tracer at a time. This article introduces a multiple radioactive particle tracking technique (MRPT) that can determine the trajectory of two free or restricted (attached to the same particle) moving tracers in a system. The accuracy (<5mm) and precision (<5mm) of the proposed technique is evaluated by tracking two stationary tracers and two moving tracers. The results confirm the reliability and validity of the MRPT technique when the two tracers have the same isotope and the distance between them is not too small (>2cm). The tracking of two sticking tracers at the two ends of a cylindrical particle in a rotating drum is also considered to illustrate the potential of this characterization method.

Keywords: radioactive particle tracking, solid mixing, rotating drum, cylindrical particle, non-spherical particle

4.2 Introduction

In chemical engineering, reliable measurement of the flow dynamics in various systems is essential. To do so, sophisticated measuring techniques have been developed and improved by

---

Correspondence concerning this article should be addressed to F. Bertrand at francois.bertrand@polymtl.ca or J.Chaouki at jamal.chaouki@polymtl.ca

advances in computer control and instrumentation technology (Chaouki, Larachi, & Dudukovic, 1997a). These improvements are of two types, namely the reduction of the measurement volume and the degree of intrusiveness, and have lead to two different categories of measurement techniques. The first category, which provides locally refined information about the flow structure, is composed, for instance, of capacitance and fiber-optic probes (Boyer, Duquenne, & Wild, 2002). The second category is characterized by the absence of side effects coming from the interaction between the medium and the measurement apparatus (Boyer et al., 2002); it includes optical techniques such as laser Doppler anemometry (LDA) and particle image velocimetry (PIV), and radioactive techniques such as radioactive particle tracking (RPT) (Boyer et al., 2002) and positron emission particle tracking (PEPT) (Parker et al., 1993). The optical methods are essentially limited to transparent systems while radioactive techniques can be applied in opaque systems, because gamma rays can penetrate relatively easily through various materials. PEPT uses two positron-sensitive detectors mounted on the opposite sides of a system to detect pairs of exactly back to back gamma rays resulting from the annihilation of a positron (Bakalis, Fryer, & Parker, 2004; Guida, Nienow, & Barigou, 2011; Leadbeater, Parker, & Gargiuli, 2012; Link et al., 2008; Ng et al., 2008; Parker et al., 1993). This technique is able to detect a tracer when this tracer is within the volume covered by the detectors. RPT employs an array of several compact Sodium Iodide (NaI-Tl) detectors, which can be flexibly arranged around the system. Since RPT and PEPT use different detectors and rely on different algorithms to reconstruct tracer trajectories, they have their own advantages and drawbacks. For instance, RPT setups are compact, flexible and cheap compared to those of PEPT (Doucet et al., 2008b). On the other hand, it is not trivial to extend RPT to systems with irregular moving boundaries (Doucet et al., 2008b).

RPT was developed by Lien et al. (1985) in the 80s to track the motion of a single particle noninvasively in fluidized beds (Lin et al., 1985). In this method, a labeled tracer particle, a data acquisition system and a location algorithm are used to calculate the tracer position, as illustrated in Figure 4.1 in the case of granular flow in a rotating drum. The tracer is a labeled particle containing an irradiated radionuclide, such as ^{46}Sc and ^{24}Na (Godfroy et al., 1997; Roy et al., 2002), which decays due to the emission of gamma rays. The data acquisition system, which consists of an array of Sodium Iodide (NaI-Tl) detectors, amplifier/discriminators and high speed counters, records the number of gamma rays- the so-called event counts- coming from the tracer ,

which are almost completely absorbed inside the detectors during the sampling time. The location algorithm will be described in detail in the following section. Several publications, principally by the groups of Chaouki and Dudukovic, on the application of RPT for gas, liquid and three-phase fluidized beds (Chen et al., 2001; Larachi, Cassanello, Chaouki, & Guy, 1996; Larachi et al., 1995; Mostoufi & Chaouki, 2004; Roy, Kernoun, Al-Dahhan, & Dudukovic, 2005), bubble columns (Degaleesan, Dudukovic, & Pan, 2001; Xu, Qu, Chaouki, & Guy, 2005), stirred tanks (Guha, Ramachandran, & Dudukovic, 2007; Guha, Ramachandran, Dudukovic, & Derksen, 2008), spouted beds (Cassanello, Larachi, Legros, & Chaouki, 1999; Larachi, Grandjean, & Chaouki, 2003), V-blender (Doucet, Bertrand, & Chaouki, 2008a; Doucet et al., 2008b) and rotating drums (Alizadeh, Dube, et al., 2013; Dube et al., 2013; Sherritt, Chaouki, Mehrotra, & Behie, 2003) have showed the capabilities of this technique for monitoring the flow dynamics in various systems. A few investigations to improve the accuracy of RPT results by choosing a proper radionuclide for the tracer (Godfroy et al., 1997; Roy et al., 2002), designing an optimal setup with respect to the sensitivity of the detectors (Roy et al., 2002) and removing saturated detectors from location calculations (Mostoufi et al., 2003), have also been reported. In addition, RPT has been modified to visualize the tracer motion on-line (Godfroy et al., 1997), and extended to systems with irregular moving boundaries (Doucet et al., 2008b) as well as systems with high velocities (Mostoufi et al., 2003).
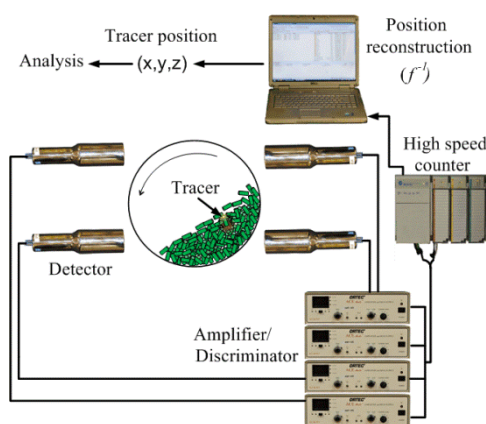
Figure 4.1: Typical RPT setup for a rotating drum.

Although RPT has showed powerful non-invasive tracking abilities in different processes, it is still limited to the tracking of only one tracer at a time. Tracking more than one particle simultaneously is definitely of interest because it could yield direct information about both the

translational and rotational motions of particles. In particular, the rotational motion of particles may play a significant role for instance on the lift force exerted on them and then have an impact on their distribution (Duchanoy & Jongen, 2003). In systems where heat transfer is involved, the rotational motion of solid particles may change the rate of heating or cooling by increasing the interphase heat transfer coefficient (Mankad & Fryer, 1997; Z. Yang et al., 2008). In addition, by tracking more than one particle at the same time, the effect of the spatial orientation of non-spherical particles when they hit the wall of a system or bubbles in a fluidized bed, as well as the relative motion of two freely moving particles, can be studied. Furthermore, the validation of discrete element based models is another reason why the tracking of multiple particles is of interest.

In this study, a so-called multiple radioactive particle tracking (MRPT) technique that is capable of simultaneously tracking two tracers, which can move freely or are constrained to stay at a fixed distance from each other, is introduced. This method will be first explained in detail, followed by two types of experiments to show its potential. It will then be applied to a rotating drum filled with cylindrical particles mixed with spherical glass beads.

4.3 Method

4.3.1 RPT location algorithm

The RPT location algorithm calculates the spatial position of the tracer ($X = (x, y, z)$) from the set of event counts ($\Phi = \{\Phi_i\}_{i=1..N}$) recorded by the data acquisition system (each of the N detectors). The latest generation of this algorithm is based on a phenomenological model that predicts the event counts for each detector for given tracer positions (Beam et al. 1978; Doucet et al., 2008b; Larachi et al., 1994). Since there is no analytical inverse function for this model, the algorithm uses a direct search method and seeks the tracer position corresponding to a given set of event counts by covering the entire domain of the system. To do so, the algorithm relies on a discretization of the domain into tetrahedra and nodes, and calculates a set of event counts for the detectors corresponding to each of these nodes. The algorithm then reconstructs the tracer position by solving a minimization problem that yields the smallest gap between the measured and calculated sets of event counts. The phenomenological model and minimization procedure

will be presented and discussed in the next two sections, followed by the introduction of the multiple radioactive particle tracking (MRPT) technique.

4.3.2 Phenomenological model

For a given system, the number of detected gamma rays (event counts) recorded by a detector is function of the relative position of the tracer and the material between this detector and this tracer. This relationship can be approximated by a phenomenological model that relates the number of events for detector j to the position of the tracer (Chaouki, Larachi, & Dudukovic, 1997b; G.F. Knoll, 2010):

$$\Phi_j(\boldsymbol{X}) = \frac{Tv R \phi \xi_j(\boldsymbol{X}, \mu_s)}{1 + \tau v R \phi \xi_j(\boldsymbol{X}, \mu_s)} \qquad\qquad 4.1$$

where T is the sampling time, v is the number of photons emitted by disintegration ($v = 2$ for ^{46}Sc) (Larachi et al., 1995), R is the tracer activity, ϕ is the photopeak-to-total ratio ($\phi = 0.40$ for ^{46}Sc) (Larachi et al., 1995), τ is the dead time of the acquisition system, and $\Phi_j(\boldsymbol{X})$ and $\xi_j(\boldsymbol{X}, \mu_s)$ represent the event counts and the efficiency of detector j with respect to position $\boldsymbol{X}$, respectively. In Eq. 4.1, the efficiency term $\xi_j(\boldsymbol{X}, \mu_s)$, which brings into play the attenuation coefficient μ_s, is the only variable that depends on the tracer position and the most challenging term to evaluate. By definition, the efficiency is the fraction of emitted gamma rays that hit a given detector as they travel across the system (Tsoulfanidis & Landsberger, 2011). Since there is no analytical solution for this efficiency, except in some simple cases, a Monte Carlo technique has been devised to compute it (Beam et al., 1978; Chaouki et al., 1997b; Doucet et al., 2008b; Larachi et al., 1995; Larachi et al., 1994).

4.3.3 Reconstruction of the tracer position

To minimize scattering and back-reflection effects, gamma rays outside of a certain energy window are rejected by using an amplifier/discriminator. In order to take into account the amplification and discrimination of the original pulses during the data acquisition process, and to obtain the attenuation coefficient of the system μ_s, a calibration test is performed prior to each RPT experiment. The tracer is positioned in n given positions $\{\boldsymbol{X}_k\}_{k=1..n}$ inside of the system.

For each detector j, the attenuation coefficient of the system μ_s, the tracer activity R and the dead time of the acquisition system τ are fitted by solving the minimization problem:

$$\min_{R,\tau,\mu_s} \sum_{k=1}^{n} \left(\frac{\Phi_j(X_k) - \Phi_j^m}{\Phi_j(X_k) + \Phi_j^m} \right)^2 \qquad 4.2$$

where $\Phi_j(X_k)$ and Φ_j^m are the calculated and measured event counts for detector j with respect to position X_k, respectively.

Since the calculation of event counts is time consuming, the algorithm saves them in a matrix, the so-called dictionary, so that this information is readily available when needed. More precisely, for each detector, a dictionary is built, which contains the calculated event counts associated with all the nodes (Dube et al., 2014) used to discretize the domain of the system V (see Dube et al. (Dube et al., 2014) for the nodal geometry). Then, for a given set of measured event counts, the algorithm seeks the node P_i yielding the smallest gap between the corresponding set of calculated event counts and these measured event counts by solving:

$$\min_{P_i \in V} \sum_{j=1}^{N} \left(\frac{\Phi_j(P_i) - \Phi_j^m}{\Phi_j(P_i) + \Phi_j^m} \right)^2 \qquad 4.3$$

After obtaining node P_i, the algorithm further refines the position of tracer X_P by searching every tetrahedron T_P that contains this node:

$$\min_{X_P \in T_P} \sum_{j=1}^{N} \left(\frac{\Phi_j(X_P) - \Phi_j^m}{\Phi_j(X_P) + \Phi_j^m} \right)^2 \qquad 4.4$$

A linear interpolation is used to compute the values of the event counts at X_P based on the values at the nodes of the corresponding tetrahedron.

4.3.4 Multiple radioactive particle tracking (MRPT) technique

When adding a second tracer, the data acquisition system records the event counts resulting from both tracers. Since the contribution of each of these tracers on the recorded event counts is not known, the location algorithm cannot be applied in a straightforward manner. To get around this problem, two approaches may be considered: (a) determine the contribution of each tracer on the

recorded event counts, or (b) create a new location algorithm that can deal with the combined recorded event counts.

In the first approach, the tracers should be built from two different isotopes, where one has a high gamma energy peak significantly different from the other energy peaks. The amplifiers/discriminators of the acquisition system can be divided into two groups. The first group only captures gamma rays that have energies within a range around the highest energy peak. The second group records gamma rays that have energies within a window covering the other energy peaks. Consequently, one possibility would consist of positioning the highest energy peak tracer (made from one of the two isotopes) using the current RPT algorithm. The phenomenological model presented in the previous section could then serve to calculate the tracer position, and the contribution of this first tracer on the events recorded by the second group of amplifiers/discriminators could be calculated and subtracted from the total event counts monitored by this group. This would enable the positioning of the second tracer with the current RPT algorithm. However, it is known that some of the gamma rays with the highest energy peak scatter when they interact (Compton scattering or pair production) so that they lose energy and end up within the range of the other energy window. Therefore, these gamma rays are recorded by the second group of amplifiers/discriminators and their contribution is not subtracted from the recorded event counts. The number of such gamma rays varies depending on their travel distance and the material that they pass through, as well as on the random nature of the radioactive interactions (further discussion is provided in the appendix of this chapter). These gamma rays represent noise for the second tracer, which increases the noise to signal ratio and leads to poor positioning. This method is then difficult to use in practice.

In the other approach, the second tracer (tracer B) is built with the same isotope as the first tracer (tracer A). Therefore, the data acquisition system records the event counts resulting from both tracers. Since the contribution of each tracer on the collected event counts is not known, the standard RPT location algorithm is not applicable. To overcome this problem, it is proposed to seek the position of the two tracers simultaneously instead of tracking each tracer individually. Consequently, the algorithm must be adapted to handle this new tracking technique. More precisely, it should be able to predict event counts resulting from two tracers located at two given positions. In fact, because of the dead time of the acquisition system, the superposition property does not hold for the measured event counts (G.F. Knoll, 2010; Tsoulfanidis & Landsberger,

2011). However, this property is still correct for the actual event count rate associated to detector j:

$$N_j^{(A,B)}(\boldsymbol{X}_A, \boldsymbol{X}_B) = N_j^A(\boldsymbol{X}_A) + N_j^B(\boldsymbol{X}_B)$$

4.5

where $N_j^{(A,B)}(\boldsymbol{X}_A, \boldsymbol{X}_B)$ is the actual event count rate resulting from both tracers A and B at positions $\boldsymbol{X}_A$ and $\boldsymbol{X}_B$, with respect to detector j. $N_j^A(\boldsymbol{X}_A)$ and $N_j^B(\boldsymbol{X}_B)$ are the actual event count rates for tracers A and B at position $\boldsymbol{X}_A$ and $\boldsymbol{X}_B$, with respect to detector j.

There is a relationship between the actual event count rate N_j, the measured event counts Φ_j for sampling time T and dead time τ (G.F. Knoll, 2010; Tsoulfanidis & Landsberger, 2011):

$$N_j^I(\boldsymbol{X}_I) = \frac{\left(\Phi_j^I(\boldsymbol{X}_I)/T\right)}{1 - \tau\left(\Phi_j^I(\boldsymbol{X}_I)/T\right)} \quad , \qquad I = A, B \text{ or } (A, B)$$

4.6

Substituting 4.6 into 4.5 then yields:

$$\frac{\left(\Phi_j^{(A,B)}(\boldsymbol{X}_A, \boldsymbol{X}_B)/T\right)}{1 - \tau\left(\Phi_j^{(A,B)}(\boldsymbol{X}_A, \boldsymbol{X}_B)/T\right)} = \frac{\left(\Phi_j^A(\boldsymbol{X}_A)/T\right)}{1 - \tau\left(\Phi_j^A(\boldsymbol{X}_A)/T\right)} + \frac{\left(\Phi_j^B(\boldsymbol{X}_B)/T\right)}{1 - \tau\left(\Phi_j^B(\boldsymbol{X}_B)/T\right)}$$

4.7

Rearranging Eq. 4.7 results in a model that can predict the total measured event counts coming from both tracers based on the individual measured event counts:

$$\Phi_j^{(A,B)}(\boldsymbol{X}_A, \boldsymbol{X}_B) = \frac{\Phi_j^A(\boldsymbol{X}_A) + \Phi_j^B(\boldsymbol{X}_B) - 2\left(\tau/T\right)\Phi_j^A(\boldsymbol{X}_A)\Phi_j^B(\boldsymbol{X}_B)}{1 - \left(\tau/T\right)^2 \Phi_j^A(\boldsymbol{X}_A)\Phi_j^B(\boldsymbol{X}_B)}$$

4.8

where $\Phi_j^{(A,B)}(\boldsymbol{X}_A, \boldsymbol{X}_B)$ is the calculated event count resulting from both tracers A and B at positions $\boldsymbol{X}_A$ and $\boldsymbol{X}_B$, with respect to detector j. $\Phi_j^A(\boldsymbol{X}_A)$ and $\Phi_j^B(\boldsymbol{X}_B)$ are the event counts calculated from Eq. 4.1 for tracers A and B at position $\boldsymbol{X}_A$ and $\boldsymbol{X}_B$, with respect to detector j.

Prior to a two-radioactive-particle tracking experiment, two calibration tests are first performed to obtain the fitted parameters of Eq. 4.1 for tracers A and B, individually. Using a procedure similar to that for the RPT algorithm, dictionaries are built for each tracer with respect to each

detector. For a given set of measured event counts, the algorithm then seeks the nodes P_i for the tracer A and P_k for the tracer B yielding the smallest gap between the sets of calculated and measured event counts by solving:

$$\min_{P_i, P_k \in V} \sum_{j=1}^{N} \left(\frac{\Phi_j^{(A,B)}(P_i, P_k) - \Phi_j^m}{\Phi_j^{(A,B)}(P_i, P_k) + \Phi_j^m} \right)^2 \qquad 4.9$$

After obtaining the pair of nodes P_i and P_k, the algorithm further refines the positions of tracers $\mathbf{X}_A$ and $\mathbf{X}_B$ by searching tetrahedra T_{P_i} and T_{P_k} that contain nodes P_i and P_k, respectively:

$$\min_{\substack{\mathbf{X}_A \in T_{P_i} \\ \mathbf{X}_B \in T_{P_k}}} \sum_{j=1}^{N} \left(\frac{\Phi_j^{(A,B)}(\mathbf{X}_A, \mathbf{X}_B) - \Phi_j^m}{\Phi_j^{(A,B)}(\mathbf{X}_A, \mathbf{X}_B) + \Phi_j^m} \right)^2 \qquad 4.10$$

A linear interpolation is used to compute the values of the event counts at $\mathbf{X}_A$ and $\mathbf{X}_B$ based on the values at the nodes of the corresponding tetrahedra.

4.4 Experimental

The isotope used for tracers A and B is scandium-46 (^{46}Sc). To choose the activities of the tracers, there were two considerations. First, for the setup used, the summation of the tracer activities should be less than 95 µCi to avoid saturation of the detectors. Secondly, the tracers should have different activities so that they can be identified. Therefore, activities of 53 µCi and 39 µCi were chosen for tracers A and B, respectively. Twelve 76mm × 76mm NaI (Tl) scintillation detectors (Teledyne Isotope S-1212-I) are positioned around the setup (Figure 4.2) on two levels in the vertical direction. Each detector is connected to a scintillation tube and the signal is amplified and discriminated by an ORTEC ACE Mate amplifier/discriminator (925-Scint). The sampling time T for the measurements is 10.0 ms, which corresponds to 100 locations per second. In this study, two types of experiments were done: (a) one for the validation of the MRPT technique and (b) one for the application of this new method. These two groups of experiments are the topic of the next two subsections, respectively.

4.4.1 a) Validation of the MRPT technique

These experiments were conducted in a plexiglass column with a 15cm diameter and filled with water up to 12cm in height. They involved: (a) two tracers that can move freely (the so-called free MRPT) or (b) two tracers at a fixed distance from each other (the so-called restricted MRPT). To assess the accuracy and precision of the MRPT technique, these experiments were carried out with stationary and moving tracers for both free and restricted MRPT.

In the stationary particle tests, the accuracy and precision of the MRPT technique were evaluated by reconstructing the tracer positions, the tracers being located at fixed positions. In the case of the free MRPT, the sources were placed at eight different distances from each other. In the case of the restricted MRPT, three rod-like tracers were built by fixing radioactive sources at the two ends of three acrylic rods with a 6mm diameter and 2, 3 and 4cm in length, respectively. Each tracer was placed in twelve different positions and six different orientations. Each such stationary particle test was performed for 12 s.

(a)   (b)
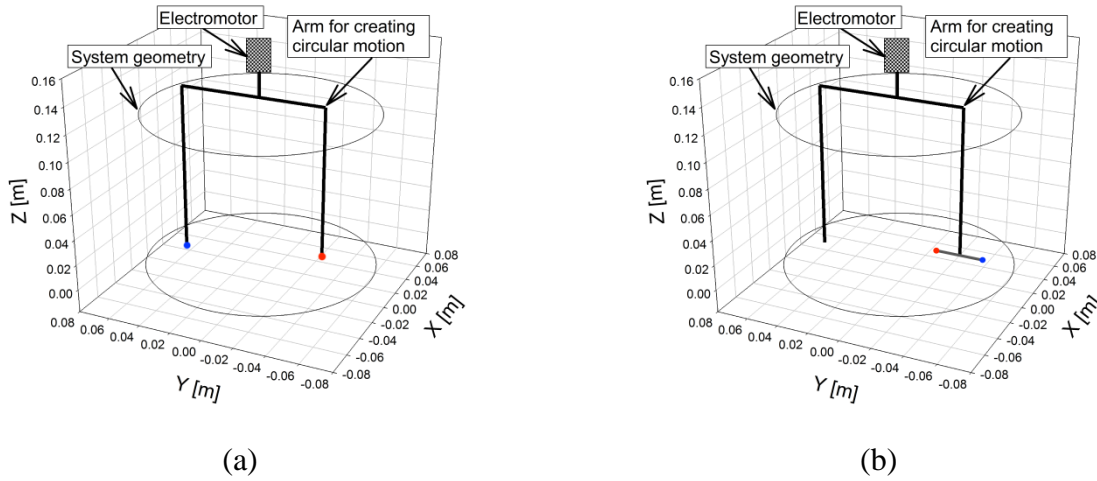
Figure 4.2: Schematic of the experimental setup for (a) moving free MRPT and (b) moving restricted MRPT test.

In the moving particle tests, the effect of the tracer speed was assessed on the basis of the quality of the reconstruction of the tracer positions, these tracers having known displacements and speeds (circular motion). To control the displacement of the tracers, an electromotor with a constant rotational speed of 10.5 rpm was vertically installed at the top of the column (see Figure 4.2).

The middle of an adjustable arm was perpendicularly joined to the shaft of the electromotor. Therefore, by fixing the tracers to the arm and adjusting the arm length, a circular motion with given radii was generated. In the case of the free MRPT (Figure 4.2a), two tracers each with its own radius were set in circular motion by attaching the two corresponding sources to the two arm tips. For the restricted MRPT (Figure 4.2b), each rod-like tracer was set in circular motion by fixing it to one tip of the arm, in such a way that the line going through the two sources is perpendicular to the axis of the shaft of the electromotor. All the moving particle experiments lasted 3 min.

4.4.2 b) Example of application

This type of experiment was conducted in a rotating drum 24 cm in diameter and 38 cm in length. The drum was filled to 35 vol % with acrylic cylindrical particles (20% v/v) 6 mm in diameter and 3 cm in length, and spherical glass beads (80% v/v) 3 mm in diameter. The drum rotational speed was set at 2.5 rpm. All the particles were uniformly mixed at the beginning. A rod-like tracer 3 cm in length was used to mimic the motion of the cylindrical particles.

4.5 Results and Discussion

4.5.1 Validation tests

The accuracy (degree of closeness of the measurements) of the MRPT technique can be evaluated by comparing the actual and measured average values of the tracer positions (p) and speeds (s) and, in the case of a rod-like tracer, of the orientations (α):

$$px_k = \left| \frac{\sum_{i=1}^{M} \hat{x}_k^i}{M} - x_k \right| \tag{4.11}$$

$$sx_k = \left| \frac{\sum_{i=1}^{M} \hat{v}x_k^i}{M} - vx_k \right| \tag{4.12}$$

$$\alpha = \left(\frac{\sum_{i=1}^{M} \mathrm{acos}\,(\vec{t_i}.\,\mathrm{t})}{M} \right) \times 180/\pi \tag{4.13}$$

The precision (reproducibility) can be assessed through the standard deviation of the measured values of the tracer positions and, in the case of a rod-like tracer, of the orientations:

$$\sigma_{xk} = \sqrt{\sum_{i=1}^{M} \left(\hat{x}_k^i - \frac{\sum_{j=1}^{M} \hat{x}_k^j}{M} \right)^2 \bigg/ M}$$

4.14

$$\sigma_k = \sqrt{\sigma_{xk}^2 + \sigma_{yk}^2 + \sigma_{zk}^2}$$

4.15

$$\sigma_\alpha = \sqrt{\sum_{i=1}^{M} \left(acos \left(\vec{t_i}.\vec{t} \right) \right)^2 \bigg/ M}$$

4.16

In these expression, x_k represents the actual position of tracer k, px_k and sx_k are the errors of the MRPT results on the position and speed of tracer k along the x axis, respectively, $\hat{x}_k^i$ and $\hat{v}x_k^i$ the ith calculated position and speed of tracer k along the x axis, respectively, $\vec{t}$ and $\vec{t_i}$ the actual and the ith calculated value of the unit vector representing the rod-like tracer, respectively, σ_{xk} the standard deviation of the position of tracer k along the x axis, and M the number of samples. More details on this can be found in the book by Tsoulfanidis and Landsberger (Tsoulfanidis & Landsberger, 2011).

In general, the quality of RPT results depends on system characteristics (size, uniformity, type, etc.) as well as RPT setup characteristics (number of detectors, arrangement of the detectors, etc.). Therefore, for comparison purposes, single tracer RPT tests were also carried out individually for tracers A and B in the same system. The averaged accuracy (p) and precision (σ) for these tracers are p_A=0.7 mm, σ_A=1.3 mm, p_B=0.8 mm and σ_B=1.6 mm, respectively. In both cases, there is scattering in the calculated tracer positions and the corresponding standard deviations σ_A and σ_B are greater than the discrepancies p_A and p_B . This scattering comes from the fluctuations in emitted gamma rays due to the random nature of the radioactive decay. The standard deviation of these fluctuations is in fact equal to the square root of their mean values (Tsoulfanidis & Landsberger, 2011). In fact, the slightly better precision of the results for tracer A (greater activity) can be explained by comparing the relative standard deviations of the measured event counts for both tracers. Although the raw event counts were passed through a

Butterworth filter in the location algorithm, the filtered event counts still exhibit some fluctuations. Another source of scattering is the non-isotropic emission of gamma rays.

4.5.1.1 Stationary particle tests for the free MRPT technique

Using a 10 ms sampling time and a 12 s experiment duration, 1200 measurements were recorded for each stationary particle test. The filtered data start at zero and then level off to a slightly oscillating value after a certain time, which depends on how the filter parameters were chosen. Therefore, the first 600 tracer positions were rejected to eliminate physically meaningless information.

(a)   (b)
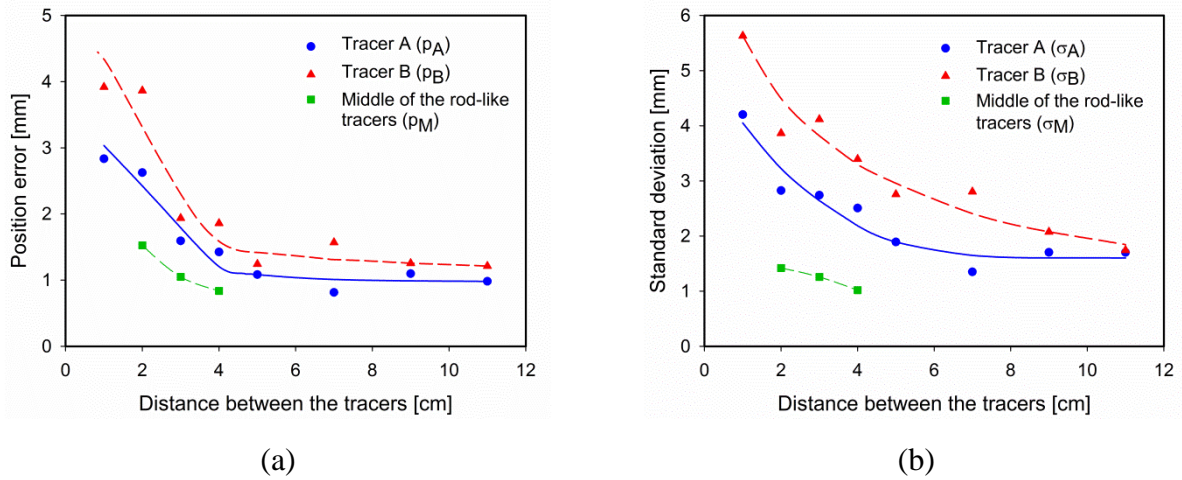
Figure 4.3: Variation of the (a) position error (accuracy) and (b) standard deviation (precision) of the position, as a function of the distance between the tracers..

The variation in the position error and standard deviation versus the distance between the tracers is displayed in Figure 4.3. It can be noticed that the accuracy and precision of the MRPT results are not as good as (larger values) than those of the RPT results (p_A=0.7 mm, σ_A=1.3 mm, p_B=0.8 mm and σ_B=1.6 mm). In MRPT, the fluctuations in the gamma rays emitted by both tracers add up, leading to a larger standard deviation of the measured event counts. To calculate the relative standard deviation for each tracer in MRPT, the total standard deviation is divided by the mean value of the event counts of each tracer individually ($\sigma_{rA} = \frac{\sigma_{(A,B)}}{\overline{\Phi}_A}$ and $\sigma_{rB} = \frac{\sigma_{(A,B)}}{\overline{\Phi}_B}$). Therefore, the relative standard deviation for each tracer is higher compared to that of RPT ($\sigma_{rA} = \frac{\sigma_A}{\overline{\Phi}_A}$ and

$\sigma_{rB} = \frac{\sigma_B}{\bar{\Phi}_B}$), resulting in lower precision. The other reason for the lower precision of MRPT is due to the fact that the gamma rays emitted come from two tracers. In some cases, the calculated position for tracer A may be such that this tracer is closer than reality to some detectors. For these detectors (set #1), the contributions of tracer A to the total calculated event counts will be larger than what it should be, and those (set #2) related to the detectors that are further than expected will be smaller. Consequently, the contributions of tracer B associated with the set #1 of the detectors will be smaller and those related to set #2 will be larger. This means that the calculated position of tracer B is closer than reality to the detectors of set #2 and further to those of set #1. In other words, the positioning error related to tracer A will increase the positioning error of tracer B.

Figure 4.3 also shows that tracer A has better accuracy and precision than tracer B. Because of its lower activity, tracer B yields fewer event counts. Its relative standard deviation σ_{rB} is also larger, resulting in a lower precision compared to tracer A. It can be seen that the error and standard deviation decrease when the distance between the tracers increases. For a detector, the higher the contribution of tracer A (resp. B) in the measured event counts (the lower the relative standard deviation), the more effective it is in positioning tracer A (resp. B). When tracers A and B are far from each other, some of the detectors (set #1) are closer to tracer A and some other detectors (set #2) are closer to tracer B. The detectors of set #1 are then effective in the positioning of tracer A for two reasons: first, the contribution of tracer A in the total event counts is high and second, the impact on the standard deviation of the total event counts due to tracer B is small. Therefore, the relative standard deviation of tracer A is close to that of RPT for the detectors of set #1 under the same conditions. For similar reasons, the set #2 of detectors is then effective in the positioning of tracer B. When tracers A and B get close to each other, the detectors of set #1 and set #2 become similar. Therefore, in comparison with the previous case, the relative contribution of tracer A to the total event counts for the set #1 of detectors is smaller and the impact on the standard deviation of the total event counts due to tracer B is higher. Therefore, the relative standard deviation of tracer A is higher compared to that of the previous case, which means that the positioning of this tracer is not as good. Similar discussion can be done for tracer B.

4.5.1.2   Stationary particle tests for the restricted MRPT technique

In the restricted stationary MRPT tests, the middle point of the rod-like tracer is calculated by averaging the positions obtained for sources A and B with the standard approach. The accuracy and precision of the middle points for the three different rod-like tracers are illustrated in Figure 4.3. These results show a better accuracy and precision of the middle point positions than those of the individual sources. In some cases, the position of one of the sources is closer than reality to a group of detectors because of the fluctuations and non-isotropic emission of gamma rays. When this occurs, the corresponding group of detectors locates the other source at a larger distance to them to be compliant with the total event counts measured. This is why the middle point can be positioned more accurately than its two surrounding sources.

One can take advantage of the fact that the middle points can be positioned more accurately and that the distance between the two tracers is known to determine their location more efficiently. Indeed, a rod-like tracer can be defined by its middle point position and the orientation vector connecting its two end points. The mean error and standard deviation of the orientation are depicted in Figure 4.4. It shows that the accuracy and precision increase with the distance between the sources. Since the position error and standard deviation are higher at smaller distances (Figure 4.3), so is the orientation error. In addition, the larger the rod, the smaller the impact of a given position error on the orientation error will be.
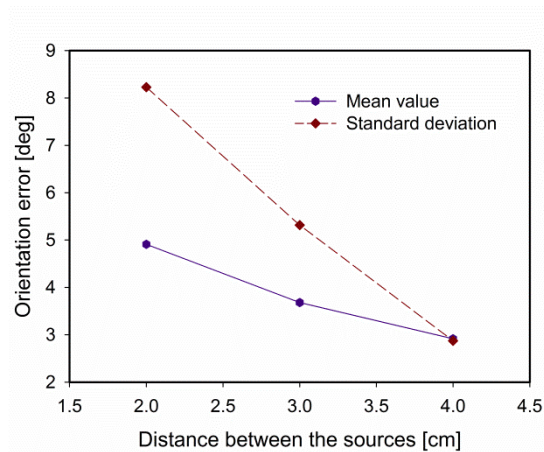
Figure 4.4: Variation of the mean error (accuracy) and standard deviation (precision) of the orientation of the rod-like tracers.

To assess the ability of this alternative approach for positioning a rod-like tracer in restricted MRPT, the positions of the two sources located at the tips of a rod-like tracer were reconstructed from its length and the measured values of its middle point position and orientation. The mean error and standard deviation of the results obtained with this approach are illustrated in Figure 4.5. It can be readily noticed that the accuracy and precision are better for all three cases, and that the improvement is more important for the 2-cm long rod-like tracer. Note that the restricted MRPT results subsequently presented were obtained with this alternative approach.

(a)   (b)
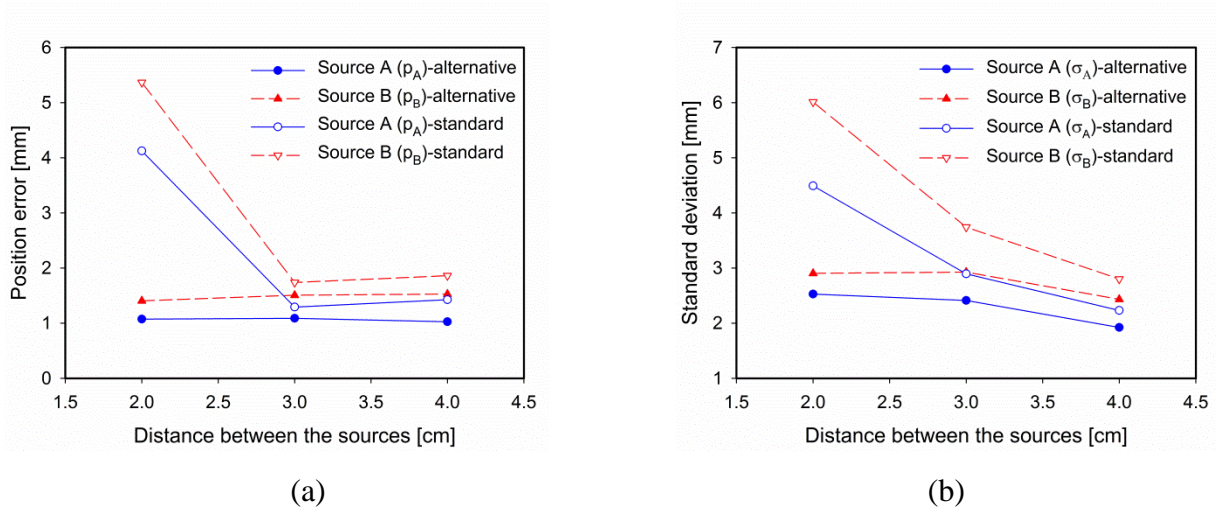
Figure 4.5: Comparison of the (a) accuracy and (b) precision obtained with the standard and alternative techniques for the restricted MRPT stationary tests.

4.5.1.3   Moving particle tests for the free MRPT technique

In the free MRPT moving particle tests, the tracers were set in motion independently along circles of radii 2, 3, 4 and 5cm (see Figure 4.6). The tracer speed was varied from 22 mm/s to 56 mm/s for the different runs. Figure 4.6a shows the average positions of tracers A and B rotating along circles of 5 and 4 cm radii (s_A=56 mm/s and s_B=46 mm/s), respectively. Figure 4.6b shows typical average velocity vectors for the tracers in an xy plane for these runs. The results obtained indicate that the proposed MRPT technique can adequately measure the positions and speeds of the two tracers.

(a)   (b)
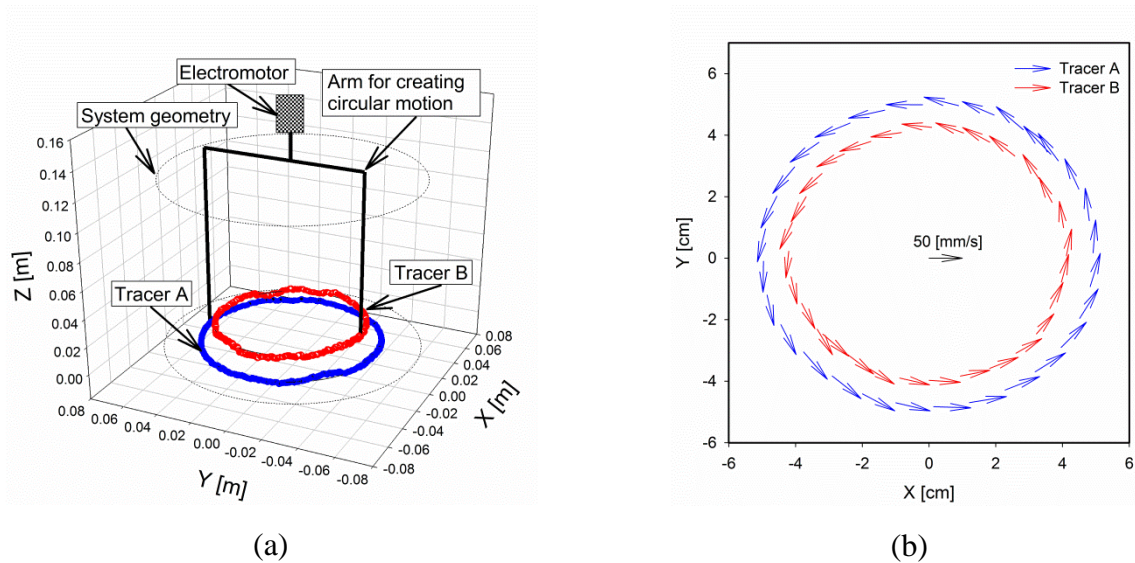
Figure 4.6: Tracers A and B rotating along 5- and 4-cm radius circles, respectively: a) average position and b) velocity vector.

The results of the variation in the average position standard deviation and speed error versus the speed of the tracers are displayed in Figure 4.7. This figure shows an adequate resolution for these tracking experiments. As already discussed, tracer A can be located more precisely than tracer B. In these free MRPT tests, since the minimum distance between the tracers is more than 4 cm, the effect of the distance between the tracers on the results is expected to be very small (see Figure 4.3). Figure 4.7 shows that the position standard deviation and speed error are mainly dominated by the corresponding contribution in the z direction. Previous work from the literature (Larachi et al., 1994; Roy et al., 2002) indicates that the results could be improved by placing the detectors on more than two levels along the z direction. In these moving particle tests, the fact that the tracers move during a recording interval causes an additional source of error compared to the stationary particle tests. This explains the small increase in the standard deviation of the tracer positions with respect to the speed of the tracers in the xy plane. Considering that the sampling time was 10 ms and the highest tracer speed was 56 mm/s, the tracers could then move a maximum of 0.56 mm during a recording interval. Since this maximum displacement is much smaller than the MRPT resolution (see Figure 4.3), the accuracy of the results (position and speed error) is not significantly affected by the variation of the tracer speed within the range of speeds considered.
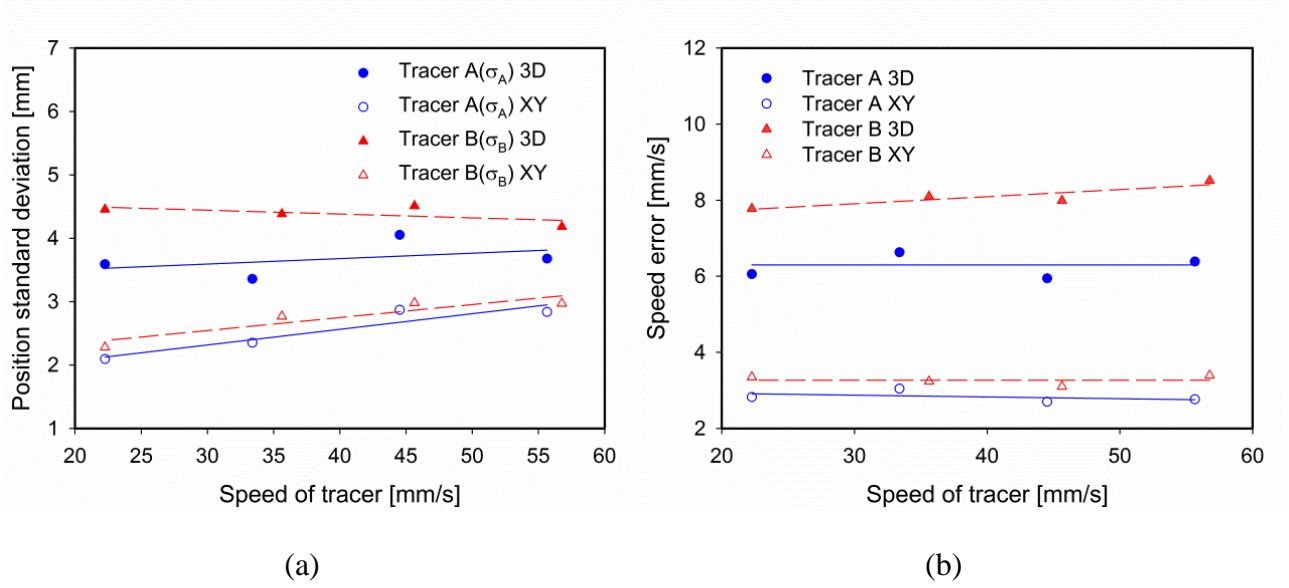
Figure 4.7: Variation of a) the average position standard deviation and b) the average speed error versus the speed of the tracer in the free MRPT tests. XY means that only the contribution in the x and y directions were taken into account in the calculation of the corresponding quantities, whereas 3D means that all three directions were considered in these calculations.

4.5.1.4 Moving particle tests for the restricted MRPT technique

In the restricted MRPT moving particle tests, the rod-like tracers were set in motion in a coupled manner along circles. The variation of the average position standard deviation and speed error corresponding to the middle point versus the speed of the tracers is given in Figure 4.8. As already discussed, the resolution for rod-like tracers improves when the distance between the sources increase. This explains the trend observed in the figure. Since the displacement of a tracer during a recording interval increases with its speed, so does its position standard deviation (Figure 4.8a). Because the electromotor has a constant rotational speed, the length of the arm was varied to adjust the speed of the tracers. Therefore, the tracers are closer to the wall of the system when their speed is higher, resulting in the decrease of the number of effective detectors and consequently, in the increase of the speed error and the position standard deviation (Figure 4.8). Despite it all, the resolution remains better than that of free MRPT (see Figure 4.7).

(a)   (b)
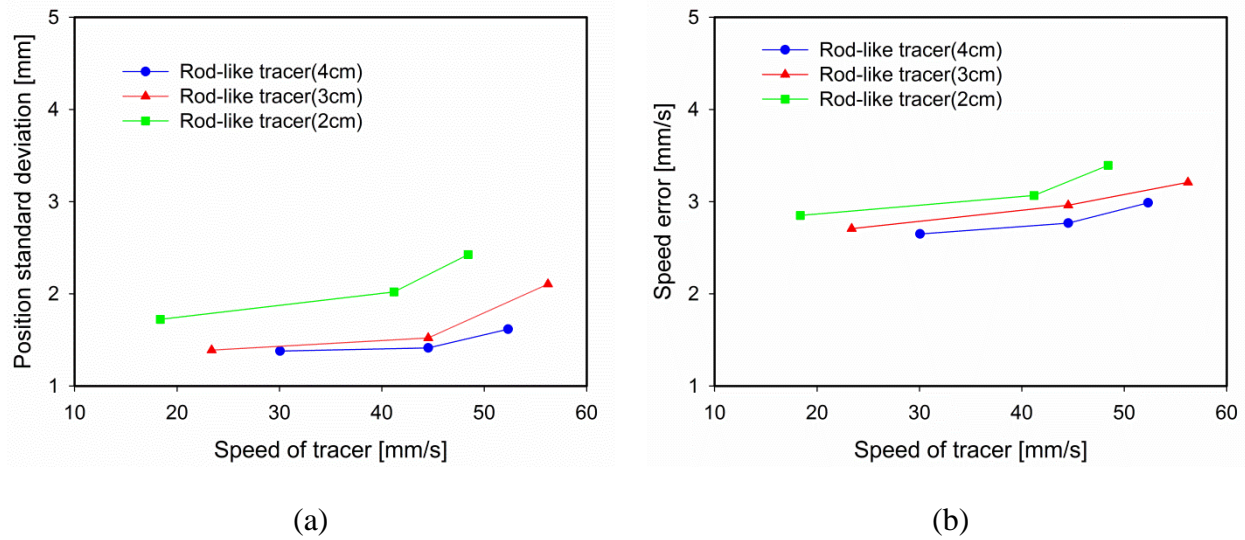
Figure 4.8: Variation in a) the average position standard deviation and b) the average speed error versus the speed of the rod-like tracers in the restricted MRPT tests.

The variation of the mean error and standard deviation of the orientation of the rod-like tracers versus the speed of these tracers is displayed in Figure 4.9. It can be noticed that the error is lower for the longer rods due to the larger distance between the sources. More precisely, it can be deduced that the orientation error and standard deviation are mainly dominated by the corresponding contributions in the z direction. The values of these quantities in the xy plane are similar to those for the stationary particle tests (Figure 4.4).
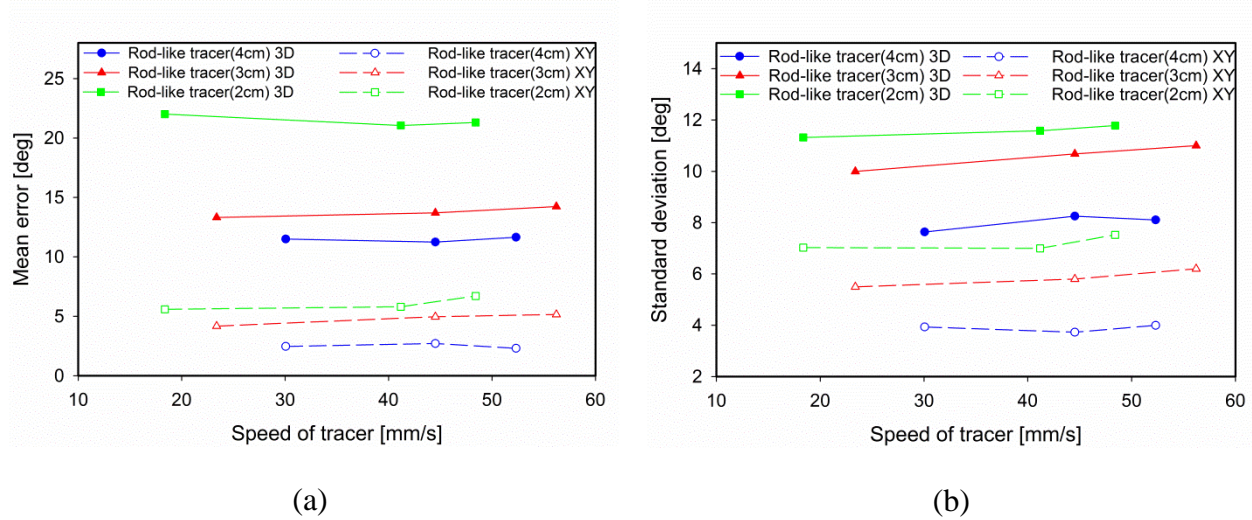
Figure 4.9: Variation of a) the mean error and b) the standard deviation of the orientation of the rod-like tracers versus the speed of these tracers in the restricted MRPT tests. XY means that only the contribution in the x and y directions were taken into account in the calculation of the corresponding quantities, whereas 3D means that all three directions were considered in these calculations.

4.5.2 Flow in the rotating drum

To demonstrate the applicability of the proposed MRPT technique to investigate the flow dynamics in a realistic application, experiments were conducted in a rotating drum (2.5 rpm) filled with acrylic cylindrical particles 6 mm in diameter and 3 cm in length, mixed with 3-mm spherical glass beads, for a duration of 30 min. A rod-like tracer 3 cm in length was used to mimic the motion of the cylindrical particles based on the so-called ergodicity assumption (the time average of one tracer is equal to a population average(Doucet et al., 2008a)). At 2.5 rpm, the speed of the rod-like tracer could reach up to 25 cm/s (at the middle of free surface). There are two reasons for mixing cylindrical particles with glass beads. First, there are many applications where large particles are mixed with smaller particles: blending, transport, pyrolysis, sintering, drying, incineration, combustion. Secondly, such a test case gives us the possibility to assess qualitatively the MRPT results by visual observation. Because of the segregation mechanism between large and small particles, the cylindrical particles will migrate to the wall of the drum and the glass beads will settle near the middle of it(Alizadeh, Dube, et al., 2013).

(a)   (b)
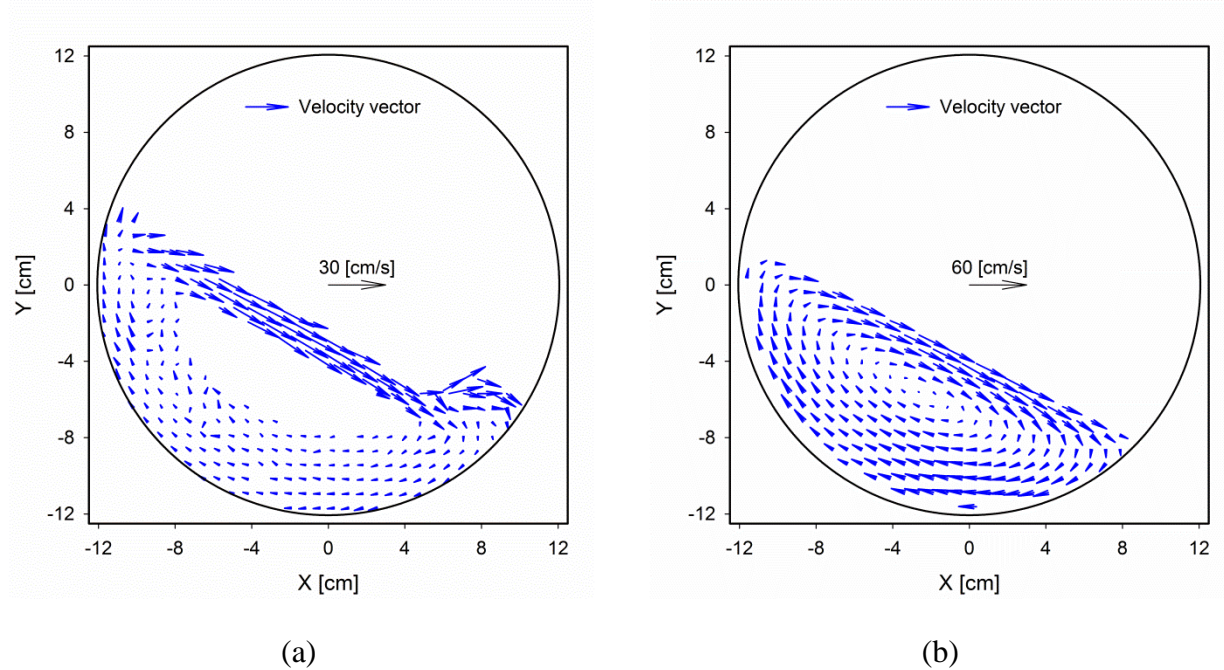
Figure 4.10: Velocity vectors in the transverse plane of the drum for (a) cylindrical particles after 30 min and a rotational speed of 2.5 rpm, (b) 3-mm glass beads and a rotational speed of 11.6 rpm (this figure is adapted from Alizadeh et al. (Alizadeh, Dube, et al., 2013)).

The speed of the tracer was calculated as the time derivative of its position. It is important to remember that the rod-like tracer position is defined by its middle point position. Since the MRPT technique tracks a tracer in a Lagrangian manner, the domain was discretized into cells and the data were converted into Eulerian data. To obtain a velocity profile in a xy transverse plane, the tracer speeds in each cell were averaged regardless of the tracer position along the z axis.

Figure 4.10a shows the velocity profile of the cylindrical particles in the transverse plane. To eliminate the errors coming from the fluctuations in the tracer position and instantaneous speed, a large number of data is required for each cell. An average of about 200 data points per cell were available to calculate the velocity profile, which is qualitatively in good agreement with that of spherical particles(Alizadeh, Dube, et al., 2013) (Figure 4.10b), except in regions where the free surface reaches the wall of the drum. It was observed that collisions between high-speed and low-speed particles occurring in the low extremity of the free surface often resulted in the jump of a few cylindrical particles. Such collisions also generated a disorder of these particles in this

section of the bed. Figure 4.10a also indicates that the rod-like tracer could not reach the core of the bed owing to segregation between the spherical and cylindrical particles.

(a)

(b)
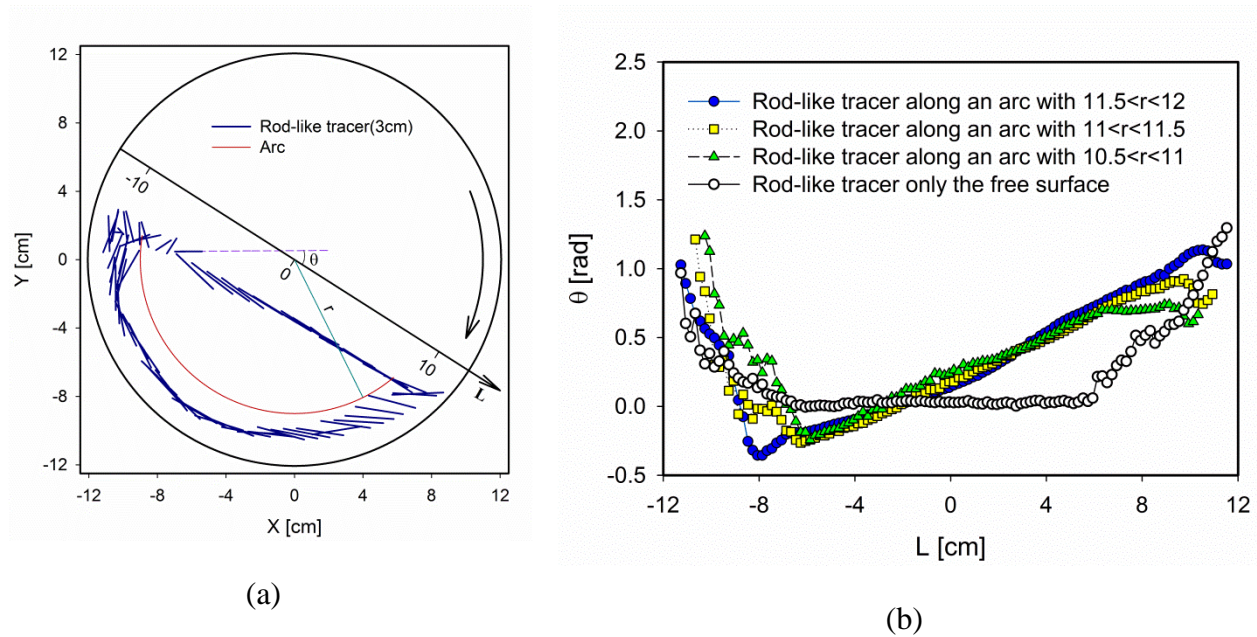
Figure 4.11: rod-like tracer position and orientation during a single circulation, and b) average angle of this tracer along the L axis during the circulations.

Figure 4.11a shows the position and orientation of the rod-like tracer during a single circulation of the tracer. To visualize in an effective manner the orientation of cylindrical particles during the circulation, the L axis is introduced and defined as the axis that passes through the center of the domain and is parallel to the free surface, while the angle θ is defined as the angle between the rod-like tracer and this L axis. We recall that the motion of the particles in a rotation drum is generally investigated by dividing the bed into two sections: (1) a thin lens-like layer beneath the free surface called active layer wherein the particles slide downward and (2) a large passive layer underneath the active layer where the particles flow along arcs of different radii. Figure 4.11b shows average values of θ in both sections. It can be observed that when the particles reach the free surface (top left part in Figure 4.11a), their orientation angles are wide. When sliding along the free surface, these angles decrease until the particles reach around L=-8 cm. Downstream from this region, the particles slide almost parallel to the free surface (θ=0) until they reach around L=6 cm, after which their orientation angles start increasing until they hit the wall of the drum. One can also notice in Figure 4.11 that particles located on the free surface near L=10 cm

can have wide orientation angles, which enable them to penetrate more easily into the passive layer of the bed. These particles then flow in a solid-like body motion, as evidenced by the constant decrease rate of their orientation angles (Figure 4.11b). Alternatively, these particles may remain in the active layer for a while before entering the passive layer. What one should appreciate here is that such information could not be provided by single tracer RPT.

4.6 Conclusion

This work shows that the proposed MRPT technique can simultaneously track two tracers that move freely or are at a fixed distance from each other. By conducting stationary and moving particle tests, it was demonstrated that MRPT can position two tracers with an error similar to that with single tracer RPT when the distance between these tracers is more than 4cm. It was also observed that when the distance between the two tracers is fixed, the middle point (<2 mm) and orientation of the tracers (<5 degrees) can be measured adequately with this technique. Finally, the MRPT technique was applied to the flow of spherical and cylindrical particles (3cm in length, speed up to 25 cm/s) in a cylindrical drum (2.5 rpm). Good results were obtained as regards the position and orientation of the cylindrical particles by using a rod-like tracer to mimic the motion of these cylindrical particles.

Future work will include the impact of the activity ratio between two tracers comprising a non-spherical particle on the efficiency of the MRPT technique, particularly when the distance between these two tracers is small.

4.7 Acknowledgments

4.8 Appendix

In this appendix, the noise coming from the tracer with higher energy peak (tracer B) on the event counts of the other tracer (tracer A) is calculated. To do so, a Monte Carlo approach is considered. In the rotating drum, 200 pair positions for tracers A and B are chosen randomly (Figure 4.12a). For a given pair of positions, to calculate the amount of gamma rays that are scattered from tracer B, two different situations are considered: first, with an empty drum and next, with a drum filled with particles. The difference between the event counts for these two situations is related to the amount of scattered gamma rays. Only a portion of these scattered gamma rays will end up in the energy window of tracer A. Here, it is assumed that this portion is 20%. Therefore, the event counts of tracer A, the noise from tracer B on the event counts of tracer A and the noise to signal ratio for tracer A can be calculated (Figure 4.12b). To ease the analysis, only 100 data points are displayed in Figure 4.12b. It shows that the noise to signal ratio varies significantly with the pair position of tracers A and B. while some cases the noise is negligible, in many cases it can be large. The averaged noise to signal ratio is about 0.6 (calculated from the 200 dada points), which is very high and likely to result in poor positioning of tracer A.

(a)   (b)
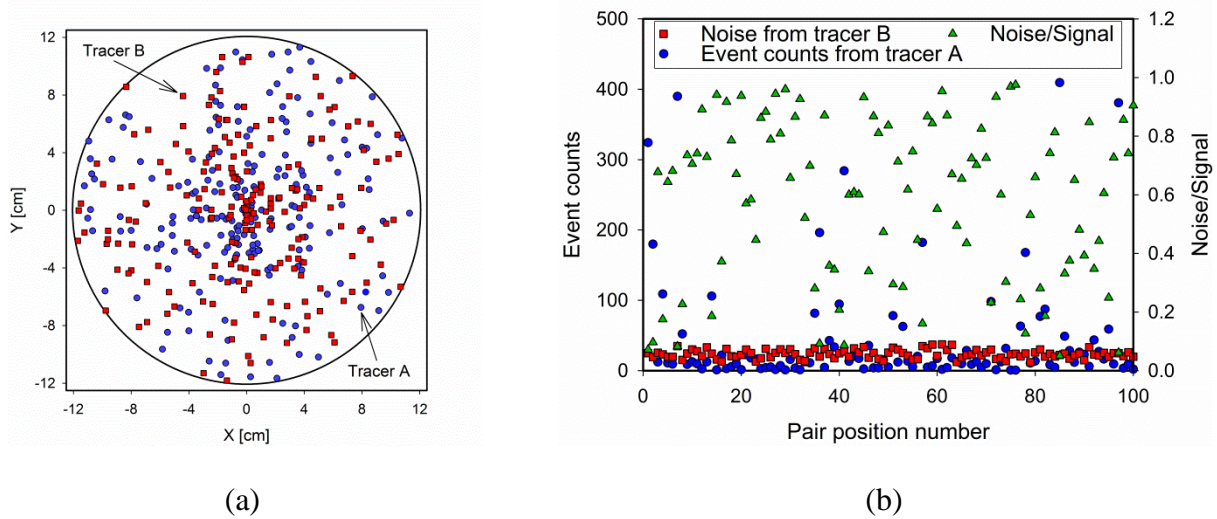
Figure 4.12: a) distribution of pair positions for tracers A (blue) and B (red) in the drum and b) event counts for tracer A, the noise from tracer B on the event counts of tracer A, and the noise to signal ratio for tracer A, for each pair position.

4.9 Literature Cited

Alizadeh, E., Dube, O., Bertrand, F., & Chaouki, J. (2013). Characterization of Mixing and Size Segregation in a Rotating Drum by a Particle Tracking Method. *Aiche Journal, 59*(6), 1894-1905. doi: 10.1002/Aic.13982

Bakalis, S., Fryer, P. J., & Parker, D. J. (2004). Measuring velocity distributions of viscous fluids using positron emission particle tracking (PEPT). *Aiche Journal, 50*(7), 1606-1613. doi: 10.1002/Aic.10153

Beam, G. B., Wielopolski, L., Gardner, R. P., & Verghese, K. (1978). Monte Carlo calculation of efficiencies of right-circular cylindrical NaI detectors for arbitrarily located point sources. *Nuclear Instruments and Methods, 154*(3), 501-508. doi: 10.1016/0029-554x(78)90081-2

Boyer, C., Duquenne, A. M., & Wild, G. (2002). Measuring techniques in gas-liquid and gas-liquid-solid reactors. *Chemical Engineering Science, 57*(16), 3185-3215. doi: 10.1016/S0009-2509(02)00193-8

Cassanello, M., Larachi, F., Legros, R., & Chaouki, J. (1999). Solids dynamics from experimental trajectory time-series of a single particle motion in gas-spouted beds. *Chemical Engineering Science, 54*(13-14), 2545-2554. doi: 10.1016/S0009-2509(98)00468-0

Chaouki, J., Larachi, F., & Dudukovic, M. P. (1997a). Noninvasive tomographic and velocimetric monitoring of multiphase flows. *Industrial & Engineering Chemistry Research, 36*(11), 4476-4503. doi: 10.1021/Ie970210t

Chaouki, J., Larachi, F., & Dudukovic, P. (1997b). *Non-Invasive Monitoring of Multiphase Flows*: Elsevier Science.

Chen, J. W., Rados, N., Al-Dahhan, M. H., Dudukovic, M. P., Nguyen, D., & Parimi, K. (2001). Particle motion in packed/ebullated beds by CT and CARPT. *Aiche Journal, 47*(5), 994-1004. doi: 10.1002/aic.690470506

Degaleesan, S., Dudukovic, M., & Pan, Y. (2001). Experimental study of gas-induced liquid-flow structures in bubble columns. *Aiche Journal, 47*(9), 1913-1931. doi: 10.1002/aic.690470904

Doucet, J., Bertrand, F., & Chaouki, J. (2008a). Experimental characterization of the chaotic dynamics of cohesionless particles: application to a V-blender. *Granular Matter, 10*(2), 133-138. doi: 10.1007/s10035-007-0075-x

Doucet, J., Bertrand, F., & Chaouki, J. (2008b). An extended radioactive particle tracking method for systems with irregular moving boundaries. *Powder Technology, 181*(2), 195-204. doi: 10.1016/j.powtec.2006.12.019

Dube, O., Alizadeh, E., Chaouki, J., & Bertrand, F. (2013). Dynamics of non-spherical particles in a rotating drum. *Chemical Engineering Science, 101*, 486-502. doi: 10.1016/j.ces.2013.07.011

Dube, O., Dube, D., Chaouki, J., & Bertrand, F. (2014). Optimization of detector positioning in the radioactive particle tracking technique. *Applied Radiation and Isotopes, 89*, 109-124. doi: 10.1016/j.apradiso.2014.02.019

Duchanoy, C., & Jongen, T. R. G. (2003). Efficient simulation of liquid-solid flows with high solids fraction in complex geometries. *Computers & Fluids, 32*(10), 1453-1471. doi: 10.1016/S0045-7930(02)00102-0

Godfroy, L., Larachi, F., Kennedy, G., Grandjean, B., & Chaouki, J. (1997). On-line flow visualization in multiphase reactors using neural networks. *Applied Radiation and Isotopes, 48*(2), 225-235. doi: 10.1016/S0969-8043(96)00183-2

Guha, D., Ramachandran, P. A., & Dudukovic, M. P. (2007). Flow field of suspended solids in a stirred tank reactor by Lagrangian tracking. *Chemical Engineering Science, 62*(22), 6143-6154. doi: 10.1016/j.ces.2007.06.033

Guha, D., Ramachandran, P. A., Dudukovic, M. P., & Derksen, J. J. (2008). Evaluation of large eddy simulation and Euler-Euler CFD models for solids flow dynamics in a stirred tank reactor. *Aiche Journal, 54*(3), 766-778. doi: 10.1002/Aic.11417

Guida, A., Nienow, A. W., & Barigou, M. (2011). Mixing of Dense Binary Suspensions: Multi-component Hydrodynamics and Spatial Phase Distribution by PEPT. *Aiche Journal, 57*(9), 2302-2315. doi: 10.1002/Aic.12456

Knoll, G. F. (2010). *Radiation Detection and Measurement*: John Wiley & Sons.

Larachi, F., Cassanello, M., Chaouki, J., & Guy, C. (1996). Flow structure of the solids in a 3-D gas-liquid-solid fluidized bed. *Aiche Journal, 42*(9), 2439-2452. doi: 10.1002/aic.690420905

Larachi, F., Chaouki, J., & Kennedy, G. (1995). 3-D Mapping of Solids Flow-Fields in Multiphase Reactors with Rpt. *Aiche Journal, 41*(2), 439-443. doi: 10.1002/aic.690410226

Larachi, F., Grandjean, B. P. A., & Chaouki, J. (2003). Mixing and circulation of solids in spouted beds: particle tracking and Monte Carlo emulation of the gross flow pattern. *Chemical Engineering Science, 58*(8), 1497-1507. doi: 10.1016/S0009-2509(02000676-0

Larachi, F., Kennedy, G., & Chaouki, J. (1994). A Gamma-Ray Detection System for 3-D Particle Tracking in Multiphase Reactors. *Nuclear Instruments & Methods in Physics Research Section a-Accelerators Spectrometers Detectors and Associated Equipment, 338*(2-3), 568-576. doi: 10.1016/0168-9002(94)91343-9

Leadbeater, T. W., Parker, D. J., & Gargiuli, J. (2012). Positron imaging systems for studying particulate, granular and multiphase flows. *Particuology, 10*(2), 146-153. doi: 10.1016/j.partic.2011.09.006

Lin, J. S., Chen, M. M., & Chao, B. T. (1985). A novel radioactive particle tracking facility for measurement of solids motion in gas fluidized beds. *Aiche Journal, 31*(3), 465-473. doi: 10.1002/aic.690310314

Link, J. M., Deen, N. G., Kuipers, J. A. M., Fan, X., Ingram, A., Parker, D. J., . . . Seville, J. P. K. (2008). PEPT and discrete particle simulation study of spout-fluid bed regimes. *Aiche Journal, 54*(5), 1189-1202. doi: 10.1002/Aic.11456

Mankad, S., & Fryer, P. J. (1997). A heterogeneous flow model for the effect of slip and flow velocities on food steriliser design. *Chemical Engineering Science, 52*(12), 1835-1843. doi: 10.1016/S0009-2509(97)00028-6

Mostoufi, N., & Chaouki, J. (2004). Flow structure of the solids in gas-solid fluidized beds. *Chemical Engineering Science, 59*(20), 4217-4227. doi: 10.1016/j.ces.2004.06.006

Mostoufi, N., Kennedy, G., & Chaouki, J. (2003). Decreasing the sampling time interval in radioactive particle tracking. *Canadian Journal of Chemical Engineering, 81*(1), 129-133.

Ng, B. H., Kwan, C. C., Ding, Y. L., Ghadiri, M., Fan, X. F., & Parker, D. J. (2008). Granular flow fields in vertical high shear mixer granulators. *Aiche Journal, 54*(2), 415-426. doi: 10.1002/Aic.11389

Parker, D. J., Broadbent, C. J., Fowles, P., Hawkesworth, M. R., & McNeil, P. (1993). Positron emission particle tracking-a technique for studying flow within engineering equipment. *Nuclear Instruments & Methods in Physics Research, Section A (Accelerators, Spectrometers, Detectors and Associated Equipment), A326*(3), 592-607. doi: 10.1016/0168-9002(93)90864-E

Roy, S., Kernoun, A., Al-Dahhan, M. H., & Dudukovic, M. P. (2005). Experimental investigation of the hydrodynamics in a liquid-solid riser. *Aiche Journal, 51*(3), 802-835. doi: 10.1002/Aic.10447

Roy, S., Larachi, F., Al-Dahhan, M. H., & Dudukovic, M. P. (2002). Optimal design of radioactive particle tracking experiments for flow mapping in opaque multiphase reactors. *Appl Radiat Isot, 56*(3), 485-503. doi: 10.1016/s0969-8043(01)00142-7

Sherritt, R. G., Chaouki, J., Mehrotra, A. K., & Behie, L. A. (2003). Axial dispersion in the three-dimensional mixing of particles in a rotating drum reactor. *Chemical Engineering Science, 58*(2), 401-415. doi: 10.1016/S0009-2509(02)00551-1

Tsoulfanidis, N., & Landsberger, S. (2011). *Measurement and Detection of Radiation*: CRC Press.

Xu, S. K., Qu, Y. H., Chaouki, J., & Guy, C. (2005). Characterization of homogeneity of bubble flows in bubble columns using RPT and fibre optics. *International Journal of Chemical Reactor Engineering, 3*.

Yang, Z., Fan, X., Bakalis, S., Parker, D. J., & Fryer, P. J. (2008). A method for characterising solids translational and rotational motions using Multiple-Positron Emission Particle Tracking (Multiple-PEPT). *International Journal of Multiphase Flow, 34*(12), 1152-1160. doi: 10.1016/j.ijmultiphaseflow.2008.06.002

CHAPTER 5   ARTICLE 2: INVESTIGATING THE DYNAMICS OF CYLINDRICAL PARTICLES IN A ROTATING DRUM USING MULTIPLE RADIOACTIVE PARTICLE TRACKING

Majid Rasouli, Olivier Dube, Francois Bertrand, Jamal Chaouki[2]

Department of Chemical Engineering, École Polytechnique de Montréal, P. O. Box 6079, Succ. Centre-ville, Montréal, QC, Canada, H3C 3A7

5.1 Abstract

The behavior of granular flows inside rotating drums is an ongoing area of research. Only a few studies have investigated non-spherical particles despite the fact that particle shape is known to have a significant impact on flow behavior. In addition, the experimental techniques limit the interpretation of the results of these studies. In this work, we compared the flow behavior of cylindrical and spherical particles using the multiple radioactive particle tracking (MRPT) technique to capture the positions and orientations of cylindrical particles simultaneously. We analyzed two important components of the transverse flow dynamics, that is, the boundary between the active and passive layers, and the velocity profile on the free surface. For the cylindrical particles, two general models are proposed to calculate the velocity profiles on the free surface and the effective particle sizes in the active and passive layers.

Keywords: Multiple Radioactive Particle Tracking, solids mixing, rotating drum, cylindrical particle

5.2 Introduction

Rotating drums are widely used to process granular materials in the chemical, pharmaceutical, metallurgical, food-processing, polymer, and waste treatment industries, among others, for applications such as mixing, size reduction, sintering, coating, heating, cooling, drying, and

---

Correspondence concerning this article should be addressed to F. Bertrand at francois.bertrand@polymtl.ca or J. Chaouki at jamal.chaouki@polymtl.ca.

chemical reactions. This broad array of applications is made possible by the ability of rotating drums to handle heterogeneous feedstock and to ensure satisfactory mixing and heat transfer of the solid phase (Boateng, 1998; Descoins et al., 2005; Dube et al., 2013). In particular, since the flow dynamics of particles determines the mass and heat transfer rates, it plays a critical role in controlling and/or limiting many of the processes mentioned above (Heydenrych et al., 2002; Liu et al., 2006; Mellmann et al., 2004). The optimal design and operation of rotating drums requires in-depth fundamental knowledge of the phenomena that occur inside them, including the transverse flow that controls primary effects such radial particle movement and particle mixing and/or segregation, as well as secondary effects such as bed temperature, reaction rates, and the rate of axial particle movement (Boateng & Barr, 1997). It is thus essential to study the transverse flow of particles to understand thoroughly the flow dynamics of particles in a rotating drum.

While the concept of rotating drums is simple, the movement of solids in these devices is rather complex. For example, for a given system, different flow regimes occur at different rotational speeds (Ding et al., 2002; Meier et al., 2007). Based on the work of Mellmann (2001), flows take the form of sliding, avalanching (surging), slumping (continuous avalanching), rolling, cascading, cataracting, and centrifuging regimes as the rotational speed increases (Mellmann, 2001). In industrial operations, rotating drums are mainly using in the rolling regime since this regime provides superior solids mixing and heat transfer (Dube et al., 2013; Fantozzi et al., 2007; Liu et al., 2006). The rolling regime is characterized by two regions: a thin, flat, rapidly flowing layer, the so-called active layer, that flows with a dynamic repose angle (β_d) with respect to the horizontal plane, and a thick layer underneath this active layer, the so-called passive layer, that undergoes a solid body rotation with the drum (Figure 5.2). At the upstream end, the particles leave the passive layer and enter the active layer. At the downstream end, the flow reverses (Alizadeh et al., 2014; Meier et al., 2007). Since particles in the passive layer undergo a solid body rotation, mixing and segregation mostly occur in the active layer where the particles can have different speeds with respect to each other (Cheng et al., 2011; Ingram et al., 2005). As such, characterizing the active layer is of primary importance. In particular, the dynamic repose angle is a distinct aspect of the active layer that depends on the properties of the rotating drum, including its dimensions, end-wall effects, and rotational speed as well as on the properties of the particles such as size, surface roughness, and shape (Meier et al., 2007). If the properties of the particles change during a process such as pyrolysis, sintering, combustion or incineration, it

becomes much more difficult to characterize the flow behavior because it may be affected by other phenomena.

The opaque nature of granular materials makes studies of such materials tedious and cumbersome. Studies on the flow behavior of particles in rotating drums have been performed using a wide variety of techniques, including fiber optic probes (Boateng & Barr, 1997), particle image velocimetry (PIV) (Alexander et al., 2002; Felix et al., 2002, 2007; Jain et al., 2002, 2004; Jain et al., 2005; Kalbag et al., 2008; Santomaso et al., 2003), laser doppler velocimetry (LDV) (Longo & Lamberti, 2002), in situ bed freeze (Wightman & Muzzio, 1998a, 1998b), magnetic resonance imaging (MRI) (Hill et al., 1997; Kawaguchi, 2010; Nakagawa et al., 1993), positron emission particle tracking (PEPT) (Ding et al., 2001; Ingram et al., 2005; Parker et al., 1997), and radioactive particle tracking (RPT) (Alizadeh et al., 2014; Alizadeh, Dube, et al., 2013; Dube et al., 2013; Sheritt et al., 2003). However, most of these studies used spherical or nearly spherical particles.

Investigations of non-spherical particles are very important since these particles usually have irregular shapes (sand, ore, and limestone grains, for example) and since they have many uses (biomass pellets, capsules, rice, candy, etc.) and, more importantly, since the shape of these particles affects their flow behavior (Dube et al., 2013; Ridgway & Rupp, 1971; Woodle & Munro, 1993) in terms of shear resistance, dilation under shear, compaction efficiency, transfer of momentum between translational and rotational movements, and their ability to form arches and block the flow (Cleary, 2010; Dube et al., 2013). Studies on the flow behavior of non-spherical particles such as limestone grains (Boateng & Barr, 1997; H. Henein et al., 1985), sand (H. Henein et al., 1985; Ingram et al., 2005), rice grains (Boateng & Barr, 1997), gravel (H. Henein et al., 1985), shale (Van Puyvelde et al., 2000), and tablets (Tobiska & Kleinebudde, 2003; Wilson & Crossman, 1997), as well as wooden ovoid, shell, and tube particles (Woodle & Munro, 1993) in rotating drums have provided useful information on the flow behavior of such non-spherical particles. However, the results of these studies are limited by the objectives and the inability to single out the effect of a given particle shape, or the experimental technique. For instance, Dube et al. (2013) used the RPT technique to capture the flow dynamics of non-spherical tablets in a rotating drum and concluded that tablets with an aspect ratio exceeding 2 had a significantly different flow behavior than spherical particles. They reported that the axial dispersion coefficient of non-spherical tablets was lower than that of spherical tablets due to their higher degree of

spatial orientation in the active layer. However, the standard RPT technique cannot capture the orientation of particles. Consequently, we developed the MRPT technique to be able to capture the positions and orientations of cylindrical particles at any time (see Rasouli et al. (2015) for more details (Rasouli, Bertrand, & Chaouki, 2015)).

The goal of the present study was to compare the flow behavior of spherical and cylindrical particles in a rotating drum. We used the RPT technique to determine the positions of the spherical particles over time, and the MRPT technique (Rasouli et al., 2015) to determine the positions and orientations of the cylindrical particles at any time, and thus calculate the essential components of the transverse flow dynamics of particles in this rotating drum, that is, the boundary between the active and passive layers and the velocity profile on the free surface. We developed two general models to calculate these components.

5.3 Methodology

The reliability and validity of results depend greatly on the technique used. Since the goal of the present study was to characterize flow behavior, it was essential to use a non-intrusive measurement technique. As mentioned previously, optical techniques such as LDV and PIV and radioactive techniques such as RPT, MRI, and PEPT have been used to study particle flows in rotating drums. Since particles are usually opaque, optical techniques are essentially limited to measuring surface flows on the side-wall of the drum and on the bed surface, which are biased due to the end-wall effect and are limited to two-dimensional systems, respectively. On the other hand, radioactive techniques are well suited for providing information on the interior of the bed because gamma rays can penetrate materials relatively easily. RPT setups have the advantage of being compact, flexible, and inexpensive compared to PEPT and MRI. On the other hand, it is not easy to use RPT in systems with irregular moving boundaries (Doucet et al., 2008b). However, we decided to use the RPT technique to study the flow behavior of spherical particles since rotating drums have simple moving boundaries. While RPT can track the positions of particles, it cannot provide information on the orientations of non-spherical particles, which is crucial for studying the flow behavior of cylindrical particles. We thus used the MRPT technique to study the flow behavior of such cylindrical particles.

5.3.1 RPT and MRPT techniques

RPT noninvasively tracks the position of a single radioactive tracer over time and can thus be used to study the flow dynamics of a variety of systems. A labeled tracer particle, a data acquisition system (detectors, amplifiers/discriminators, and high-speed counters), and a location algorithm are used to calculate the position of the tracer, as shown in Figure 5.1 for granular flows in a rotating drum (for more details, see references (Dube et al., 2013; Larachi et al., 1994; Rasouli et al., 2015; Tsoulfanidis & Landsberger, 2011)).
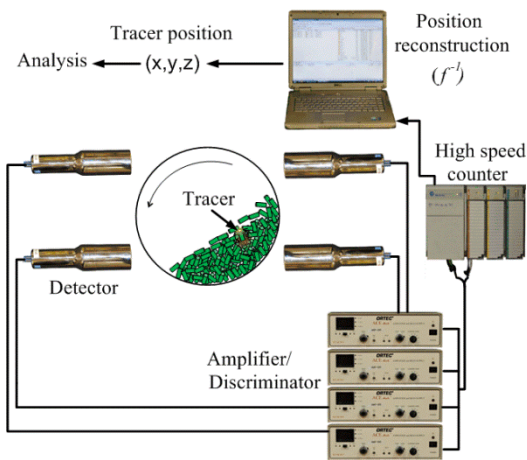
Figure 5.1: RPT setup in a rotating drum Rasouli et al. (2015)

We used two different tracer particles, ^{64}Sc for cylindrical and ^{24}Na for spherical particles. We explain why we used these two isotopes in the Experimental section.

While the MRPT technique can simultaneously track two tracers that move freely (free MRPT) or that remain at a fixed distance from each other (restricted MRPT), it uses the same basic setup as RPT (see Figure 5.1), with two main differences. First, it uses two radioactive sources (source A and source B) with the same isotope that are inserted into two different tracer particles (free MRPT) or into a single tracer particle (restricted MRPT; at both ends of a single cylindrical particle). Second, it uses a different location algorithm since the gamma rays measured by the acquisition system come from two different radioactive sources (see Rasouli et al. (2015) for more details).

Since we wanted to study cylindrical particles, we used the restricted MRPT technique, with one source fixed at one end of a cylindrical particle and the other source fixed at the opposite end of

the particle (the rod-like tracer). The position of the middle of the rod-like tracer was calculated by averaging the positions determined for sources A and B. The orientation of the rod-like tracer was equal to the orientation of the line passing through the positions determined for sources A and B.

5.4 Experimental

The experiments were conducted using a 24.13-cm diameter, 35.56-cm long, 16.3-L acrylic rotating drum. A single filling fraction (35vol%) was used for all the experiments. Two different particle shapes were chosen for the study: spherical (6-mm glass beads) and cylindrical (6-mm-diameter, 2-cm-long acrylic particles). We decided to study cylindrical particles because of the many industrial applications for such particles, including manufacturing capsules, candies, and biomass pellets. Since we also wanted to determine the effect of particle shape on flow behavior, we needed a readily identifiable shape that was not spherical. The cylinder is one of the most basic curvilinear geometric shapes. In addition, many shapes, especially those with a high aspect ratio, can be approximated as cylinders, including ovoid and bottle-shaped candies. We used 2-cm-long cylindrical particles because, in order to have reliable measurement, the current MRPT technique is limited to a lower threshold of 2 cm between the radioactive sources (Rasouli et al., 2015).

The tracer should have the same physical properties (size, shape, weight, etc.) as the particles being studied to ensure reliable and valid RPT and MRPT measurements. Scandium (^{64}Sc, half-life ~85 days) is generally preferred to sodium (^{24}Na, half-life ~15 h) due to its longer half-life. However, we used ^{24}Na for the spherical tracer because the glass beads contained sodium, which was activated in the Slowpoke reactor of École Polytechnique de Montreal. This ensured that the glass bead tracer had the same physical properties as the other glass beads. To make the rod-like tracer, two tiny holes were drilled in the center of each end of a cylindrical particle. A tiny radioactive scandium metal sheet ($1 \times 1 \times 0.2$ mm^3) was placed in each of the holes and was fixed in place with glue, making sure that the surface remained flat. This ensured that the rod-like tracer had the same size, shape, and weight as the other cylindrical particles (Table 5.1). We used 6-mm-diameter cylindrical particles to make it easier to insert the radioactive scandium metal sheets in the cylinder without changing its physical properties.

The rod-like tracer was used to mimic the motion of the cylindrical particles. With this type of particle and a 35vol% fill level, the rolling regime starts at approximately 5 RPM and stops at approximately 15 RPM. The drum was thus operated at five different rotational speeds (5, 7.5, 10, 12.5, and 15 RPM) that covered the entire rolling regime used in most applications. To compare the flow behavior of the cylindrical and spherical particles, one RPT test with the glass beads was performed at 10 RPM and a 35vol% fill level. To avoid saturation of the detectors, the activity of the tracer should be less than 70 µCi for our system. The two sources of the rod-like tracer were activated at 32 µCi and the glass bead tracer was activated at 60 µCi. Thirteen 76 mm × 76 mm NaI (Tl) scintillation detectors (Teledyne Isotope S-1212-I) were positioned around the setup. Each detector was connected to a scintillation tube, and the signal was amplified and discriminated using an ORTEC ACE Mate amplifier/discriminator (925-Scint).

Table 5.1: Material properties

	Shape	Length [cm]	Diameter [cm]	Isotope	Weight [g]	Material
Particles	cylinder	2.0 ± 0.2	0.6	---	0.77	acrylic
	sphere	---	0.6	---	0.3	class
Tracer	cylinder	2.0 ± 0.0	0.6	^{64}Sc	0.77	acrylic, scandium
	sphere	---	0.6	^{24}Na	0.3	glass
Drum	cylinder	35.5	24.1	---	---	acrylic

5.5 Results and Discussion

After a detailed analysis of the data, we will present the two aspects of the flow dynamics inside that rotating drum that were most affected by the shape of the particles. We will thus present and analyze the boundary between the active and passive layers as well as the velocity profile on the free surface after describing some primary parameters (the dynamic repose angle, the dynamic filling fraction, and the rotational speed of the bed of particles). Figure 5.2 presents a schematic

cross-sectional view of the drum operating in the rolling regime as well as the variables used. As can be seen, the bed consisted of active and passive layers. In the boundary between the two layers, the two curved lines are defined as the yield line $\delta(x)$ (Boateng & Barr, 1997) and the turning point line (Alizadeh, Dube, et al., 2013) $\alpha(x)$, which are shown in Figure 5.2b. The yield line is defined as the interface that separates the solid body rotation region from the other region, while the turning point line is defined as the point where the direction of the streamwise velocity [$u(x, y)$], changes [$u(x, y) = 0$]. δ_0 and α_0 give the depth of the active layer based on the yield or the turning point line at $x = 0$, respectively.The area between the two curved lines is the transition region. While this region is frequently neglected because of its relatively small size (Khakhar, McCarthy, Shinbrot, et al., 1997), we took this boundary into consideration. Table 5.2 lists the variables displayed in Figure 5.2.

(a)   (b)
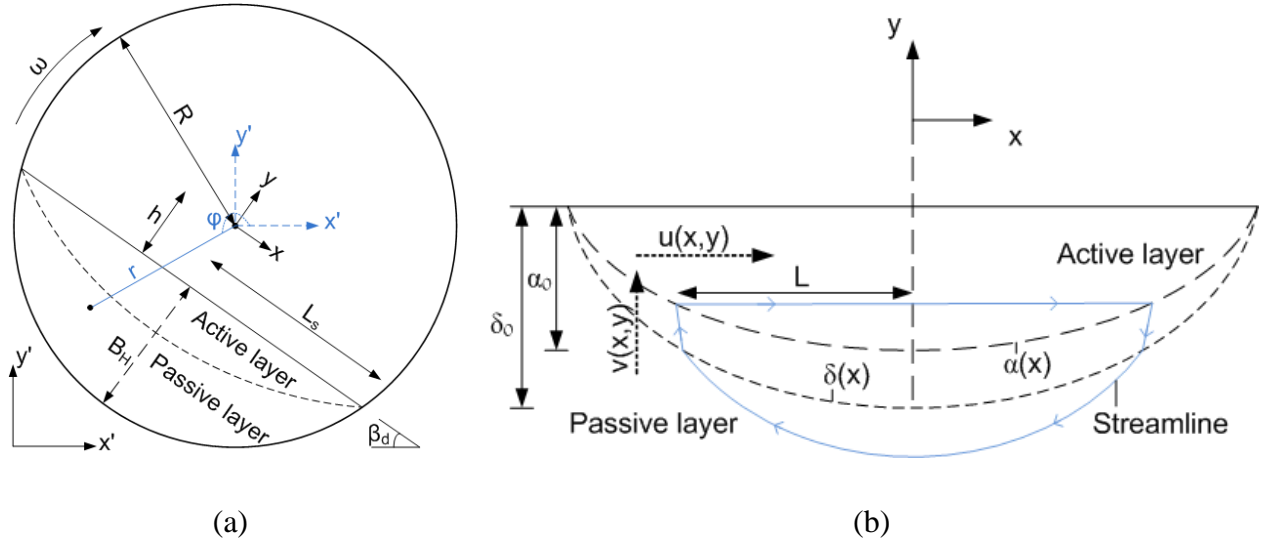
Figure 5.2: (a) Cross-sectional view of the rotating drum and (b) a close-up of the active layer.

Table 5.2: Definition of the variables

Variable	Definition
x	Streamwise direction [cm]
y	Transverse direction [cm]
u	Streamwise velocity [cm/s]
v	Transverse velocity [cm/s]
R	Drum radius [cm]
h	Normal distance between the center of the bed surface and the center of the drum [cm]
L_s	Half-length of the bed surface [cm]
L	Half-length of a streamline in the active layer [cm]
β_d	Dynamic repose angle [deg]
ω	Angular velocity [rad/s]
B_H	Bed height at x=0 [cm]
r	Radial distance [cm]
φ	Azimuth angle [deg]

In our conditions, the RPT technique tracked the position of the spherical tracer with an accuracy of 2.5 mm and a precision of 2.0 mm, while the MRPT technique tracked the orientation and position of the mid-point of the rod-like tracer with an accuracy of 6 degrees and 2.0 mm, and a precision of 10 degrees and 2.5 mm, respectively. Certain circular movements were created by fixing the tracers at different known radii while the drum was rotating to verify the accuracy and precision of the measurement techniques. The tracer speed was calculated as the time derivative of its position. Since the RPT and MRPT techniques track tracers in a Lagrangian manner, the

domain (2D transverse plane) was discretized into cells and the data were converted into Eulerian data (Alizadeh, Dube, et al., 2013). Given the accuracy of the results, the cell size was set at 2.5 x 2.5 mm^2. To avoid the end-wall effect, only data with an axial position within 20 cm of the center of the drum were taken into consideration. Each experiment lasted at least 3 h and used a 10-ms sampling time. This gave enough data points (between 200 and 1400 data points for each cell) for statistically relevant measurements.

5.5.1 Primary parameters

The flow behavior of the cylindrical particles was markedly different from that of the spherical particles. Among the parameters of interest in granular rheology are the static and dynamic repose angles. The static repose angle was obtained by measuring the angle between the horizontal plane and the free surface of the particles when the drum stopped rotating. The dynamic repose angle was calculated from the RPT or MRPT results using the velocity field (Figure 5.3). To obtain the velocity field in a x'y' transverse plane (see Figure 5.2), the tracer speeds in each cell were averaged regardless of the tracer position along the z axis. The method used by Dube et al. (2013) was applied here to calculate the dynamic repose angle. The mean values of the angles between the horizontal plane and the velocity vectors in the x'y' plane, for vectors belonging to $-5.0 \leq x \leq +5.0$ and $-(h + 0.5) \leq y \leq -h$, were considered as the dynamic repose angles. Table 5.3 lists the dynamic and static repose angle values. In this table, the uncertainties correspond to the standard deviations of the data measured on the transverse plane. As can be seen, the dynamic and static repose angles for the cylindrical particles were significantly higher than for the spherical particles, as previously reported by Dube et al. (2013) and Boateng et al. (1997) The dynamic repose angle is a measure of the ability of a particle lattice structure to transmit shear loads. Cylindrical particles can make stable structures that resist shear better than spherical particles. To overcome this higher resistance, more shear has to be applied to the bed of cylindrical particles using a higher repose angle. The difference between the dynamic and static repose angles of the cylindrical particles was much higher than those of the spherical particles. This is likely due to the stable structures formed by cylindrical particles once the bed becomes static. Shear resistance depends on how the particles are oriented when they form local structures. The non-isotropic shape of the cylindrical particles would explain the wider variation in the repose angles. During the 5-RPM run, the cylindrical particles displayed a mixed behavior

of rolling and avalanching regimes. The particles flowed continuously on the free surface while a thin layer of the particles periodically avalanched downward (slumping regime). Since the 5-RPM run was not a pure rolling regime, it was excluded from the rest of the analysis.

The filling fraction, which was calculated from the bed height at $x = 0$, B_h, (Table 5.3), could also be obtained from the velocity field. Note that the static filling fraction of the bed was 35vol%. The values obtained clearly showed that significant bed dilation occurred with the moving cylindrical particles, as reported previously by Dube et al. (2013) and Cleary (2010) (Cleary, 2010). More precisely, a bed dilation of more than 25% was observed for the cylindrical particles at all rotational speeds. The structures formed by the dynamic and static cylindrical particles were notably different due to the bed dilation and resulted in a larger difference between their dynamic and static repose angles. Table 5.3 also shows that there was a relatively constant filling fraction ($\sim$45%) for the cylindrical particles at different rotational speeds (from 7.5 to 15 RPM). An explanation as to why a constant filling fraction for the cylindrical particles was obtained is provided in the section discussing the orientations of the particles.

Lastly, it is also important to measure the rotational speed of the bed of particles in the passive layer (Table 5.3). To adequately evaluate the rotational speed of the bed, the velocity vectors satisfying $0.8R \leq r$ and $215^\circ \leq \varphi \leq 235°$ were taken into consideration to calculate the angular velocity of the bed (Figure 5.2). Selecting this region ensured that the data used for this calculation came from the passive layer. The rotational speed of the bed of spherical particles was slightly lower than that of the drum due to the lack of friction between the bulk of particles and the wall of the drum (Dube et al., 2013). It can also be observed that rotational speed of the bed of cylindrical particles systematically slightly higher, which is a priori surprising. This can however be attributed to the measurement uncertainties related to MRPT technique and the fact that the drum rotational speed could only be raised by 0.5 RPM steps.

Table 5.3: Primary parameters

Rotational speed [RPM]	Static repose angle [deg]	Dynamic repose angle [deg]	Filling fraction [%]	Bed dilation [%]	Rotational speed of the bed of particles [RPM]
Cylindrical particles					
0	34.9 ± 2.3	---	35.3 ± 0.9	0.0	---
5	34.9 ± 2.3	45.8 ± 1.4	42.4 ± 0.2	20.1	5.5 ± 0.6
7.5	34.9 ± 2.3	43.6 ± 1.5	44.5 ± 0.5	26.0	8.0 ± 1.1
10	34.9 ± 2.3	43.5 ± 2.0	44.7 ± 0.5	26.6	10.2 ± 1.3
12.5	34.9 ± 2.3	42.2 ± 3.2	45.0 ± 0.6	27.4	12.6 ± 1.3
15	34.9 ± 2.3	42.2 ± 4.3	45.4 ± 0.4	28.6	15.2 ± 1.4
Spherical particles					
0	25.1 ± 1.2	---	34.9 ± 0.8	0.0	---
10	25.1 ± 1.2	26.8 ± 0.7	35.5 ± 0.3	1.1	9.7 ± 0.3

5.5.2 Velocity profile

Figure 5.3 shows the velocity fields for the spherical and cylindrical particles at 10 RPM. As can be seen, the flow behaviors of the two types of particles were significantly different in terms of dynamic repose angle and bed dilation. In addition, the velocity vectors of the cylindrical particles had a slightly different pattern than those of the spherical particles in the region where the free surface reached the wall of the drum at the downward extremity of the free surface. This can be explained by the fact that collisions between high-speed and low-speed particles in the downward extremity of the free surface often results in the jump of a few cylindrical particles (Rasouli et al., 2015).
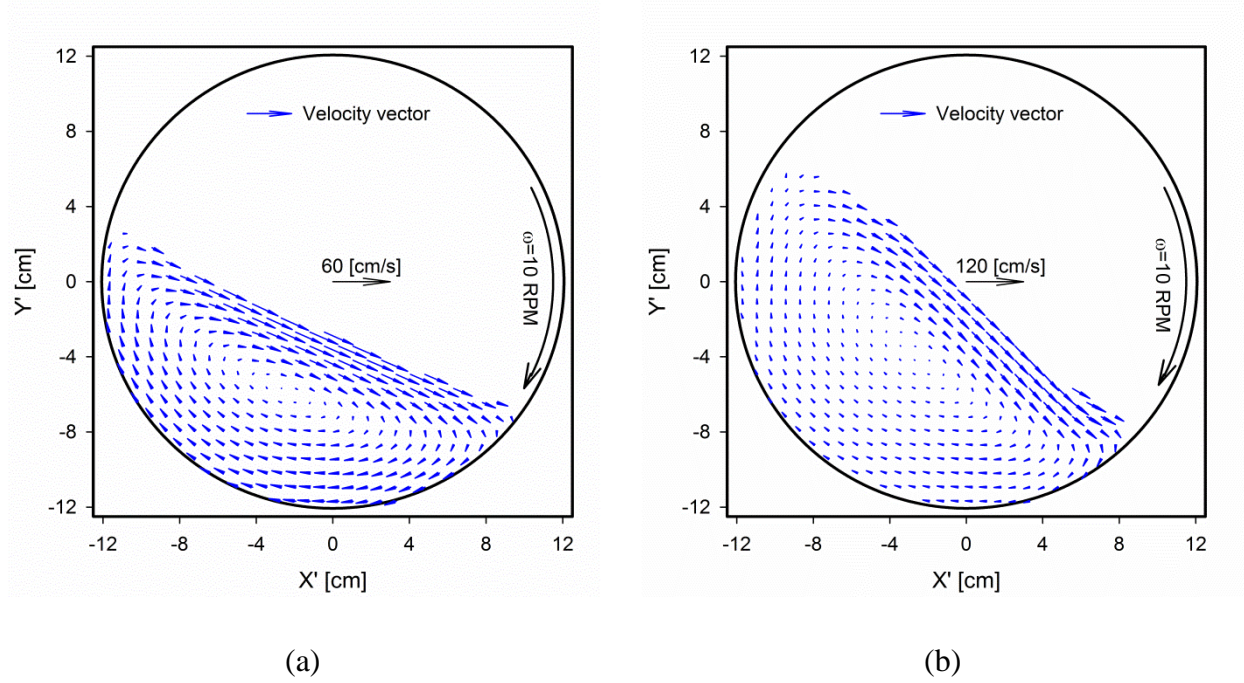
Figure 5.3: Velocity vectors for (a) spherical and (b) cylindrical particles at a rotational speed of 10 RPM

Despite the differences between the two velocity fields, they were similar in that the flows of the cylindrical and spherical particles both consisted of active and passive layers, which is characteristic of a rolling regime. Hence, to compare their flow dynamics for quantitative and modeling purposes, the passive and active layers should both be analyzed. As mentioned before, our comparison will focus on the two components of the flow dynamics that differ the most for the spherical and cylindrical particles. Consequently, the two following sections will present the dynamics of the boundary between the active and passive layers, and the streamwise velocity profile on the free surface.

5.5.3 Boundary between the active and passive layers

Mixing, segregation and heat transfer in the solid phase mostly occur in the active layer where particles can have different speeds with respect to each other (Alizadeh, Dube, et al., 2013; Cheng et al., 2011; Dube et al., 2013; Ingram et al., 2005). As such, modeling and calculating the extent of the active layer is essential for assessing the degree of such phenomena. Several correlations have been proposed to calculate the thickness of the active layer (Alizadeh, Dube, et

al., 2013; Ding et al., 2001; Liu et al., 2006; Meier et al., 2007; Mellmann et al., 2004; A. V. Orpe & Khakhar, 2001). These correlations mainly rely on the operating conditions, the geometrical properties of the system, and the properties of the particles to calculate the thickness of the active layer based on the yield line or the turning point line (Alizadeh, Dube, et al., 2013; Dube et al., 2013). In the present study, we used the MRPT and RPT results to obtain the two boundary lines and then compared them with the predictions of several correlations proposed in the literature.

The boundary line was obtained based on the points where the tracer entered or exited the active or passive layer and, as such, their trajectories. Figure 5.4a and b show the trajectories of the spherical and rod-like tracers in two different tracer cycles obtained using the RPT and MRPT techniques, respectively.

Based on the definition of the turning point, the exit points from the active layer were the points where the streamwise velocity of the tracer changed from a positive to a negative value, and the reverse for the entry points (the blue triangles in Figure 5.4). Note that these entry and exit points were a bit noisy because the turning point lines were slightly different for the different cycles and because of measurement uncertainty. The turning point line, which was calculated by smoothing these entry and exit points, is depicted in Figure 5.4 as a blue dashed line.

(a) (b)

Figure 5.4: The yield line and turning point line based on the streamwise and angular velocities for (a) the spherical and (b) the cylindrical particles at a rotational speed of 10 RPM. The tracer trajectories within two different cycles are shown.

The yield line can be obtained using the tracer trajectories and their instantaneous angular velocity ($d\varphi/dt$). The tracer is considered to be in the passive layer if its angular velocity is equal to that of the drum (ω as calculated in Table 5.3). Note that, due to measurement uncertainty, the angular velocities obtained were slightly noisy. Consequently, using $d\varphi/dt = \omega$ led to a non-continuous trajectory in the passive layer during one cycle. To overcome this problem, a threshold of 20% was considered, which means that any point that met the $d\varphi/dt < 0.8\omega$ condition was considered to be in the passive layer. Based on this criterion, the entry and exit points of the passive layer (the green diamond points in Figure 5.4) were obtained, and the yield line was calculated by smoothing them (the green dashed line in Figure 5.4).

Ingram et al. (2005) used the angular velocity ($d\varphi/dt$) instead of the streamwise velocity of the tracer to calculate the turning point line (the red square points in Figure 5.4) (Ingram et al., 2005). The turning point line based on the angular velocity was obtained by smoothing these entry, and exit points and is displayed in Figure 5.4 as a red dashed line. Ingram et al. (2005) claimed that the turning point line based on the angular velocity would lie somewhere between the yield line and the turning point line based on the streamwise velocity (Ingram et al., 2005). However, Figure 5.4 clearly shows that, for the present work, the turning point line based on the angular velocity is located above the turning point line based on the streamwise velocity. This is shown in Figure 5.4 as blue and red solid lines. They are drawn from the center of the drum to the entry points to the active layer, where the blue triangle point (based on the streamwise velocity) and the red square point (based on the angular velocity) can be seen. The trajectories of the tracers from the green diamond point to the blue triangle point (u and $d\varphi/dt$) are both negative, whereas from the blue triangle point to the red square point, u is positive while $d\varphi/d$ remains negative. This can be explained by the fact that, even though the streamwise velocity became positive after the blue triangle point, the transverse velocity (v) contributed to reducing angle φ. Hence, the change in angle φ depended on the ratio of the streamwise to the transverse velocity. This may explain why the two turning point lines overlap each other in a small region around the center

point ($x = 0$) and why the (red) turning point line based on the angular velocity approaches the free surface faster than the (blue) turning point based on the streamwise velocity when the distance from the center point increases.

Other correlations have been proposed to calculate the yield and/or turning point lines. These correlations often use physical parameters that are difficult to measure experimentally, including the angle between the horizontal plane and the yield line (Alizadeh, Dube, et al., 2013; A. V. Orpe & Khakhar, 2001), the angle between the free surface and the turning point line at the wall of the drum(Liu et al., 2006), and the maximum velocity at the surface (Khakhar, McCarthy, & Ottino, 1997). Note that the angle between the horizontal plane and the yield line at $x = 0$ is equal to the dynamic repose angle. The correlation containing this parameter can thus be used to calculate the depth of the active layer at $x = 0$. Mellmann et al. (2004) proposed a correlation to calculate the angle between the free surface and the turning point line at the wall of the drum based on the radius and rotational speed of the drum, the dynamic repose angle, and the filling fraction.

Table 5.4: Values of the turning point line-based active layer thickness (α_0) at $x = 0$

Rotational speed [RPM]	Measured α_0 ($u = 0$) [cm (%)[a]]	Measured α_0 ($d\varphi/dt = 0$) [cm (%)[a]]	Liu et al. (2006) [cm (%)[a]]	Alizadeh et al. (2013) [cm (%)[a]]
Spherical particles				
10	3.6 (38)	3.6 (38)	1.7 (19)[b]	3.9 (41)[b]
Cylindrical particles				
7.5	2.8 (27)	2.8 (27)	2.9 (28)[b], 3.6 (34)[c] 3.4 (32)[d]	2.3 (22)[b], 3.0 (29)[c] 2.8 (27)[d]
10	3.0 (28)	3.0 (28)	3.2 (30)[b], 4.0 (39)[c] 3.7 (35)[d]	2.6 (25)[b], 3.4 (33)[c] 3.1 (30)[d]
12.5	3.1 (30)	3.1 (30)	3.5 (34)[b], 4.7 (45)[c] 4.2 (40)[d]	2.9 (28)[b], 3.8 (36)[c] 3.4 (33)[d]
15	3.3 (32)	3.3 (32)	4.2 (40)[b], 6.1 (59)[c] 5.1 (49)[d]	3.1 (29)[b], 3.9 (38)[c] 3.5 (34)[d]
Average error (%)	---	---	12[b], 50[c] 32[d]	10[b], 15[c] 6[d]

[a] The percentage of bed depth; [b] 6-mm particle size, [c] 20-mm particle size, and [d] 12-mm particle size were used in the calculations.

The values for α_0, the active layer thickness based on streamwise and angular velocities, are presented in Table 5.4 and are compared to those obtained using the models proposed by Liu et al. (2006) and Alizadeh et al. (2013). While the measured turning point lines based on the streamwise and angular velocities are different, it can be seen that similar values for α_0 were measured. The turning point line based on angular velocity is thus valid for calculating α_0 but not for calculating the boundary line (see Figure 5.4). For the cylindrical particles, α_0 and the percentage of bed depth occupied by the active layer were increased by increasing the rotational

speed, which is in agreement with the predictions of the two models. Table 5.4 also shows that α_0 and this percentage for the cylindrical particles were 6 mm and 10% less, respectively, than those for the spherical particles at the same rotational speed (10 RPM). At first glance, this means that the bed of cylindrical particles is less efficient than the bed of spherical particles. On the other hand, the two models predict that these values would increase by increasing the particle size. The models also predict that α_0 would increase when the filling fraction is increased, while the percentage of the bed occupied by the active layer would decrease. Since the size and the filling fraction of the cylindrical particles in our experiments were larger than that of the spherical particles, there is then a prioir a contradiction between our results and the correlations. The fact that the dynamic and static repose angles for the cylindrical and spherical particles were different (see Table 5.3) may explain why there are discrepancies between the predicted and the measured values. Another possibility would be to use in the models an apparent size for the cylindrical particles in order to bring the predicted values into line with the measured values.

Since the cylindrical particles have two distinct dimensional characteristics (diameter and length), two different particle sizes (6 and 20 mm) were used in the correlations. As can be seen in Table 5.4 the correlation proposed by Liu et al. (2006) under-predicts α_0 for spherical particles while it overestimates it for cylindrical particles, for both particle sizes. The correlation of Alizadeh et al. (2013) gives a better prediction of α_0 for both the spherical and cylindrical particles than the correlation proposed by Liu et al. (2006). However, both models provide better predictions when the particle size is set at 6 mm.

Table 5.5: Values of the yield line-based active layer thickness (δ_0) at $x = 0$

Rotational speed [RPM]	Measured δ_0 [cm (%)[a]]	Alizadeh et al. (2013) [cm (%)[a]]	Ding et al. (2001) [cm (%)[a]]	Orpe and Khakhar (2001) [cm (%)[a]]
		Spherical particles		
10	4.6 (49)	4.7 (50)[b]	5.9 (63)[b]	5.2 (55)[b]
		Cylindrical particles		
7.5	3.7 (35)	2.5 (24)[b], 3.3 (32)[c]	6.9 (66)[b], 6.9 (66)[c]	2.7 (26)[b], 3.7 (25)[c]
		3.2 (30)[d]	6.9 (66)[d]	3.5 (34)[d]
10	3.9 (37)	2.9 (27)[b], 3.9 (37)[c]	7.0 (67)[b], 7.0 (67)[c]	3.2 (30)[b], 4.3 (41)[c]
		3.6 (35)[d]	7.0 (67)[d]	4.0 (38)[d]
12.5	4.0 (39)	3.2 (31)[b], 4.4 (42)[c]	6.8 (65)[b], 6.8 (65)[c]	3.6 (34)[b], 4.8 (46)[c]
		4.1 (39)[d]	6.8 (65)[d]	4.5 (43)[d]
15	4.4 (44)	3.4 (32)[b], 4.6 (44)[c]	7.1 (68)[b], 7.1 (68)[c]	3.8 (36)[b], 5.1 (49)[c]
		4.3 (41)[d]	7.1 (68)[d]	4.8 (46)[d]
Average error (%)	---	25[b], 5[c]	73[b], 73[c]	17[b], 11[c]
		6[d]	73[d]	6[d]

[a] The percentage of bed depth; [b] 6-mm particle size, [c] 20-mm particle size, and [d] 16-mm particle size were used for the calculations.

The values measured for δ_0, the active layer thickness based on the yield line, are presented in Table 5.5 and are compared to those obtained using the models developed by Alizadeh et al. (2013), Ding et al. (2001), and Orpe and Khakhar (2001) (A. V. Orpe & Khakhar, 2001). Table 5.5 shows that the value of δ_0 can be increased by increasing the rotational speed, which is in agreement with the predictions of two of the models, but not for the model proposed by Ding et

al. (2001). While this model uses the experimentally measured value of the ratio $\Lambda = \alpha/\delta$, its predictive power is poor. The other two models are based on the model proposed by Makse (1999) (Makse, 1999). The only difference is related to the fitting parameter. The same discussion as for α_0 applies here. Two particle sizes (6 and 20 mm) were used to assess the prediction of the models (we will get back to the 16-mm particle size). When the particle size was set at 6 mm, both models under-predict the yield line depth while their predictions are more accurate when the particle size was set at 20 mm. Unexpectedly, this finding is the opposite of that obtained for the turning point depth, where the 6-mm particle gives a better prediction. Since the models proposed by Alizadeh et al. (2013) show the same trend for both cases (i.e., α_0 and δ_0), this discrepancy cannot be the result of the differences between the assumptions made for the development of the models, but may be the result of the difference between the orientations of the cylindrical particles (same effective particle size) in the active and passive layers.
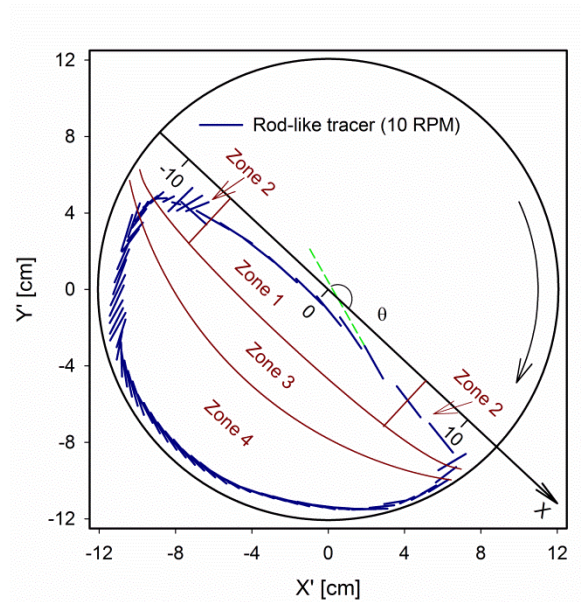
Figure 5.5: Rod-like tracer position and orientation during a single cycle at a rotational speed of 10 RPM.

Figure 5.5 shows the position and orientation of the rod-like tracer measured by the MRPT technique during a single cycle of the tracer. To keep the orientation of the rod-like tracer in the xy plane, angle θ was defined as the angle between the rod-like tracer and the x axis. Note that angle φ (see Figure 5.2) is linked to the position of the tracer while angle θ is linked to the

orientation of the tracer. Figure 5.5 shows that the rod-like tracer was almost aligned with the x axis in the active layer (Zone 1) and that the effective particle size of the cylindrical particles, that is the dimension of the cylindrical particles aligned with their flow direction, was thus equal to their diameter (6 mm). On the other hand, in the passive layer (Zone 4), the rod-like tracer underwent a solid body rotation that gave angle θ a larger value. The effective particle size of the tracer in the passive layer was thus larger than in the active layer. This would explain the contradictory effects of particle size in the calculation of α_0 (related to the turning point line) and δ_0 (related to the yield line) by the models.
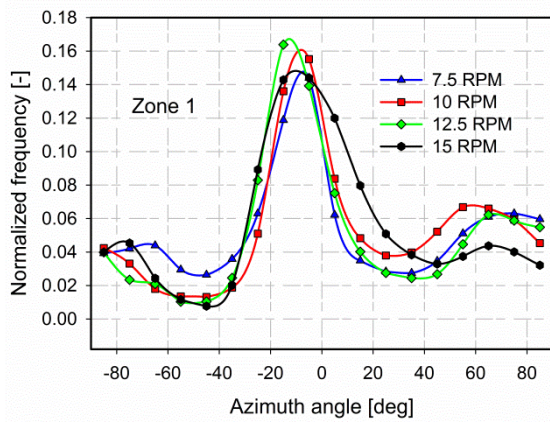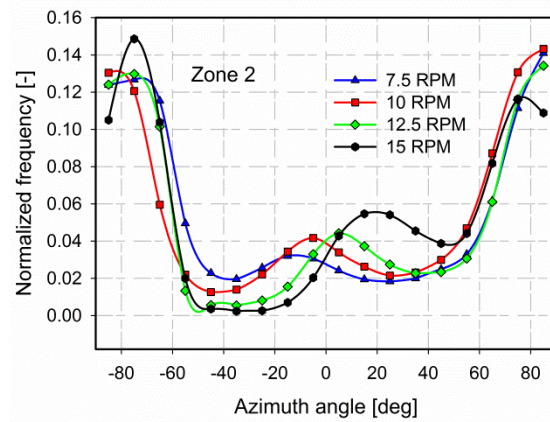
(a)   (b)
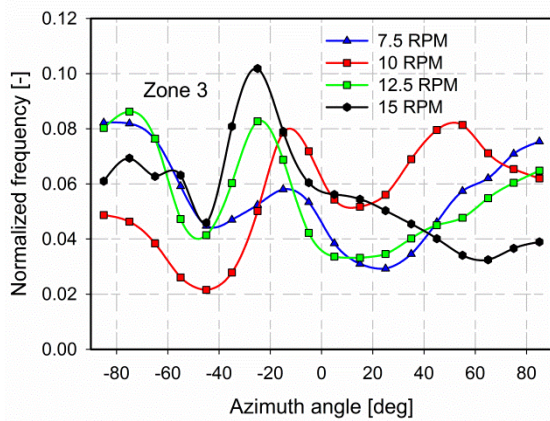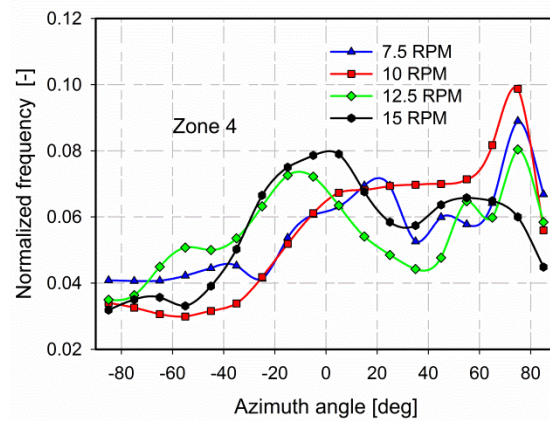
(c)   (d)

Figure 5.6: Distribution of the azimuth angle **θ** of the rod-like tracer located in (a) Zone 1, (b) Zone 2, (c) Zone 3, and (d) Zone 4 (see Figure 5.5 for the zone locations)

Clearly, the rod-like tracer can have a different set of orientations during different cycles. The calculation of the effective particle size based on the distribution of these orientations should thus give better model predictions. The distribution of angle θ was thus calculated for the different zones for the entire duration of an experiment and is shown in Figure 5.6. All four zones (see Figure 5.5) were considered in these calculations, while the values of Zones 1 and 4 were considered in the calculation of the effective particle size for the active and passive layers, respectively. For a given orientation (θ), the effective particle size was approximated by Eq. 5.1, and then considering the distribution of θ for a given zone, the average effective particle size was computed for this zone.

$$Effective\ particle\ size = diameter + (length - diameter) \times |\sin\theta| \qquad 5.1$$

The calculated values for the effective particle size were about 12 and 16 mm for the active and passive layers, respectively, for all rotational speeds. The predictions of the models using these values as well as the particle sizes are indicated in Table 5.4 and 5 with the superscript "d". The model proposed by Liu et al. (2006) overestimates α_0 for the 6- and 20-mm particles (Table 5.4), as it does for the 12-mm particle. The model proposed by Ding et al. (2001) for δ_0 is independent of particle size and the new values do not change the quality of its predictions (Table 5.5). Interestingly, the other models produce better predictions of α_0 and δ_0 using the new values for the particle sizes. In particular, the models proposed by Alizadeh et al. (2013) predict the values of α_0 and δ_0 with the greatest accuracy.

Since particle orientation (and the effective particle size) was shown to have impact on the distribution of the active and passive layers, it would be useful to be able to predict the effective particle size of each zone in a rotating drum containing cylindrical particles of any size. We feel that the orientation presented in Figure 5.6 would be similar to the orientations of cylindrical particles of any size because the shear applied to the particles would align them with the free surface in the active layer. In addition, in Zone 2, downstream (resp. upstream) cylindrical particles have a wider angle in such a way that they can more easily penetrate into the passive (resp. active) layer. Furthermore, in the passive layer, cylindrical particles tend to enter at a wide

angle and, given the effect of the clockwise solid body rotation, the angle decreases until they leave the passive layer. Rasouli et al. (2015) observed similar behavior with 3-cm-long cylindrical particles. Therefore, to calculate the effective particle sizes of cylindrical particles of other sizes, the measured distributions of the orientations in Figure 5.6 can be used. To do so, the following effective azimuth angle obtained from Figure 5.6 is proposed:

$$\theta_{effective} = \sin^{-1}\left(\frac{Effective\ particle\ size - diameter}{length - diameter}\right) \qquad 5.2$$

An effective particle size based on this effective azimuth angle can then be evaluated by substituting $\theta_{effective}$ into Eq. 5.1. Based on Eq. 5.2 and the MRPT results of Figure 5.6, the effective azimuth angle ($\theta_{effective}$) for Zones 1, 2, 3, and 4 were calculated and are presented in Table 5.6. The values in this table were rounded off. Of course, more work involving other sizes of cylindrical particles would be needed to assess the accuracy of this approach.

Table 5.6: The effective particle size for the cylindrical particle and the azimuth angle ($\boldsymbol{\theta_{effective}}$) for Zones 1, 2, 3, and 4

	Effective particle size [mm]	Effective azimuth angle [deg]
Active layer (**Zone 1**)	12	25
Active layer near the wall (**Zone 2**)	18	60
Transient region (**Zone 3**)	17	50
Passive layer (**Zone 4**)	16	45

The distributions of the azimuth angles display a similar trend for all the rotational speeds (see Figure 5.6). Since the packing density of a bed of cylindrical particles is a function of the distribution of their orientations, this packing density is expected to be similar in all the zones. This explains why there is an almost constant dynamic filling fraction ($\sim$45% in Table 5.3) for the cylindrical particles at all rotational speeds.

5.5.4 The streamwise velocity profile on the free surface

To obtain the dynamics of the granular flow inside a rotating drum, it is essential to evaluate the streamwise velocity profile on the free surface. This component is important for studying inter- and intra-tablet coating variability, for example, when a rotating drum is used as a pan coater (Kalbag et al., 2008; Ketterhagen, 2011). Figure 5.7a shows that the shape and scale of the streamwise velocity profiles of the spherical and cylindrical particles on the free surface are significantly different. The cylindrical particles have a higher velocity peak than the spherical particles, as has been reported by others (Dube et al., 2013; Suzzi et al., 2012; Wilson & Crossman, 1997). For particles with a relatively flat shape, Dube et al. (2013) and Suzzi et al. (2012) proposed that they align in a preferred spatial orientation in the active layer and slide down rather than rotate, which is why they can attain a higher velocity peak than spherical particles. To our knowledge, Figure 5.6a reveals this preferred orientation of relatively flat-shaped particles for the first time (cylindrical particles in this case). Previous studies used numerical simulations (Suzzi et al., 2012) or the RPT technique, which cannot measure the orientation of particles inside the active layer (Dube et al., 2013).
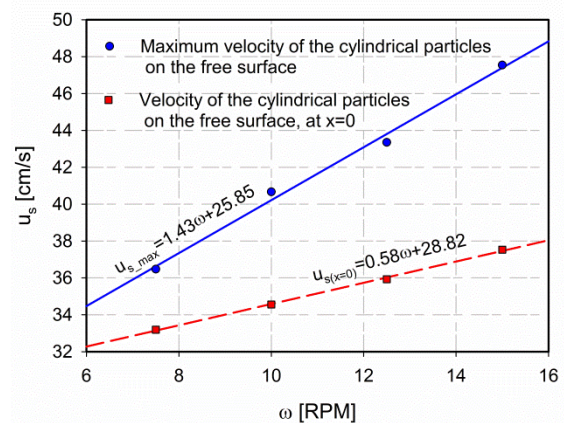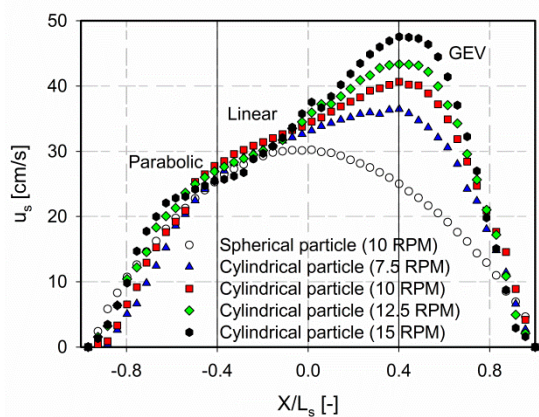
(a)   (b)

Figure 5.7: (a) streamwise velocity profile on the free surface and (b) variations of maximum velocity and velocity at x=0 on the free surface for cylindrical particles based on the rotational speed of the drum

Khakhar et al. (1997) suggested that the maximum velocity on the free surface is proportional to the rotational speed of the drum in the rolling regime (Khakhar, McCarthy, & Ottino, 1997). The variations in the maximum velocity on the free surface (u_{s_max}) versus the rotational speed for the cylindrical particles are presented in Figure 5.7b. Given that the maximum velocity of the spherical particles in the rolling regime occurs at $x/Ls = 0$ when Ls is the half-length of the bed surface, the corresponding velocity of the cylindrical particles, $u_{s(x=0)}$, is also displayed. This result confirms the existence of a linear relationship between u_{s_max} and $u_{s(x=0)}$ and the rotational speed of the drum.

According to Alexander et al. (2002), the velocity profile of spherical particles on the free surface has two general shapes, that is, symmetrical and asymmetrical with respect to $x/Ls = 0$ (Alexander et al., 2002). When a particle reaches the upstream part of the free surface, it starts to accelerate, and after going a certain distance l, it stops accelerating. After this, the particle continues its path at a constant speed or it begins to decelerate until it hits the wall of the drum. In the case of a symmetric velocity profile, the particle stops accelerating somewhere before or at the half-length of the bed surface (i.e., at $l/Ls \leq 1$), which happens with a low to normal rotational speed. However, in the case of a non-symmetric velocity profile, the particle stops accelerating somewhere after the half-length of the bed surface (i.e., at $1 < l/Ls$), which happens with a high rotational speed. Alexander et al. (2002) showed that l/Ls increases with an increase in rotational speed ($l/Ls \propto \sqrt[3]{\omega}$). However, they also noted that there is a certain distance ($l/Ls = 1.15$ for their experiments) beyond which the particle cannot accelerate even by further increasing the rotational speed (above 30 RPM for their experiments). Alexander et al. (2002) also asserted that this distance ($l/Ls = 1.15$) and the rotational speed (30 RPM) are not universal and that the values of these parameters depend on the properties of the particles and the drum. It should be noted that above such a high rotational speed, the flow regime is no longer in a rolling regime.

The spherical particles have a symmetric velocity profile (l/L $= 1$). A simple parabolic curve can represent the velocity profile as follows (Alizadeh, Dube, et al., 2013; Dube et al., 2013; Khakhar, McCarthy, & Ottino, 1997; Khakhar, McCarthy, Shinbrot, et al., 1997):

$$\frac{u_s(x, \omega)}{u_{s\_max\_sp}(\omega)} = 1 - \left(\frac{x}{L_s}\right)^2 \qquad\qquad 5.3$$

However, as can be seen in Figure 5.7a, the cylindrical particles exhibit non-symmetric velocity profiles at all the rotational speeds. Interestingly, the distance within which the particles accelerate is the same for all the rotational speeds, that is, $l/Ls = 1.4$. Suzzi et al. (2012) obtained the same l/Ls for oval and bi-convex tablets using numerical simulations. Models for determining the velocity profile should thus take this finding into account.

Figure 5.7a also shows that the shapes of the velocity profiles of the cylindrical particles are more complicated than those of the spherical particles. A polynomial function with a degree of 2 (Eq. 5.3) is adequate for determining the velocity profiles of spherical particles. However, such a polynomial function is inadequate as a model for determining the velocity profiles of cylindrical particles unless a polynomial with degree of 6 or higher is used, which indicates that the velocity profiles of cylindrical particles are very complex. While a polynomial equation with degree of 6 can accurately predict a velocity profile, in such a case it requires seven fitting parameters for each rotational speed. Given this, a general model with fewer or even no fitting parameters would be more useful for predicting velocity profiles, even if the predictions are less accurate.

Examining the measured velocity profiles (Figure 5.7) reveal that the increase in the velocity of the cylindrical particles is similar to that of the spherical particles from $x/Ls = -1$ to $x/Ls = -0.4$, after which it increases in a relatively linear fashion until it peaks at $x/Ls = 0.4$ and then decelerates toward the wall of the drum. In general, increasing the rotational speed of the drum results in a more rapid increase in the velocity profile. While this can be observed at the very beginning of the movement of the cylindrical particles (upstream region), the velocity profiles quickly approach each other at a point, $-l_b$, just before $x/Ls = -0.4$ due to resistance against the sliding down of the cylindrical particles caused by the rotation of other cylindrical particles in this region (see Figure 5.5). $x/Ls = -l_b$ is thus the point where the particle flow becomes fully developed and where the cylindrical particles become aligned with the free surface and start

sliding down without any resistance from the rotation of the other particles. This fully developed region ends at the velocity peak point where resistance due to the rotation of other particles and hitting the wall affect the movement of the particles and reduce their velocity. It is reasonable to assume that the required length (from $x/Ls = -1$ to $x/Ls = -l_b$) for a fully developed flow from the upstream wall is similar to the length of a non-fully developed flow to the downstream wall, that is, the length from the velocity peak point to the downstream wall. l_b is thus considered to be equal to 0.4. As such, the velocity profile from $x/Ls = -1$ to $x/Ls = -l_b$ follows Eq. 5.3, shifts to a linear trend (Eq. 5.4) ($x/Ls = -l_b$) until the peak point ($x/Ls = l_b$) is reached, and then decelerates (Eq. 5.5) from the peak point to $x/Ls = 1$. More precisely, the velocity profile for the fully developed flow region can thus be expressed as:

$$u_s(x,\omega) - u_{s\_max}(\omega) = \frac{u_{s\_max\_sp}(1 - (l_b)^2) - u_{s\_max}(\omega)}{2l_b}\left(-\frac{x}{Ls} + l_b\right) , -l_b \leq \frac{x}{LS} \leq l_b \quad 5.4$$

where $u_{s\_max\_sp}$ comes from Eq. 5.3 and u_{s_max} is the maximum velocity of the cylindrical particles. The results for the velocity profiles of the cylindrical particles during the deceleration phase indicate there are three specific components, namely, deceleration, which starts at $x/Ls = l_b$, velocity peak, which is located at the same point ($x/Ls = l_b$), and velocity, which reaches zero at the wall of the drum. Since the deceleration phase has three components and looks like a distribution function with a negative skewness, a generalized extreme value (GEV) distribution, which has three variables (σ, λ and κ), is used for modeling the deceleration phase:

$$\frac{u_s(x,\omega)}{u_{s\_max}(\omega)} = \frac{1}{\sigma}\left(1 + \lambda\left(\frac{(x/L_s) - \kappa}{\sigma}\right)\right)^{-1/\lambda - 1} . exp\left(-\left(1 + \lambda\left(\frac{(x/L_s) - \kappa}{\sigma}\right)\right)^{-1/\lambda}\right) \quad 5.5$$

where $\sigma = 0.43$, $\lambda = -0.5036$, and $\kappa = 0.1462$.

The maximum velocity values in Figure 5.7 and the strategy mentioned above were used to generate the velocity profiles on the free surface shown in Figure 5.8a for the cylindrical particles at different rotational speeds.

(a)   (b)
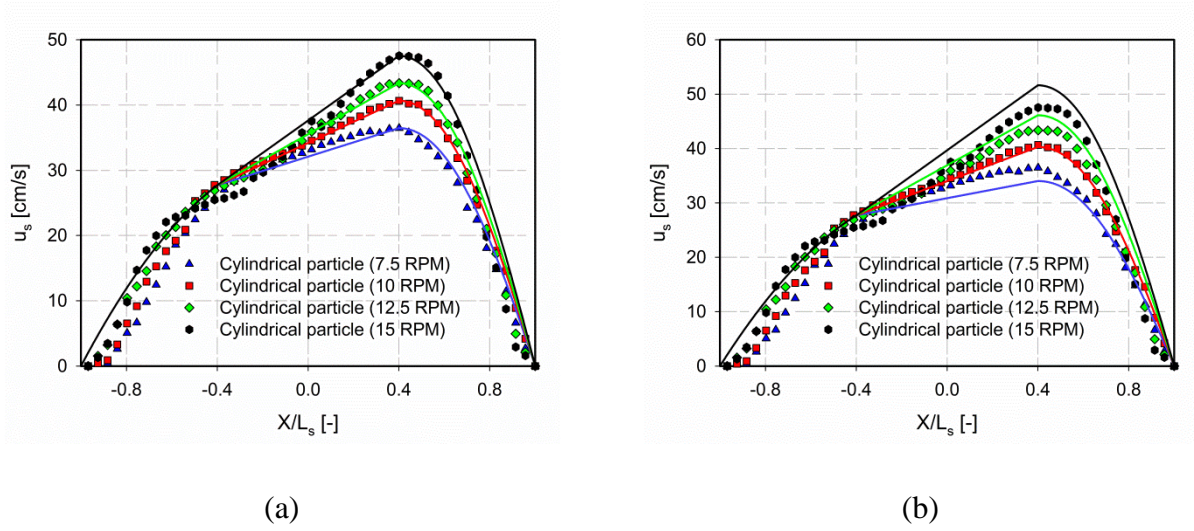
Figure 5.8: Streamwise velocity profiles on the free surface predicted with the model using maximum velocity values obtained by (a) experiments and (b) Eq. 5.9

Figure 5.8a shows that there is fairly good agreement between the prediction of the model (solid lines) and the experimental data (points). Since the only parameter in this model is the maximum velocity on the free surface u_{s_max}, the quality of its prediction depends to a great extent on the accuracy of this maximum velocity value. The experimentally (MRPT) obtained maximum velocity values were used to generate the plots in Figure 5.8a, which could be improved by finding a way to predict the value of u_{s_max}. This could be done by assuming that the maximum velocity for the cylindrical particles is similar to that of spherical particles under similar operating conditions, which means that the dilation of the bed of cylindrical particles should be taken into consideration. In other words, to obtain the maximum velocity for the cylindrical particles, which have a 45% dynamic filling fraction (see Table 5.3), we took a bed of spherical particles with a 45% filling fraction into consideration using the correlation proposed by Khakhar et al. (1997) Note that the filling fraction directly affects the values of h and L_s. According to Khakhar et al. (1997), the maximum velocity of spherical particles is given by:

$$u_{s\_max}(\omega) = \frac{\omega L_s^2}{\alpha_0}$$

5.6

In Eq. 5.6, α_0 is a function of the rotational speed (ω), which can be determined using the model proposed by Alizadeh et al. (2013):

$$\frac{L_s^2}{\alpha_0^2}\frac{\delta_0 - \alpha_0}{h + \delta_0} = 1 \implies \alpha_0 = L_s^2 \frac{\sqrt{1 + 4\delta_0\,(h + \delta_0)/L_s^2} - 1}{2(h + \delta_0)} \qquad\qquad 5.7$$

Eq. 5.7 links α_0 to δ_0. In addition, δ_0, the depth of the active layer based on the yield line, is proportional to the square root of the rotational speed (Alizadeh, Dube, et al., 2013; Makse, 1999; Meier et al., 2007):

$$\delta_0(\omega) = \delta_0^* \sqrt{\frac{\omega}{\omega^*}} \qquad\qquad 5.8$$

where δ_0^* is the depth of the active layer corresponding to a rotational speed of ω^*. Based on the values in Table 5.5, for a rotational speed of 10 RPM ($\omega^* = 10$), δ_0^* is equal to 4.6 cm and 4.7 cm based on experimental results and the model of Alizadeh et al. (2013), respectively. It should be remembered that the model of Alizadeh et al. (2013) is accurate and can thus be used to predict the maximum velocity of cylindrical particles on the free surface by introducing Eqs. 5.7 and 8 into Eq. 5.6 as follows:

$$u_{s\_max}(\omega) = \frac{2\omega\left(h + \delta_0^*\sqrt{\frac{\omega}{\omega^*}}\right)}{\sqrt{1 + 4\delta_0^*\sqrt{\frac{\omega}{\omega^*}}\left(h + \delta_0^*\sqrt{\frac{\omega}{\omega^*}}\right)/L_s^2} - 1} \qquad\qquad 5.9$$

Figure 5.8b shows the prediction of the model (solid lines) using Eq. 5.9 to calculate the maximum velocity u_{s_max}, which is reasonably accurate given that no fitting parameter is used in this model.

Given the shape of the velocity profile for the cylindrical particles and the results of Alexander et al. (2002), we can infer a priori that the cylindrical particles in our experiments were not in a rolling regime, but rather in a cascading regime. The main difference between the rolling and cascading regimes is that the free surface is almost flat in the rolling regime while the free surface has an "S" shape in the cascading regime (Mellmann, 2001). However, while the free surface of the cylindrical particles that we observed was slightly bumpy, it did not have an "S" shape. Therefore, this indicates that the cylindrical particles were in a rolling regime.

5.6 Conclusion

We investigated and compared the behavior of cylindrical (2 cm in length and 6 mm in diameter) and spherical (6 mm in diameter) particles in a rotating drum. We used the MRPT technique to capture the positions and orientations of the cylindrical particles and the RPT techniques to capture the positions of the spherical particles. The dilation of the bed during the rotation, the static and dynamic repose angles, and the streamwise velocity on the free surface of the cylindrical particles were significantly higher than those of the spherical particles at the same rotational speed. In addition, the depth of active layer at $x = 0$ and the percentage of the bed occupied by the active layer based on the turning point (α_0) and yield (δ_0) lines for the cylindrical particles were lower than those of the spherical particles at the same rotational speed. The turning point line based on the angular velocity was higher than the line based on the streamwise velocity.

The spherical particles in the active layer rolled down while the cylindrical particles slid down due to their alignment with their dynamic repose angle. A model was proposed to calculate the spatial orientation of the cylindrical particles in different zones inside the drum. Even at low rotational speeds, the cylindrical particles on the free surface continued their acceleration beyond the half length of the bed surface, unlike the spherical particles. At rotational speeds ranging from 7.5 to 15 RPM, the velocity of the cylindrical particles peaked at 0.7 of the length of the bed surface. Lastly, a no-fitting-parameter model was proposed to calculate the velocity profile on the free surface.

5.7 Acknowledgments

5.8 Literature Cited

Alexander, A., Shinbrot, T., & Muzzio, F. J. (2002). Scaling surface velocities in rotating cylinders as a function of vessel radius, rotation rate, and particle size. *Powder Technology, 126*(2), 174-190. doi: 10.1016/S0032-5910(02)00010-4

Alizadeh, E., Bertrand, F., & Chaouki, J. (2014). Comparison of DEM Results and Lagrangian Experimental Data for the Flow and Mixing of Granules in a Rotating Drum. *Aiche Journal, 60*(1), 60-75. doi: 10.1002/Aic.14259

Alizadeh, E., Dube, O., Bertrand, F., & Chaouki, J. (2013). Characterization of Mixing and Size Segregation in a Rotating Drum by a Particle Tracking Method. *Aiche Journal, 59*(6), 1894-1905. doi: 10.1002/aic.13982

Boateng, A. A. (1998). Boundary layer modeling of granular flow in the transverse plane of a partially filled rotating cylinder. *International Journal of Multiphase Flow, 24*(3), 499-521. doi: 10.1016/S0301-9322(97)00065-7

Boateng, A. A., & Barr, P. V. (1997). Granular flow behaviour in the transverse plane of a partially filled rotating cylinder. *Journal of Fluid Mechanics, 330*, 233-249. doi: 10.1017/S0022112096003680

Cheng, N.-S., Zhou, Q., Keat Tan, S., & Zhao, K. (2011). Application of incomplete similarity theory for estimating maximum shear layer thickness of granular flows in rotating drums. *Chemical Engineering Science, 66*(12), 2872-2878. doi: 10.1016/j.ces.2011.03.050

Cleary, P. W. (2010). DEM prediction of industrial and geophysical particle flows. *Particuology, 8*(2), 106-118. doi: 10.1016/j.partic.2009.05.006

Descoins, N., Dirion, J. L., & Howes, T. (2005). Solid transport in a pyrolysis pilot-scale rotary kiln: preliminary results—stationary and dynamic results. *Chemical Engineering and Processing: Process Intensification, 44*(2), 315-321. doi: 10.1016/j.cep.2004.02.025

Ding, Y. L., Forster, R., Seville, J. P. K., & Parker, D. J. (2002). Granular motion in rotating drums: bed turnover time and slumping-rolling transition. *Powder Technology, 124*(1-2), 18-27. doi: 10.1016/S0032-5910(01)00486-7

Ding, Y. L., Seville, J. P. K., Forster, R., & Parker, D. J. (2001). Solids motion in rolling mode rotating drums operated at low to medium rotational speeds. *Chemical Engineering Science, 56*(5), 1769-1780. doi: 10.1016/S0009-2509(00)00468-1

Doucet, J., Bertrand, F., & Chaouki, J. (2008). An extended radioactive particle tracking method for systems with irregular moving boundaries. *Powder Technology, 181*(2), 195-204. doi: 10.1016/j.powtec.2006.12.019

Dube, O., Alizadeh, E., Chaouki, J., & Bertrand, F. (2013). Dynamics of non-spherical particles in a rotating drum. *Chemical Engineering Science, 101*, 486-502. doi: 10.1016/j.ces.2013.07.011

Fantozzi, F., Colantoni, S., Bartocci, P., & Desideri, U. (2007). Rotary kiln slow pyrolysis for syngas and char production from biomass and waste - Part I: Working envelope of the

reactor. *Journal of Engineering for Gas Turbines and Power, 129*(4), 901-907. doi: 10.1115/1.2720521

Felix, G., Falk, V., & D'Ortona, U. (2002). Segregation of dry granular material in rotating drum: Experimental study of the flowing zone thickness. *Powder Technology, 128*(2-3), 314-319. doi: 10.1016/S0032-5910(02)00171-7

Felix, G., Falk, V., & D'Ortona, U. (2007). Granular flows in a rotating drum: The scaling law between velocity and thickness of the flow. *European Physical Journal E, 22*(1), 25-31. doi: 10.1140/epje/e2007-00002-5

Henein, H., Brimacombe, J. K., & Watkinson, A. P. (1985). Experimental Study of Segregation in Rotary Kilns. *Metallurgical transactions. B, Process metallurgy, 16 B*(4), 763-774.

Heydenrych, M. D., Greeff, P., Heesink, A. B. M., & Versteeg, G. F. (2002). Mass transfer in rolling rotary kilns: A novel approach. *Chemical Engineering Science, 57*(18), 3851-3859. doi: 10.1016/S0009-2509(02)00312-3

Hill, K. M., Caprihan, A., & Kakalios, J. (1997). Bulk segregation in rotated granular material measured by magnetic resonance imaging. *Physical Review Letters, 78*(1), 50-53. doi: 10.1103/PhysRevLett.78.50

Ingram, A., Seville, J. P. K., Parker, D. J., Fan, X., & Forster, R. G. (2005). Axial and radial dispersion in rolling mode rotating drums. *Powder Technology, 158*(1-3), 76-91. doi: 10.1016/j.powtec.2005.04.030

Jain, N., Ottino, J. M., & Lueptow, R. M. (2002). An experimental study of the flowing granular layer in a rotating tumbler. *Physics of Fluids, 14*(2), 572-582. doi: 10.1063/1.1431244

Jain, N., Ottino, J. M., & Lueptow, R. M. (2004). Effect of interstitial fluid on a granular flowing layer. *Journal of Fluid Mechanics, 508*, 23-44. doi: 10.1017/S0022112004008869

Jain, N., Ottino, J. M., & Lueptow, R. M. (2005). Regimes of segregation and mixing in combined size and density granular systems: An experimental study. *Granular Matter, 7*(2-3), 69-81. doi: 10.1007/s10035-005-0198-x

Kalbag, A., Wassgren, C., Sumana Penumetcha, S., & Pérez-Ramos, J. D. (2008). Inter-tablet coating variability: Residence times in a horizontal pan coater. *Chemical Engineering Science, 63*(11), 2881-2894. doi: 10.1016/j.ces.2008.03.009

Kawaguchi, T. (2010). MRI measurement of granular flows and fluid-particle flows. *Advanced Powder Technology, 21*(3), 235-241. doi: 10.1016/j.apt.2010.03.014

Ketterhagen, W. R. (2011). Modeling the motion and orientation of various pharmaceutical tablet shapes in a film coating pan using DEM. *International Journal of Pharmaceutics, 409*(1–2), 137-149. doi: 10.1016/j.ijpharm.2011.02.045

Khakhar, D. V., McCarthy, J. J., & Ottino, J. M. (1997). Radial segregation of granular mixtures in rotating cylinders. *Physics of Fluids, 9*(12), 3600-3614. doi: 10.1063/1.869498

Khakhar, D. V., McCarthy, J. J., Shinbrot, T., & Ottino, J. M. (1997). Transverse flow and mixing of granular materials in a rotating cylinder. *Physics of Fluids, 9*(1), 31-43. doi: 10.1063/1.869172

Larachi, F., Kennedy, G., & Chaouki, J. (1994). A Gamma-Ray Detection System for 3-D Particle Tracking in Multiphase Reactors. *Nuclear Instruments & Methods in Physics Research Section a-Accelerators Spectrometers Detectors and Associated Equipment, 338*(2-3), 568-576. doi: 10.1016/0168-9002(94)91343-9

Liu, X. Y., Specht, E., Gonzalez, O. G., & Walzel, P. (2006). Analytical solution for the rolling-mode granular motion in rotary kilns. *Chemical Engineering and Processing, 45*(6), 515-521. doi: 10.1016/j.cep.2005.10.009

Longo, S., & Lamberti, A. (2002). Grain shear flow in a rotating drum. *Experiments in Fluids, 32*(3), 313-325. doi: 10.1007/s003480100359

Makse, H. A. (1999). Continuous avalanche segregation of granular mixtures in thin rotating drums. *Physical Review Letters, 83*(16), 3186-3189. doi: 10.1103/PhysRevLett.83.3186

Meier, S. W., Lueptow, R. M., & Ottino, J. M. (2007). A dynamical systems approach to mixing and segregation of granular materials in tumblers. *Advances in Physics, 56*(5), 757-827. doi: 10.1080/00018730701611677

Mellmann, J. (2001). The transverse motion of solids in rotating cylinders-forms of motion and transition behavior. *Powder Technology, 118*(3), 251-270. doi: 10.1016/S0032-5910(00)00402-2

Mellmann, J., Specht, E., & Liu, X. (2004). Prediction of rolling bed motion in rotating cylinders. *Aiche Journal, 50*(11), 2783-2793. doi: 10.1002/aic.10266

Nakagawa, M., Altobelli, S. A., Caprihan, A., Fukushima, E., & Jeong, E. K. (1993). Non-invasive measurements of granular flows by magnetic resonance imaging. *Experiments in Fluids, 16*(1), 54-60. doi: 10.1007/BF00188507

Orpe, A. V., & Khakhar, D. V. (2001). Scaling relations for granular flow in quasi-two-dimensional rotating cylinders. *Physical Review E - Statistical, Nonlinear, and Soft Matter Physics, 64*(3 I), 313021-3130213. doi: 10.1103/PhysRevE.64.031302

Parker, D. J., Dijkstra, A. E., Martin, T. W., & Seville, J. P. K. (1997). Positron emission particle tracking studies of spherical particle motion in rotating drums. *Chemical Engineering Science, 52*(13), 2011-2022. doi: 10.1016/S0009-2509(97)00030-4

Rasouli, M., Bertrand, F., & Chaouki, J. (2015). A multiple radioactive particle tracking technique to investigate particulate flows. *Aiche Journal, 61*(2), 384-394. doi: 10.1002/aic.14644

Ridgway, K., & Rupp, R. (1971). Mixing of powder layers on a chute. The effect of particle size and shape. *Powder Technology, 4*(4), 195-202. doi: 10.1016/0032-5910(71)80035-9

Santomaso, A. C., Ding, Y. L., Lickiss, J. R., & York, D. W. (2003). Investigation of the granular behaviour in a rotating drum operated over a wide range of rotational speed. *Chemical Engineering Research and Design, 81*(8), 936-945. doi: 10.1205/026387603322482176

Sheritt, R. G., Chaouki, J., Mehrotra, A. K., & Behie, L. A. (2003). Axial dispersion in the three-dimensional mixing of particles in a rotating drum reactor. *Chemical Engineering Science, 58*(2), 401-415. doi: 10.1016/S0009-2509(02)00551-1

Suzzi, D., Toschkoff, G., Radl, S., Machold, D., Fraser, S. D., Glasser, B. J., & Khinast, J. G. (2012). DEM simulation of continuous tablet coating: Effects of tablet shape and fill level

on inter-tablet coating variability. *Chemical Engineering Science, 69*(1), 107-121. doi: 10.1016/j.ces.2011.10.009

Tobiska, S., & Kleinebudde, P. (2003). Coating uniformity and coating efficiency in a Bohle Lab-Coaterusing oval tablets. *European Journal of Pharmaceutics and Biopharmaceutics, 56*(1), 3-9. doi: 10.1016/S0939-6411(03)00026-2

Tsoulfanidis, N., & Landsberger, S. (2011). *Measurement and Detection of Radiation*: CRC Press.

Van Puyvelde, D. R., Young, B. R., Wilson, M. A., & Schmidt, S. J. (2000). Modelling transverse segregation of particulate solids in a rolling drum. *Chemical Engineering Research and Design, 78*(4), 643-650. doi: 10.1205/026387600527590

Wightman, C., & Muzzio, F. J. (1998a). Mixing of granular material in a drum mixer undergoing rotational and rocking motions I. Uniform particles. *Powder Technology, 98*(2), 113-124. doi: 10.1016/S0032-5910(98)00010-2

Wightman, C., & Muzzio, F. J. (1998b). Mixing of granular material in a drum mixer undergoing rotational and rocking motions II. Segregating particles. *Powder Technology, 98*(2), 125-134. doi: 10.1016/S0032-5910(98)00011-4

Wilson, K. E., & Crossman, E. (1997). The Influence of Tablet Shape and Pan Speed on Intra-tablet Film Coating Uniformity. *Drug Development and Industrial Pharmacy, 23*(12), 1239-1243. doi: 10.3109/03639049709146164

Woodle, G. R., & Munro, J. M. (1993). Particle motion and mixing in a rotary kiln. *Powder Technology, 76*(3), 241-245.

CHAPTER 6 EXPERIMENTAL MODELING OF THE DYNAMICS OF CYLINDRICAL PARTICLES IN A ROTATING DRUM USING RADIOACTIVE PARTICLE TRACKING

This chapter is essentially a further analysis of the data obtained by the MRPT and RPT techniques in the previous chapter (Chapter 5). It aims to provide equations of motion for the cylindrical and spherical particles in the active and passive layers, as well as equations of the yield and turning point curve lines. Having these equations enables us to gain further knowledge about the system, which is inaccessible by experimental techniques, by means of numerical simulation. For instance, through simulation one can study the effect of advection (without considering the effects of diffusion (dispersion)) on the mixing of particles without further experiments. While advection and diffusion phenomena coexist in real experiments.

To do so, the velocity of granular flow based on the position ($\vec{V}(x, y)$) should be available. Thus, firstly, the velocity profile of transverse flow will be calculated and presented. Afterwards, this chapter will present the flow motion within the passive layer. Subsequently, to determine the extent of the passive layer, the boundary between the active and passive layers must be identified. Therefore, equations for the yield and turning point curve line will be obtained. This chapter will then analyze the active layer and obtain its equation of motion. Furthermore, to complete the modeling of flow motion, the velocity profile on the free surface will be obtained. Finally, a case simulation will show the potential of these equations of motion to aid in further studies.

6.1 Velocity profile
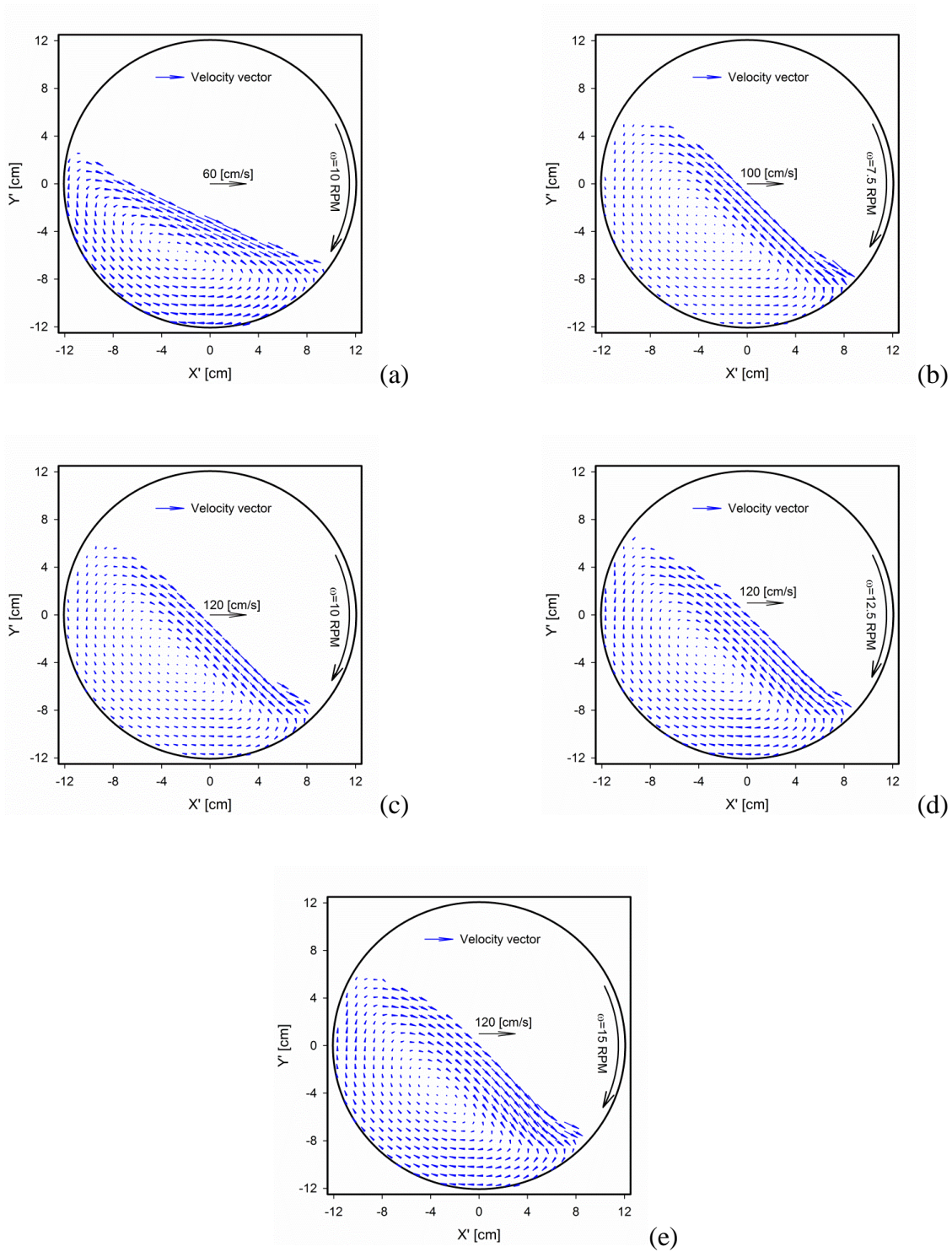
Figure 6.1: Velocity vectors for (a) spherical particles at 10 RPM rotational speed, and cylindrical particles at (b) 7.5 RPM , (c) 10 RPM , (d) 12.5 RPM and (e) 15 RPM

Figure 6.1 shows the velocity field for spherical and cylindrical particles. Despite the differences between velocity fields, there is a key similarity between them: the flow motions for all of them consist in the active and passive layers, which are characteristic of rolling regime. Therefore, to compare their flow dynamics quantitatively as well as for modeling purpose, the passive and actively layers must be analyzed. To model the transverse flow dynamic, one should ascertain the dynamic of the passive and active layer, as well the boundary between these two layers.

6.2 Passive layer

The passive layer is a region where the bed of the particles undergoes a solid body rotational motion the same as the drum. Therefore, the flow dynamic of this region is well known and can be described as follows (Meier et al., 2007):

$$u_{passive} = -\omega y \tag{6.1}$$

$$v_{passive} = \omega x \tag{6.2}$$

Note that the value of angular velocity (ω) is negative due to the clockwise rotation of the drum. The validity of this prediction should be verified by the results of the experiments. To do so, the streamwise (u) and transverse (v) component of velocity at a specific x are necessary data to be obtained.

6.3 Streamwise and transverse velocity profiles

Figure 6.2 displays the streamwise and transverse components of the velocity profile through the whole bed at $x = 0$ for spherical and cylindrical particles for a rotational speed of 10 RPM. It can be readily observed that there are some regions, for the both particle shapes, where their velocities follow Eq. 6.1 and 6.2.
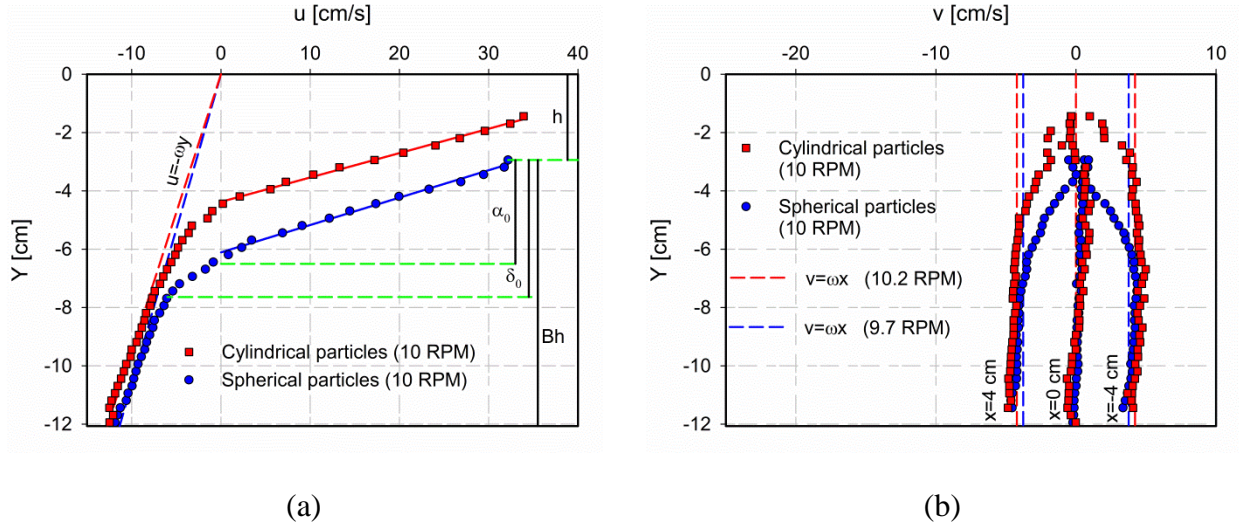
Figure 6.2: (a) streamwise and (b) transverse velocity profiles for spherical and cylindrical particles at x=0 and a rotational speed of 10 RPM.

In Figure 6.2b, the transverse velocity v for x equal to -4, 0 and 4 cm along the whole bed is presented. This figure shows that transverse velocity is almost zero all along the bed height at $x = 0$, while its value changes along the y axis at other x values. Therefore, considering streamwise velocity u at $x = 0$ is enough to determine the interface between the passive and active layers. One can obtain the thickness of the yield line (δ_0) at $x = 0$ by considering that the first point out of the passive layer is the point where its streamwise velocity deviates more than the threshold value from Eq. 6.1. This threshold value depends on the accuracy of the measurements. In this work, 10% is considered the threshold value. In Figure 6.2a, the green dashed line (at around $y = -8$ cm) was obtained with the above-mentioned criterion, showing δ_0 for spherical particles. In addition, in this figure one can obtain the turning point (α_0) by finding the point where the streamwise velocity direction changes. Finally, the bed height (Bh) can be defined by the point with the highest y. For example, in Figure 6.2a, α_0 and Bh are presented by the green dashed lines at y equal to -6 and -3 cm for spherical particles, respectively. To complete the modeling of the passive layer, the boundaries of this layer (the yield line and/or turning point line) should be defined beside its equations of motion (Eq. 6.1 and 6.2).

6.4 Boundary between the active and passive layers

In general, mixing, segregation and heat transfer in the solid phase mostly happen in the active layer where particles can have different speeds with respect to each other (Alizadeh, Dube, et al., 2013; Cheng et al., 2011; Dube et al., 2013; Ingram et al., 2005). Thus the modeling and calculation of the extent of active layer is essential to assess the degree of such phenomena. Determining the thickness of the active layer has been the subject of many studies, and different correlations have been proposed for its calculation (Alizadeh, Dube, et al., 2013; Ding et al., 2001; Liu et al., 2006; Meier et al., 2007; Mellmann et al., 2004; A. V. Orpe & Khakhar, 2001). The method outlined in the previous section can find the boundary between the active and passive layers at $x = 0$. However, the method based on instantaneous velocity, also mentioned in the previous chapter (Chapter 5), is preferred due to the fact that in the positions where $x \neq 0$, the transverse component of velocity is not zero ($v(x \neq 0, y) \neq 0$).

Table 6.1: Values of the turning point and yield line thickness (α_0 and δ_0) at $x = 0$

Rotational Speed [RPM]	Measured α_0 [cm (%)[a]]	Measured δ_0 [cm (%)[a]]
Spherical particles		
10	3.6 (38)	4.6 (49)
Cylindrical particles		
7.5	2.8 (27)	3.7 (35)
10	3.0 (28)	3.9 (37)
12.5	3.1 (30)	4.0 (39)
15	3.3 (32)	4.4 (44)

[a] Percentage of bed depth.
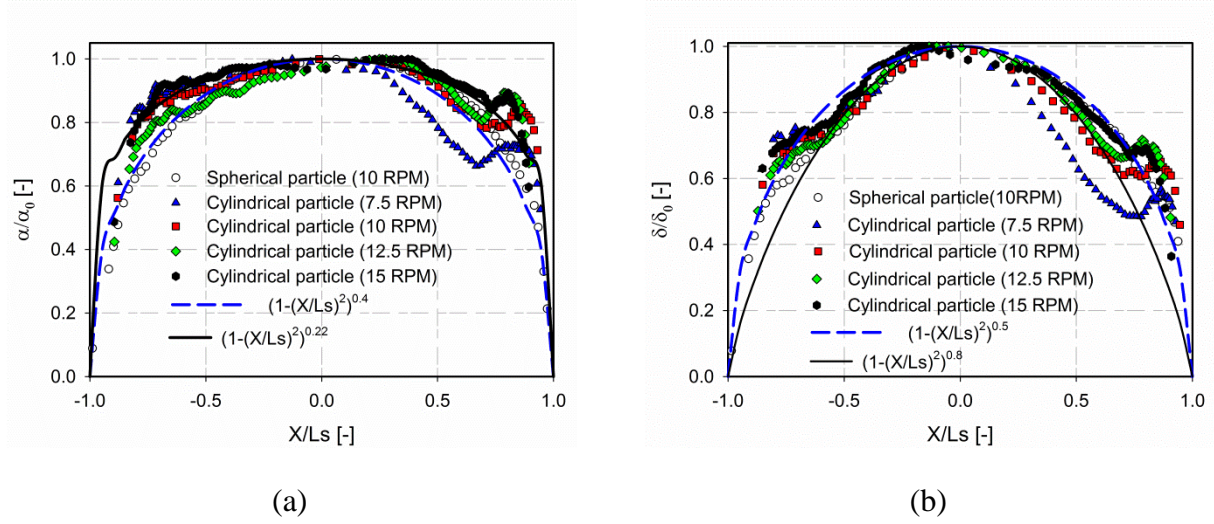
Figure 6.3: Normalized active layer boundary based on (a) the turning point line and (b) the yield line.

The normalized active layer boundary based on the turning point and yield lines are calculated from the RPT and MRPT results and presented in Figure 6.3. Using this dimensionless presentation of the boundary lines enables a better comparison between the cylindrical and spherical particles (Dube et al., 2013). Figure 6.3 shows the active layer boundary lines (δ and α) are more symmetrical and smooth for spherical particles in comparison with those of cylindrical particles, which are more noisy and asymmetrical, particularly for the run of 7.5 RPM. This is a consequence of the fact that cylindrical particles can have many different orientations in a random manner in the transition region (see Figure 5.6, Zone 3). For cylindrical particles, in both of the boundary lines there is an unusual local summit around $x/Ls = 0.8$. This could be the effect of rotation of the cylindrical particles (see Figure 5.6, Zone 2) when they impact the wall of the drum. To model the active layer boundary lines, the general form of Eq. 6.3 and 6.4 was considered and their power numbers (n_δ and n_α) were fitted (Alizadeh, Dube, et al., 2013; Dube et al., 2013; Meier et al., 2007).

$$\delta(x,\omega) = \delta_0(\omega).\left(1 - \left(\frac{x}{L_S}\right)^2\right)^{n_\delta(\omega)} \tag{6.3}$$

$$\alpha(x,\omega) = \alpha_0(\omega).\left(1 - \left(\frac{x}{L_S}\right)^2\right)^{n_\alpha(\omega)} \tag{6.4}$$

The power numbers of the active layer boundary based on the yield line (n_δ in Eq. 6.3) and the turning point line (n_α in Eq. 6.4) were computed as $n_\delta = 0.5, 0.8$ and $n_\alpha = 0.4, 0.22$ for spherical and cylindrical particles, respectively, considering all the rotational speeds together. The corresponding boundary lines based on these power numbers are presented in Figure 6.3, where the blue dashed curve is related to the spherical particles and the black solid curve is related to the cylindrical particles. It shows that Eq. 6.3 and 6.4 offer a good representative of the boundary lines for spherical particles in all areas. However, the agreement between these equations and the measured values for cylindrical particles is not as good as spherical particles, especially for the yield line (δ) in the regions near the wall of the drum. As already mentioned in the previous chapter, near the wall of the drum two boundary layers approach each other. Therefore, to calculate the active layer boundary line for cylindrical particles, one can use Eq. 6.3 for the area in the middle of the drum, and then use Eq. 6.4 for the regions near the wall of the drum. In addition, to improve the agreement for cylindrical particles, the power numbers were fitted for each rotational speed individually, and the results are displayed in Figure 6.4. The other parameter (α_0 and δ_0 from Table 6.1) of Eq. 6.3 and 6.4 is shown in this figure as well. Interestingly, the power numbers and depth at $x = 0$ for the yield line and turning point have a linear relationship with the rotational speed of the drum. Each of these relationships is presented in the figure near to the corresponding line. Such a relationship is definitely of interest for any numerical investigation of the effect of the drum rotational speed, for example, a study of the effect of a periodical rotational speed on quality of mixing. To complete the modeling of the transverse flow dynamic, considering the equations provided in this section, what remains is the equation of motion of the active layer, which is the topic of the next section.
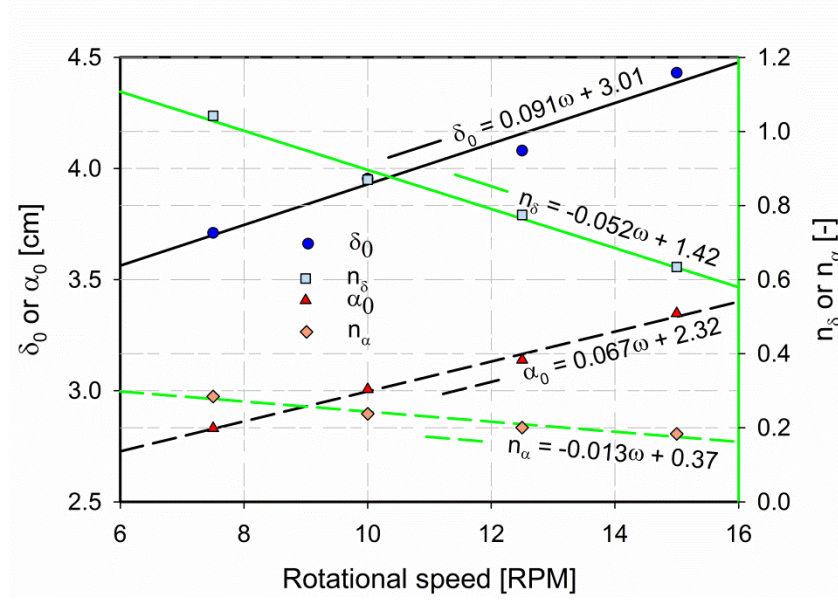
Figure 6.4: Variation of the active layer depth (δ_0 and α_0) and the power numbers of Eq. 6.3 and 6.4 as a function of the rotational speed for the cylindrical particles.

6.5 Active layer

In the literature a linear behaviour for the streamwise and transverse velocity profile in the active layer is widely reported (Alizadeh et al., 2014; Alizadeh, Dube, et al., 2013; Dube et al., 2013; Fiedor & Ottino, 2005; Makse, 1999; Meier et al., 2007; Nakagawa et al., 1993). This means that the shear rate is constant ($\gamma^{\cdot} \neq \gamma^{\cdot}(y)$) in the active layer, while some models with a non-constant shear rate ($\gamma^{\cdot} = \gamma^{\cdot}(y)$) have been reported as well (Boateng, 1998; Ding et al., 2001; Khakhar, McCarthy, Shinbrot, et al., 1997). Figure 6.2 verifies the existence of such a linear trend for spherical and cylindrical particles in the active layer ($-h - \delta(x) \leq y \leq -h$), except the transient region ($-h - \delta(x) \leq y \leq -h - \alpha(x)$). To handle this exception, there are two simple approaches: 1) one can assume another constant shear rate ($\gamma^{\cdot}_{transient} \neq \gamma^{\cdot}_{active}$) for the transient region, which different from the shear rate of the rest, and 2) consider only the shear rate of the active layer ($\gamma^{\cdot}_{active}$) and ignore the error from the discrepancy of this region since the size of this region in comparison with the whole active layer is small. Figure 6.2b suggests a non-constant shear rate ($\gamma^{\cdot} = \gamma^{\cdot}(x)$) for the transverse velocity profile of the both particle shapes. However, for modeling purposes, a constant shear rate ($\gamma^{\cdot} \neq \gamma^{\cdot}(x)$) is often assumed (Dube et al., 2013; Meier et al., 2007).

(a)   (b)
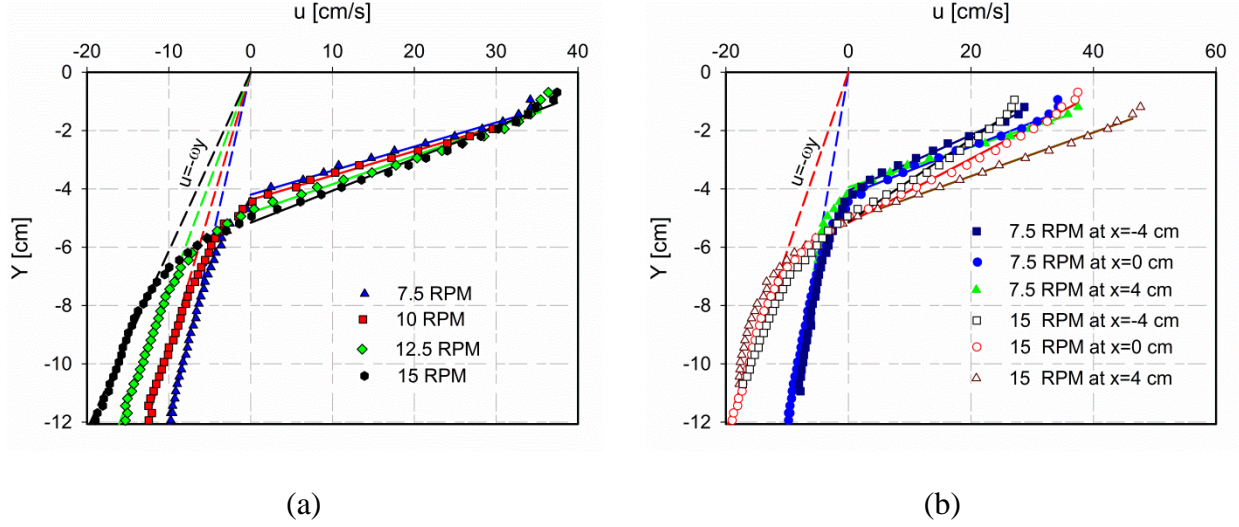
Figure 6.5: Streamwise velocity profiles for cylindrical particles (a) at x=0 for all the rotational speeds and (b) at x= -4,0 and 4 cm for rotational speeds of 7.5 and 15 RPM.

To verify the existence of a similar trend for the other rotational speed, the streamwise velocity profile of the cylindrical particles at $x = 0$ for all the rotational speeds of the drum is illustrated in Figure 6.5a. In addition, to confirm the existence of a similar trend for the other x axis values, in Figure 6.5b shows the streamwise velocity profile for the lowest (7.5 RPM) and highest (15 RPM) rotational speeds at three different x values ($x = -4, 0, 4\ cm$). Figure 6.5 clearly confirms that a linear velocity profile approximation can rather accurately represent the reality. Therefore, by using two appropriate boundary conditions (B.C.), one can obtain the equation of motion of the active layer. The expected boundary conditions for the streamwise and transverse velocity in the active layer are listed in Eq. 6.5 and 6.6, respectively:

$$\begin{cases} B.C.1: at\ y = -h & \Rightarrow & u_{active} = u_s(x) \\ B.C.2: at\ y = -h - \alpha(x) \Rightarrow & u_{active} = u_{transient} = 0 \\ B.C.3: at\ y = -h - \delta(x) \Rightarrow u_{transient} = u_{passive} = -\omega(-h - \delta(x)) \end{cases} \qquad 6.5$$

$$\begin{cases} B.C.4: at\ y = -h & \Rightarrow v_{active} = 0 \\ B.C.5: at\ y = -h - \delta(x) \Rightarrow v_{active} = v_{passive} = \omega x \end{cases} \qquad 6.6$$

where u_{active} and v_{active} are the streamwise and transverse velocity in the active layer, respectively, and $u_s(x)$ is the streamwise velocity profile on the free surface. Using boundary conditions 1 and 2 will give the equation of the streamwise velocity in the active layer $-h -$

$\alpha(x) \leq y \leq -h$ (Eq. 6.7) (Alizadeh, Dube, et al., 2013; Dube et al., 2013), while using boundary conditions 2 and 3 will result in the equation of the streamwise velocity in the transient region (Eq. 6.8). Obviously the equation resulting from boundary conditions 1 and 3 will not be as accurate as these to equations, due to the nonlinearity of the velocity profile from the transient region to the active layer (see Figure 6.2a and Figure 6.5). In Eq. 6.7 the only unknown is the streamwise velocity profile on the free surface (u_s), which is topic of the next section.

$$u_{active}(x,y) = u_s(x)\left(1 + \frac{y+h}{\alpha(x)}\right) \qquad\qquad 6.7$$

$$u_{transient}(x,y) = \frac{\omega\big(h+\delta(x)\big)\big(y+h+\alpha(x)\big)}{\alpha(x) - \delta(x)} \qquad\qquad 6.8$$

Using boundary conditions 4 and 5 will give the equation of the transverse velocity as follows (Dube et al., 2013; Meier et al., 2007):

$$v_{active}(x,y) = \frac{-\omega x(y+h)}{\delta(x)} \qquad\qquad 6.9$$

6.6 The streamwise velocity profile on the free surface

To obtain the dynamic of granular flow inside the rotating drum, it is essential to evaluate another major element, the streamwise velocity profile on the free surface. Figure 6.6a displays the streamwise velocity profile on the free surface for both spherical and cylindrical particles. The cylindrical particles show a higher velocity peak in comparison with spherical particles, as has been reported by others (Dube et al., 2013; Suzzi et al., 2012; Wilson & Crossman, 1997).
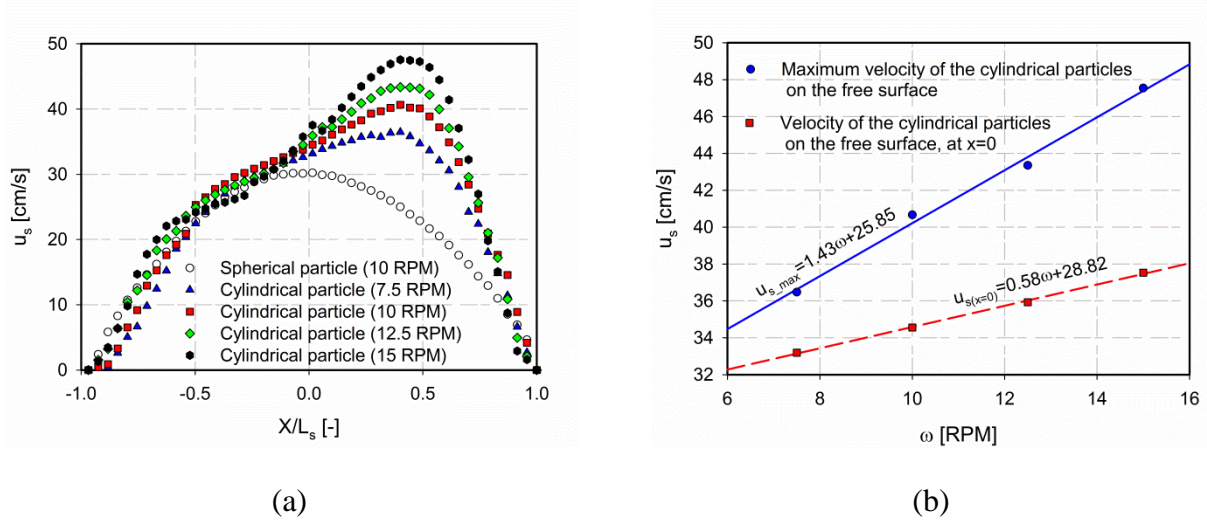
Figure 6.6: a) streamwise velocity profile on the free surface, and b) variation of the maximum velocity and velocity at x=0 on the free surface based on the rotational speed of the drum for cylindrical particles.

Khakhar et al. (Khakhar, McCarthy, & Ottino, 1997) suggested that the maximum velocity on the free surface is proportional to the rotational speed of the drum in the rolling regime. Therefore, the variation of the maximum velocity on the free surface (u_{s_max}) versus the rotational speed for cylindrical particles is presented in Figure 6.6b. In the rolling regime, as the maximum velocity for spherical particles is at $x/Ls = 0$, for comparison reason, the corresponding velocity ($u_{s(x=0)}$) of cylindrical particles are displayed in this figure as well. The result confirms the existence of a linear relationship between u_{s_max} and $u_{s(x=0)}$ with the rotational speed of the drum. These relationships are presented in Figure 6.6b. Moreover, the maximum velocity u_{s_max} is used to make the dimensionless velocity profiles in Figure 6.7 (Dube et al., 2013).

According to Alexander et al. (Alexander et al., 2002), for spherical particles, the velocity profile on the free surface has two general shapes, namely, symmetrical and asymmetrical. In the case of the symmetrical velocity profile, the particle stops accelerating somewhere before or at half the length of the bed surface (i.e. $l/Ls \leq 1$). We recall that l is the distance from the wall of drum uphill until the acceleration of the particle is finished. However, in the case of the asymmetrical velocity profile, the particle stops accelerating somewhere after half the length of the bed surface (i.e. $1 < l/Ls$). Alexander et al. that showed l/Ls is increases with an increase in rotational

speed. However, they discovered that there is a certain distance a particle cannot accelerate beyond, even by further increasing the rotational speed.

Figure 6.7a displays the dimensionless form of the velocity profile on the free surface for the both particles shapes. For spherical particles, the results show a symmetrical velocity profile and $l/Ls = 1$. Therefore, a simple parabolic curve can represent the velocity profile as follows (Alizadeh, Dube, et al., 2013; Dube et al., 2013; Khakhar, McCarthy, & Ottino, 1997; Khakhar, McCarthy, Shinbrot, et al., 1997):

$$\frac{u_s(x, \omega)}{u_{s\_max}(\omega)} = 1 - \left(\frac{x}{L_s}\right)^2 \qquad\qquad 6.10$$

(a) (b)
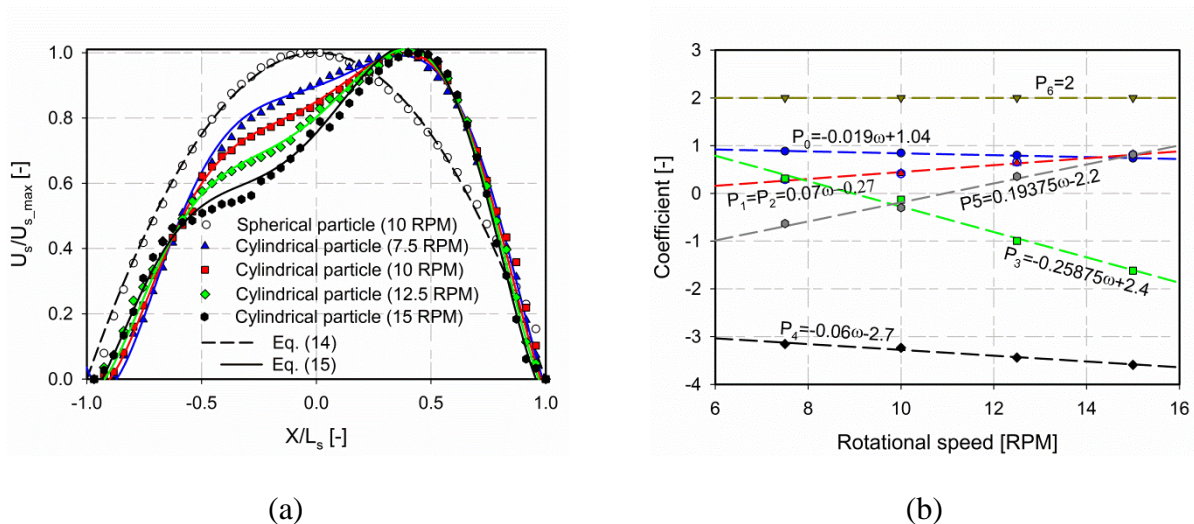
Figure 6.7: a) normalized streamwise velocity profile on the free surface based on x axis, and b) variation of the coefficients of Eq. 6.11 based on the rotational speed of the drum.

However, for cylindrical particles, the results certainly show an asymmetrical velocity profile for all rotational speeds. Interestingly, the distance of the acceleration for all rotational speeds is the same, $l/Ls = 1.4$. More interestingly, Suzzi et al. (Suzzi et al., 2012) obtained the same l/Ls for oval and bi-convex tablets using numerical simulation. Therefore, any proposed model for the velocity profile should appreciate this finding.

Figure 6.7 shows that the shape of the velocity profile for cylindrical particles is much more complicated than that for spherical particles. With a polynomial function as a model for the velocity profile, it was not successful using a polynomial with degree of 6 (Eq. 6.11) or higher, while for spherical particles a polynomial function with degree of 2 (Eq. 6.10) was fine. This fact strongly suggests a more complicated velocity profile for cylindrical particles.

$$\frac{u_s(x,\omega)}{u_{s\_max}(\omega)} = P_0(\omega) + P_1(\omega).\left(\frac{x}{L_s}\right)^1 + P_2(\omega).\left(\frac{x}{L_s}\right)^2 + P_3(\omega).\left(\frac{x}{L_s}\right)^3 + P_4(\omega).\left(\frac{x}{L_s}\right)^4$$
$$+ P_5(\omega).\left(\frac{x}{L_s}\right)^5 + P_6(\omega).\left(\frac{x}{L_s}\right)^6$$

6.11

For each rotational speed, a set of seven coefficients for Eq. 6.11 was obtained by fitting this equation and the experimental results. The solid line in Figure 6.7a shows the quality of Eq. 6.11 in predicting the velocity profile for cylindrical particles. Interestingly, it was found that all seven coefficients of Eq. 6.11 exhibit a linear relationship with the rotational speed, which is definitely of interest, as already mentioned. The obtained values for the coefficients and their linear correlation with the rotational speed are presented in Figure 6.7b.

In addition, the velocity profile can be modeled using the summation of two distributions, whereby one distribution contributes primarily to the acceleration part of the velocity profile, and the other one to deceleration. Considering the points mentioned previously regarding the velocity profile of cylindrical particles, there are three specific conditions, namely, that deceleration starts at $x/Ls = 0.4$, the velocity peak is located at the same point ($x/Ls = 0.4$), and the velocity reaches zero at the wall of the drum. As deceleration has three conditions and a distribution shape with a negative skewness, a generalized extreme value (GEV) distribution, which has three variables (σ, λ and κ), is appropriate for modeling this part. Therefore, using these three conditions one can obtain the three variables of the GEV distribution, as follows:

$$\begin{cases} Mode\ of\ GEV(\sigma,\lambda,\kappa) = \begin{cases} \kappa + \sigma\dfrac{(1+\lambda)^{-\lambda}+1}{\lambda} & if\ \lambda \neq 0 \\ \kappa & if\ \lambda = 0 \end{cases} = 0.4 \\ \qquad GEV\big((x/L_s) = 0.4; \sigma,\lambda,\kappa\big) = 1 \\ \qquad GEV\big((x/L_s) = 1; \sigma,\lambda,\kappa\big) = 0 \\ \Longrightarrow \begin{cases} \sigma = 0.43 \\ \lambda = -0.5036 \\ \kappa = 0.1462 \end{cases} \end{cases}$$

6.12

For the acceleration part, a Weibull distribution is considered, and the velocity profile on the free surface can therefore be modeled by:

$$\frac{u_s(x,\omega)}{u_{s\_max}(\omega)} = \left[\begin{array}{c} Generalized\ extreme\ value\ \big(GEV((x/L_s); \sigma,\lambda,\kappa)\big) \\ + P_1(\omega) \times Weibull\big((x/L_s); P_2(\omega), P_3(\omega)\big) \end{array} \right]$$

$$= \left[\frac{1}{\sigma}\left(1 + \lambda\left(\frac{(x/L_s) - \kappa}{\sigma}\right)\right)^{-1/\lambda - 1} . exp\left(-\left(1 + \lambda\left(\frac{(x/L_s) - \kappa}{\sigma}\right)\right)^{-1/\lambda}\right) \right.$$

6.13

$$\left. + P_1(\omega). \frac{P_2(\omega)}{P_3(\omega)}.\left(\frac{(x/L_s) + 1}{P_3(\omega)}\right)^{P_2(\omega) - 1} . exp\left(-\left(\frac{(x/L_s) + 1}{P_3(\omega)}\right)^{P_2(\omega)}\right) \right]$$

where P_1 is an adjusting parameter, and P_2 and P_3 are the parameters of the Weibull distribution. These parameters were calculated by fitting the experimental data with Eq. 6.13, and then presented in Figure 6.8b. Interestingly, these parameters have a linear relationship with the rotational speed of the drum, which is certainly of interest, as already mentioned. As depicted by the solid lines in Figure 6.8a, Eq. 6.13 can represent the velocity profile of the cylindrical particles with quite good agreement.
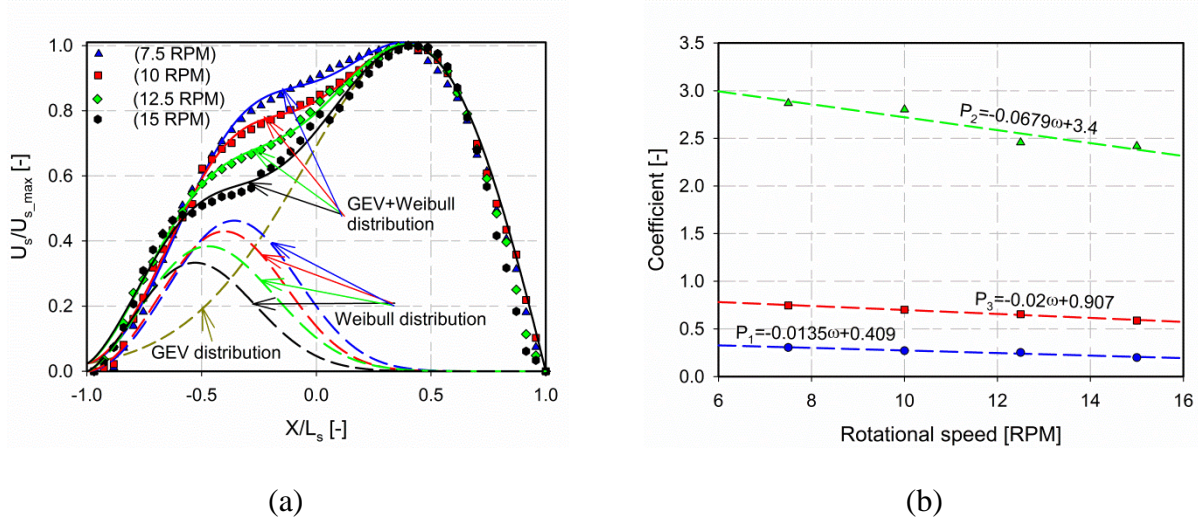
Figure 6.8: a) normalized streamwise velocity profile on the free surface based on x axis, and b) variation of the coefficients of Eq. 6.13 based on the rotational speed of the drum.

6.7 Effect of the flow dynamics on mixing

In general, in a rotating drum, particles are mixed under the effect of advection – which is covered in this work – and diffusion (dispersion). Even though the obtained flow dynamics do not contain the elements of the dispersion, it yet is interesting to evaluate the effects of the flow motion of both cylindrical and spherical particles in the mix. A useful way to see the effect of the flow dynamics on the mixing is by using a numerical simulation (Fiedor & Ottino, 2005). To do so, some particles are initially placed at various positions inside the rotation drum. The particles' next positions are calculated by numerically integrating the equations of motion in time. In this work, for a particle located in the passive layer, Eq. 6.1 and 6.2 are considered as its equation of motion. If the particle lies in the active layer, Eq. 6.7 and 6.9 are used, considering that $u_s(x)$ is calculated from Eq. 6.10 and 6.13 for spherical and cylindrical particles, respectively. Finally, the positions of the particles are depicted at a certain time.
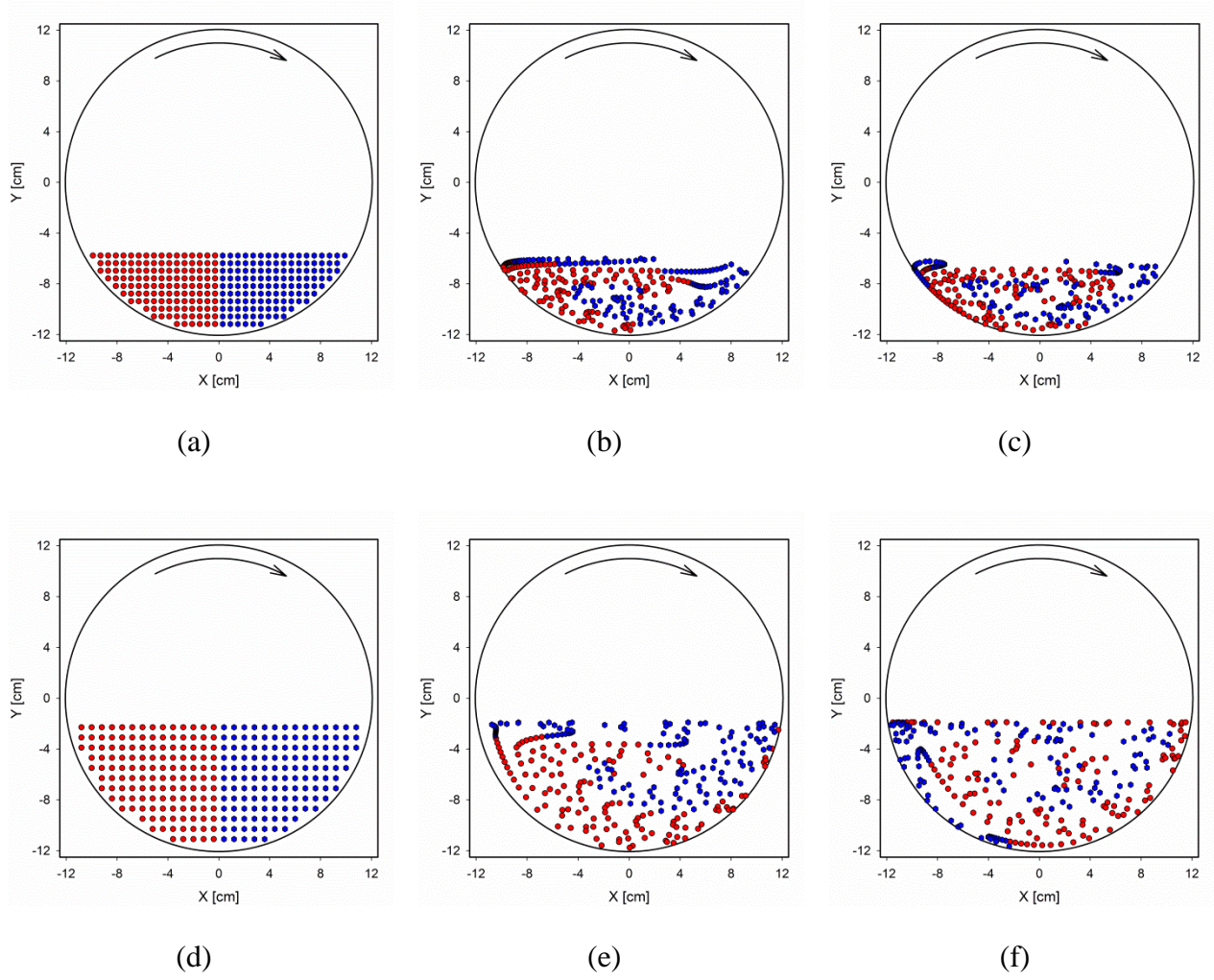
Figure 6.9: Snapshot for the spherical particles after (a) 0, (b) 0.5 and (c) 1 revolution as well as the cylindrical particles after (d) 0, (e) 0.5 and (f) 1 revolution, for a constant rotational speed of the drum.

Figure 6.9 shows snapshots for the spherical and cylindrical particles at an initial point, after half a revolution, and one full revolution of the drum at the rotational speed of 10 RPM. Considering the distribution of the blue and red particles in Figure 6.9c and f, one can qualitatively evaluate better mixing for the cylindrical particles. Conversely, it was observed that the depth and percentage of the active layer for spherical particles are larger, thus they should have better mixing. To answer this contradictory finding, we should recall that the streamwise velocity profile on the free surface for the spherical particles was symmetrical, while the profile for the cylindrical particles was extremely asymmetrical. It is well known that any asymmetry in the

system will help the mixing. Indeed, this example demonstrates the importance of flow dynamics for the outcome of a process.

6.8 Conclusion

In this chapter, the equations of motion for cylindrical and spherical particles in a rolling regime were obtained using the RPT and MRPT techniques. These equations of motion are based on the continuum approaches and can be used to do system simulations. A case study simulation demonstrated the abilities of the models for further investigations of the system. The results of the simulation indicated that the quality of mixing was better for cylindrical particles due to the asymmetrical velocity profile on the free surface, but if only the effects of advection were considered.

6.9 Literature Cited

Alexander, A., Shinbrot, T., & Muzzio, F. J. (2002). Scaling surface velocities in rotating cylinders as a function of vessel radius, rotation rate, and particle size. *Powder Technology, 126*(2), 174-190. doi: 10.1016/S0032-5910(02)00010-4

Alizadeh, E., Bertrand, F., & Chaouki, J. (2014). Comparison of DEM Results and Lagrangian Experimental Data for the Flow and Mixing of Granules in a Rotating Drum. *Aiche Journal, 60*(1), 60-75. doi:10.1002/Aic.14259

Alizadeh, E., Dube, O., Bertrand, F., & Chaouki, J. (2013). Characterization of Mixing and Size Segregation in a Rotating Drum by a Particle Tracking Method. *Aiche Journal, 59*(6), 1894-1905. doi: 10.1002/aic.13982

Boateng, A. A. (1998). Boundary layer modeling of granular flow in the transverse plane of a partially filled rotating cylinder. *International Journal of Multiphase Flow, 24*(3), 499-521. doi:10.1016/S0301-9322(97)00065-7

Cheng, N.-S., Zhou, Q., Keat Tan, S., & Zhao, K. (2011). Application of incomplete similarity theory for estimating maximum shear layer thickness of granular flows in rotating drums. *Chemical Engineering Science, 66*(12), 2872-2878. doi: 10.1016/j.ces.2011.03.050

Ding, Y. L., Seville, J. P. K., Forster, R., & Parker, D. J. (2001). Solids motion in rolling mode rotating drums operated at low to medium rotational speeds. *Chemical Engineering Science, 56*(5), 1769-1780. doi: 10.1016/S0009-2509(00)00468-1

Dube, O., Alizadeh, E., Chaouki, J., & Bertrand, F. (2013). Dynamics of non-spherical particles in a rotating drum. *Chemical Engineering Science, 101*, 486-502. doi: 10.1016/j.ces.2013.07.011

Fiedor, S. J., & Ottino, J. M. (2005). Mixing and segregation of granular matter: multi-lobe formation in time-periodic flows. *Journal of Fluid Mechanics, 533*, 223-236. doi: 10.1017/S0022112005003952

Ingram, A., Seville, J. P. K., Parker, D. J., Fan, X., & Forster, R. G. (2005). Axial and radial dispersion in rolling mode rotating drums. *Powder Technology, 158*(1-3), 76-91. doi: 10.1016/j.powtec.2005.04.030

Khakhar, D. V., McCarthy, J. J., & Ottino, J. M. (1997). Radial segregation of granular mixtures in rotating cylinders. *Physics of Fluids, 9*(12), 3600-3614. doi: 10.1063/1.869498

Khakhar, D. V., McCarthy, J. J., Shinbrot, T., & Ottino, J. M. (1997). Transverse flow and mixing of granular materials in a rotating cylinder. *Physics of Fluids, 9*(1), 31-43. doi: 10.1063/1.869172

Liu, X. Y., Specht, E., Gonzalez, O. G., & Walzel, P. (2006). Analytical solution for the rolling-mode granular motion in rotary kilns. *Chemical Engineering and Processing, 45*(6), 515-521. doi: 10.1016/j.cep.2005.10.009

Makse, H. A. (1999). Continuous avalanche segregation of granular mixtures in thin rotating drums. *Physical Review Letters, 83*(16), 3186-3189. doi: 10.1103/PhysRevLett.83.3186

Meier, S. W., Lueptow, R. M., & Ottino, J. M. (2007). A dynamical systems approach to mixing and segregation of granular materials in tumblers. *Advances in Physics, 56*(5), 757-827. doi: 10.1080/00018730701611677

Mellmann, J., Specht, E., & Liu, X. (2004). Prediction of rolling bed motion in rotating cylinders. *Aiche Journal, 50*(11), 2783-2793. doi: 10.1002/aic.10266

Nakagawa, M., Altobelli, S. A., Caprihan, A., Fukushima, E., & Jeong, E. K. (1993). Non-invasive measurements of granular flows by magnetic resonance imaging. *Experiments in Fluids, 16*(1), 54-60. doi: 10.1007/BF00188507

Orpe, A. V., & Khakhar, D. V. (2001). Scaling relations for granular flow in quasi-two-dimensional rotating cylinders. *Physical Review E - Statistical, Nonlinear, and Soft Matter Physics, 64*(3 I), 313021-3130213. doi: 10.1103/PhysRevE.64.031302

Suzzi, D., Toschkoff, G., Radl, S., Machold, D., Fraser, S. D., Glasser, B. J., & Khinast, J. G. (2012). DEM simulation of continuous tablet coating: Effects of tablet shape and fill level on inter-tablet coating variability. *Chemical Engineering Science, 69*(1), 107-121. doi: 10.1016/j.ces.2011.10.009

Wilson, K. E., & Crossman, E. (1997). The Influence of Tablet Shape and Pan Speed on Intra-tablet Film Coating Uniformity. *Drug Development and Industrial Pharmacy, 23*(12), 1239-1243. doi:10.3109/03639049709146164

CHAPTER 7 　 GENERAL DISCUSSION

Understanding the dynamics of granular flow could potentially benefit many industries, due to the widespread presence of granular materials in both industry and daily life. Among the three main granular flow regimes (quasi-static, dense (liquid) and fast (gaseous)), the dense flow regime is the most complicated and the one with the least investigation. A rotating drum is a standard experimental setup to study a dense granular flow regime. In addition, rotating drums have many industrial applications, were they are used mostly in the rolling regime, which provides superior solid mixing and heat transfer.

It is well known that the physical properties of particles affect the flow dynamics of granular materials. Although particle shape is one of the main factors affecting flow dynamics, the majority of studies in this field used spherical or nearly spherical particles. To study the effect of particle shape on flow dynamics, the shape characteristics should be readily identified, and distinct from those of a sphere. A cylinder is one of the most basic curvilinear geometric shapes, and many other curvilinear shapes, especially with a high aspect ratio, can be approximated as a cylinder. Therefore, for this study the cylinder was the particle shape chosen. Moreover, there are many industrial applications for cylindrical particles.

The employed measurement technique for studying granular flow dynamics should be nonintrusive (i.e. the flow is not disturbed by a probe) and radioactive based (i.e. able to get information from inside the bed). Radioactive particle tracking (RPT) is one of the common measurement techniques and chosen to conduct this investigation. However, it is limited to tracking the position of a single tracer. As cylindrical particles are used in the context of this study, it is essential for the employed measurement technique to be able to simultaneously track the position and orientation of a cylindrical particle.

To do so, RPT needed an improvement to track two tracers at the same time. Therefore, multiple radioactive particle tracking technique (MRPT) is required, as it can determine the trajectory of two free or restricted (attached to the same particle) moving tracers in a system. Therefore, the MRPT technique can measure the position and orientation of a cylindrical particle at the same time. The concept of MRPT technique is to search a pair positions for two tracers in such way that the gap between the recorded and calculated event count-rates is minimum. The accuracy (<5

mm) and precision (<5 mm) of the proposed technique was evaluated by tracking two stationary tracers and two moving tracers. The results confirm the reliability and validity of the MRPT technique when the distance between the two tracers is not too small (>2 cm). The accuracy and precision of MRPT increase as the distance between the tracers increases. However, after a certain distance (related to the conditions of system), any increase in the distance between the tracers will not increase the accuracy and precision of the results. This maximum accuracy and precision is roughly similar to that of single tracer RPT. Note that with RPT one of the sources of imperfection comes from the measurement during the calibration step. It was also observed that when the distance between the two tracers is fixed (so-called restricted MRPT), the middle point (<2 mm) and orientation of the tracers (<5 degrees) can be measured adequately with this technique. Due to the context of this study, the restricted MRPT technique was used to obtain the position and orientation of cylindrical particles. Note that the current MRPT technique can gain information about two axes of particles in a 3D system.

Two different particle shapes were chosen for the study: spherical (6-mm glass beads) and cylindrical (6-mm-diameter, 2-cm-long acrylic particles). We used 2-cm-long cylindrical particles because, in order to have reliable measurement, the current MRPT technique is limited to a lower threshold of 2 cm between the radioactive sources. To compare the flow dynamics of the cylindrical and spherical particles, we analyzed all components of the transverse flow, namely, the active and passive layers, the boundaries (the turning point and yield lines) between the active and passive layers, the velocity profile on the surface, the static and dynamic repose angles, and dilation bed, in a rolling regime (7.5-15 RPM for cylindrical particles under the conditions of this study). The flow dynamics of cylindrical particles differ significantly from that of spherical particles. The dilation of the bed during the rotation, the static and dynamic repose angles, and the streamwise velocity on the free surface of the cylindrical particles were significantly higher than those of the spherical particles at the same rotational speed. In addition, the depth at $x = 0$ and the percentage of the active layer based on the turning point (α_0) and yield (δ_0) lines for the cylindrical particles were lower than those of the spherical particles at the same rotational speed. As opposed to Ingram et al. (2005), we found that the turning point line based on angular velocity was higher than the line based on streamwise velocity.

For the first time in the literature, we measured the orientation of cylindrical particles inside the bed. The results confirm the existence of a preferred spatial orientation (at roughly a 25- degree

deviation from the dynamic repose angle) for cylindrical particles in the active layer. The results show that the spatial orientations of the cylindrical particles within the bed are not sensitive to the rotational speed of the drum. Therefore, for cylindrical particles at all rotational speeds, the bed dilation was constant (about 25%), while the bed dilation for spherical particles is about 1%. The obtained velocity profiles on the free surface for cylindrical particles show an asymmetrical shape (the peak of velocity profile is located at 70% of the free surface length) while the profile for spherical particles is symmetrical (the peak of velocity profile is located at 50% of the free surface length). For the first time in the literature, two general models are proposed to calculate the velocity profiles for cylindrical particles on the free surface and effective particle size in the active and passive layers. We thus obtained the equations of motion for both cylindrical and spherical particles in the active and passive layers, as well as the equations for the yield and turning point curve lines.

CHAPTER 8   CONCLUSION AND RECOMMENDATIONS

The main objective of this thesis was to characterize the cylindrical particle flow dynamics inside a rotating drum using a multiple radioactive particle tracking (MRPT) technique.

To do so, it was firstly required to develop the MRPT technique. Therefore, this work presents a radioactive-based measurement technique (i.e. MRPT) which can simultaneously track two tracers (with similar isotopes) that move freely or are at a fixed distance from each other. We developed for the first time in the literature a model that links the number of events recorded by detectors to the positions of two tracers (with similar isotopes). It was demonstrated MRPT can position two tracers with a margin of error similar to that of a single tracer RPT when the distance between these tracers is more than a certain length (4 cm under the conditions of this study). The results confirm the reliability and validity of the MRPT technique when the distance between the two tracers is not too small (>2 cm under the conditions of this study). It was also observed that when the distance between the two tracers is fixed, the middle point and orientation of the tracers can be measured adequately with this technique.

It was reconfirmed that particle shape can considerably change flow dynamics. For example, in a rotating drum in the rolling regime, it was found that the dynamics of cylindrical particles differ significantly from that of spherical particles at a similar rotational speed. These differences in the flow dynamics based on particle shape can be seen in all characteristics of flow dynamics. For instance, some aspects of flow dynamics are much greater for cylindrical particles (i.e. the dilation of the bed during the rotation, the static and dynamic repose angles, as well as the streamwise velocity on the free surface), while some other items are greater for spherical particles (i.e. the depth at $x = 0$ and the percentage of the active layer based on the turning point (α_0) and yield (δ_0) lines) at the same rotational speed. These differences are a result of the anisotropic shape of cylindrical particles, which cause them to assume a preferred spatial orientation within the active layer. This preferred spatial orientation (a 25-degree deviation from the dynamic repose angle) was measured for the first time in the literature. Based on these measurements, we proposed a general equation to calculate the effective particle size for cylindrical particles of any size for different zones inside a rotating drum.

The cylindrical particles in the active layer align with their dynamic repose angle and then slide down rather than rolling, contrary to spherical particles. Even at a low rotational speed,

cylindrical particles on the free surface continue their acceleration beyond half the length of the bed surface, contrary to the behaviour of spherical particles. At a rotational speed of 7.5 to 15 RPM, cylindrical particles show their velocity peak at 0.7 of the length of the bed surface. Thus, we proposed a general model to calculate the velocity profiles on the free surface. To complete the modeling of flow dynamics, we derived the equations of motion for both cylindrical and spherical particles in the active and passive layers, as well as the equations of the yield and turning point curve lines.

Finally, contrary to claims within the existing literature, we show that the turning point line based on the angular velocity calculation is above the turning point, based on the streamwise velocity.

Based on the discussions, the following recommendations for future research can be made:

1. To develop an RPT technique without a calibration step;

2. To study the impact of the activity ratio between two tracers comprising a non-spherical particle on the efficiency of the MRPT technique, particularly when the distance between these two tracers is small;

3. To improve the MRPT technique to be able to track three tracers simultaneously, using same concept as the MRPT technique;

4. To obtain the diffusion (dispersion) term to complete the modeling of cylindrical particles;

5. To compare the extent of mixing and segregation of cylindrical and spherical particles, considering both advection and diffusion terms;

6. To study the effect of the length of cylindrical particles in terms of flow dynamics; and

7. To investigate the flow dynamics of poly-dispersed cylindrical particles.

BIBLIOGRAPHY

Alexander, A., Shinbrot, T., & Muzzio, F. J. (2002). Scaling surface velocities in rotating cylinders as a function of vessel radius, rotation rate, and particle size. *Powder Technology, 126*(2), 174-190. doi: 10.1016/S0032-5910(02)00010-4

Alizadeh, E. (2013). *Numerical and experimental investigation of solid mixing and segregation in tumbling blenders.* (NR95205 Ph.D.), Ecole Polytechnique, Montreal (Canada), Ann Arbor. Retrieved from http://search.proquest.com/docview/1460765102?accountid=40695 ProQuest Dissertations & Theses Full Text database.

Alizadeh, E., Bertrand, F., & Chaouki, J. (2014). Comparison of DEM Results and Lagrangian Experimental Data for the Flow and Mixing of Granules in a Rotating Drum. *Aiche Journal, 60*(1), 60-75. doi: 10.1002/Aic.14259

Alizadeh, E., Dube, O., Bertrand, F., & Chaouki, J. (2013). Characterization of Mixing and Size Segregation in a Rotating Drum by a Particle Tracking Method. *Aiche Journal, 59*(6), 1894-1905. doi: 10.1002/aic.13982

Alizadeh, E., Hajhashemi, H., Bertrand, F., & Chaouki, J. (2013). Experimental investigation of solid mixing and segregation in a tetrapodal blender. *Chemical Engineering Science, 97*, 354-365.

Bakalis, S., Fryer, P. J., & Parker, D. J. (2004). Measuring velocity distributions of viscous fluids using positron emission particle tracking (PEPT). *Aiche Journal, 50*(7), 1606-1613. doi: 10.1002/Aic.10153

Beam, G. B., Wielopolski, L., Gardner, R. P., & Verghese, K. (1978). Monte Carlo calculation of efficiencies of right-circular cylindrical NaI detectors for arbitrarily located point sources. *Nuclear Instruments and Methods, 154*(3), 501-508. doi: 10.1016/0029-554x(78)90081-2

Bertrand, F., Leclaire, L. A., & Levecque, G. (2005). DEM-based models for the mixing of granular materials. *Chemical Engineering Science, 60*(8-9 SPEC. ISS.), 2517-2531.

Boateng, A. A. (1998). Boundary layer modeling of granular flow in the transverse plane of a partially filled rotating cylinder. *International Journal of Multiphase Flow, 24*(3), 499-521. doi: 10.1016/S0301-9322(97)00065-7

Boateng, A. A., & Barr, P. V. (1997). Granular flow behaviour in the transverse plane of a partially filled rotating cylinder. *Journal of Fluid Mechanics, 330*, 233-249. doi: 10.1017/S0022112096003680

Bonamy, D., Daviaud, F., & Laurent, L. (2002). Experimental study of granular surface flows via a fast camera: a continuous description. *Physics of Fluids (1994-present), 14*(5), 1666-1673.

Boyer, C., Duquenne, A. M., & Wild, G. (2002). Measuring techniques in gas-liquid and gas-liquid-solid reactors. *Chemical Engineering Science, 57*(16), 3185-3215. doi: 10.1016/S0009-2509(02)00193-8

Broadbent, C. J., Bridgwater, J., Parker, D. J., Keningley, S. T., & Knight, P. (1993). Phenomenological study of a batch mixer using a positron camera. *Powder Technology, 76*(3), 317-329.

Brone, D., Alexander, A., & Muzzio, F. (1998). Quantitative characterization of mixing of dry powders in V-blenders. *Aiche Journal, 44*(2), 271-278.

Campbell, C. S. (1990). Rapid granular flows. *Annual Review of Fluid Mechanics, 22*(1), 57-90.

Campbell, C. S. (2006). Granular material flows – An overview. *Powder Technology, 162*(3), 208-229. doi: http://dx.doi.org/10.1016/j.powtec.2005.12.008

Cassanello, M., Larachi, F., Legros, R., & Chaouki, J. (1999). Solids dynamics from experimental trajectory time-series of a single particle motion in gas-spouted beds. *Chemical Engineering Science, 54*(13-14), 2545-2554. doi: 10.1016/S0009-2509(98)00468-0

Chaouki, J., Larachi, F., & Dudukovic, M. P. (1997a). Noninvasive tomographic and velocimetric monitoring of multiphase flows. *Industrial & Engineering Chemistry Research, 36*(11), 4476-4503. doi: 10.1021/Ie970210t

Chaouki, J., Larachi, F., & Dudukovic, P. (1997b). *Non-Invasive Monitoring of Multiphase Flows*: Elsevier Science.

Chen, J. W., Rados, N., Al-Dahhan, M. H., Dudukovic, M. P., Nguyen, D., & Parimi, K. (2001). Particle motion in packed/ebullated beds by CT and CARPT. *Aiche Journal, 47*(5), 994-1004. doi: 10.1002/aic.690470506

Cheng, N.-S., Zhou, Q., Keat Tan, S., & Zhao, K. (2011). Application of incomplete similarity theory for estimating maximum shear layer thickness of granular flows in rotating drums. *Chemical Engineering Science, 66*(12), 2872-2878. doi: 10.1016/j.ces.2011.03.050

Chung, Y., Hsiau, S., Liao, H., & Ooi, J. (2010). An improved PTV technique to evaluate the velocity field of non-spherical particles. *Powder Technology, 202*(1), 151-161.

Cleary, P. W. (2010). DEM prediction of industrial and geophysical particle flows. *Particuology, 8*(2), 106-118. doi: 10.1016/j.partic.2009.05.006

Cundall, P. A., & Strack, O. D. (1979). A discrete numerical model for granular assemblies. *Geotechnique, 29*(1), 47-65.

Degaleesan, S., Dudukovic, M., & Pan, Y. (2001). Experimental study of gas-induced liquid-flow structures in bubble columns. *Aiche Journal, 47*(9), 1913-1931. doi: 10.1002/aic.690470904

Descoins, N., Dirion, J. L., & Howes, T. (2005). Solid transport in a pyrolysis pilot-scale rotary kiln: preliminary results—stationary and dynamic results. *Chemical Engineering and Processing: Process Intensification, 44*(2), 315-321. doi: 10.1016/j.cep.2004.02.025

Ding, Y. L., Forster, R., Seville, J. P. K., & Parker, D. J. (2002). Granular motion in rotating drums: bed turnover time and slumping-rolling transition. *Powder Technology, 124*(1-2), 18-27. doi: 10.1016/S0032-5910(01)00486-7

Ding, Y. L., Seville, J. P. K., Forster, R., & Parker, D. J. (2001). Solids motion in rolling mode rotating drums operated at low to medium rotational speeds. *Chemical Engineering Science, 56*(5), 1769-1780. doi: 10.1016/S0009-2509(00)00468-1

Doucet, J. (2008). *Mesure et caracterisation du melange dans les systemes granulaires denses.* (NR41746 Ph.D.), Ecole Polytechnique, Montreal (Canada), Ann Arbor. Retrieved from

http://search.proquest.com/docview/304818311?accountid=40695 ProQuest Dissertations & Theses Full Text database.

Doucet, J., Bertrand, F., & Chaouki, J. (2008a). Experimental characterization of the chaotic dynamics of cohesionless particles: application to a V-blender. *Granular Matter, 10*(2), 133-138. doi: 10.1007/s10035-007-0075-x

Doucet, J., Bertrand, F., & Chaouki, J. (2008b). An extended radioactive particle tracking method for systems with irregular moving boundaries. *Powder Technology, 181*(2), 195-204. doi: 10.1016/j.powtec.2006.12.019

Dube, O. (2013). *Dynamique particulaire dans des lits fixes et rotatifs.* (NR95219 Ph.D.), Ecole Polytechnique, Montreal (Canada), Ann Arbor. Retrieved from http://search.proquest.com/docview/1460765202?accountid=40695 ProQuest Dissertations & Theses Full Text database.

Dube, O., Alizadeh, E., Chaouki, J., & Bertrand, F. (2013). Dynamics of non-spherical particles in a rotating drum. *Chemical Engineering Science, 101*, 486-502. doi: 10.1016/j.ces.2013.07.011

Dube, O., Dube, D., Chaouki, J., & Bertrand, F. (2014). Optimization of detector positioning in the radioactive particle tracking technique. *Applied Radiation and Isotopes, 89*, 109-124. doi: 10.1016/j.apradiso.2014.02.019

Duchanoy, C., & Jongen, T. R. G. (2003). Efficient simulation of liquid-solid flows with high solids fraction in complex geometries. *Computers & Fluids, 32*(10), 1453-1471. doi: 10.1016/S0045-7930(02)00102-0

Elperin, T., & Vikhansky, A. (1998). Kinematics of the mixing of granular material in slowly rotating containers. *EPL (Europhysics Letters), 43*(1), 17.

Fantozzi, F., Colantoni, S., Bartocci, P., & Desideri, U. (2007). Rotary kiln slow pyrolysis for syngas and char production from biomass and waste - Part I: Working envelope of the reactor. *Journal of Engineering for Gas Turbines and Power, 129*(4), 901-907. doi: 10.1115/1.2720521

Felix, G., Falk, V., & D'Ortona, U. (2002). Segregation of dry granular material in rotating drum: Experimental study of the flowing zone thickness. *Powder Technology, 128*(2-3), 314-319. doi: 10.1016/S0032-5910(02)00171-7

Felix, G., Falk, V., & D'Ortona, U. (2007). Granular flows in a rotating drum: The scaling law between velocity and thickness of the flow. *European Physical Journal E, 22*(1), 25-31. doi: 10.1140/epje/e2007-00002-5

Fiedor, S. J., & Ottino, J. M. (2005). Mixing and segregation of granular matter: multi-lobe formation in time-periodic flows. *Journal of Fluid Mechanics, 533*, 223-236. doi: 10.1017/S0022112005003952

Forrest, S., Bridgwater, J., Mort, P. R., Litster, J., & Parker, D. J. (2003). Flow patterns in granulating systems. *Powder Technology, 130*(1-3), 91-96.

Godfroy, L., Larachi, F., Kennedy, G., Grandjean, B., & Chaouki, J. (1997). On-line flow visualization in multiphase reactors using neural networks. *Applied Radiation and Isotopes, 48*(2), 225-235. doi: 10.1016/S0969-8043(96)00183-2

Goldhirsch, I. (2003). Rapid granular flows. *Annual Review of Fluid Mechanics, 35*(1), 267-293.

Gray, J. M. N. T. (2001). Granular flow in partially filled slowly rotating drums. *Journal of Fluid Mechanics, 441*, 1-29.

Guha, D., Ramachandran, P. A., & Dudukovic, M. P. (2007). Flow field of suspended solids in a stirred tank reactor by Lagrangian tracking. *Chemical Engineering Science, 62*(22), 6143-6154. doi: 10.1016/j.ces.2007.06.033

Guha, D., Ramachandran, P. A., Dudukovic, M. P., & Derksen, J. J. (2008). Evaluation of large eddy simulation and Euler-Euler CFD models for solids flow dynamics in a stirred tank reactor. *Aiche Journal, 54*(3), 766-778. doi: 10.1002/Aic.11417

Guida, A., Nienow, A. W., & Barigou, M. (2011). Mixing of Dense Binary Suspensions: Multi-component Hydrodynamics and Spatial Phase Distribution by PEPT. *Aiche Journal, 57*(9), 2302-2315. doi: 10.1002/Aic.12456

Harnby, N., Edwards, M. F., & Nienow, A. W. (1992). *Mixing in the process industries* (Second ed.): Butterworth-Heinemann.

Henein, H., Brimacombe, J., & Watkinson, A. (1983). Experimental study of transverse bed motion in rotary kilns. *Metallurgical transactions B, 14*(2), 191-205.

Henein, H., Brimacombe, J. K., & Watkinson, A. P. (1985). Experimental Study of Segregation in Rotary Kilns. *Metallurgical transactions. B, Process metallurgy, 16 B*(4), 763-774.

Herminghaus, S. (2005). Dynamics of wet granular matter. *Advances in Physics, 54*(3), 221-261.

Heydenrych, M. D., Greeff, P., Heesink, A. B. M., & Versteeg, G. F. (2002). Mass transfer in rolling rotary kilns: A novel approach. *Chemical Engineering Science, 57*(18), 3851-3859. doi: 10.1016/S0009-2509(02)00312-3

Hill, K. M., Caprihan, A., & Kakalios, J. (1997). Bulk segregation in rotated granular material measured by magnetic resonance imaging. *Physical Review Letters, 78*(1), 50-53. doi: 10.1103/PhysRevLett.78.50

Hiseman, M. J. P., Laurent, B. F. C., Bridgwater, J., Wilson, D. I., Parker, D. J., North, N., & Merrifield, D. R. (2002). Granular flow in a planetary mixer. *Chemical Engineering Research and Design, 80*(5), 432-440.

Ingram, A., Seville, J. P. K., Parker, D. J., Fan, X., & Forster, R. G. (2005). Axial and radial dispersion in rolling mode rotating drums. *Powder Technology, 158*(1-3), 76-91. doi: 10.1016/j.powtec.2005.04.030

Jackson, R. (1983). Some mathematical and physical aspects of continuum models for the motion of the granular materials.

Jain, N., Ottino, J. M., & Lueptow, R. M. (2002). An experimental study of the flowing granular layer in a rotating tumbler. *Physics of Fluids, 14*(2), 572-582. doi: 10.1063/1.1431244

Jain, N., Ottino, J. M., & Lueptow, R. M. (2004). Effect of interstitial fluid on a granular flowing layer. *Journal of Fluid Mechanics, 508*, 23-44. doi: 10.1017/S0022112004008869

Jain, N., Ottino, J. M., & Lueptow, R. M. (2005). Regimes of segregation and mixing in combined size and density granular systems: an experimental study. *Granular Matter, 7*(2-3), 69-81.

Jones, J. R., & Bridgwater, J. (1998). Case study of particle mixing in a ploughshare mixer using Positron Emission Particle Tracking. *International Journal of Mineral Processing, 53*(1-2), 29-38.

Kalbag, A., Wassgren, C., Sumana Penumetcha, S., & Pérez-Ramos, J. D. (2008). Inter-tablet coating variability: Residence times in a horizontal pan coater. *Chemical Engineering Science, 63*(11), 2881-2894. doi: 10.1016/j.ces.2008.03.009

Kawaguchi, T. (2010). MRI measurement of granular flows and fluid-particle flows. *Advanced Powder Technology, 21*(3), 235-241. doi: 10.1016/j.apt.2010.03.014

Ketterhagen, W. R. (2011). Modeling the motion and orientation of various pharmaceutical tablet shapes in a film coating pan using DEM. *International Journal of Pharmaceutics, 409*(1–2), 137-149. doi: 10.1016/j.ijpharm.2011.02.045

Khakhar, D. V. (2011). Rheology and mixing of granular materials. *Macromolecular Materials and Engineering, 296*(3-4), 278-289.

Khakhar, D. V., McCarthy, J. J., & Ottino, J. M. (1997). Radial segregation of granular mixtures in rotating cylinders. *Physics of Fluids, 9*(12), 3600-3614. doi: 10.1063/1.869498

Khakhar, D. V., McCarthy, J. J., Shinbrot, T., & Ottino, J. M. (1997). Transverse flow and mixing of granular materials in a rotating cylinder. *Physics of Fluids, 9*(1), 31-43. doi: 10.1063/1.869172

Khakhar, D. V., Orpe, A. V., & Ottino, J. (2001). Continuum model of mixing and size segregation in a rotating cylinder: concentration-flow coupling and streak formation. *Powder Technology, 116*(2), 232-245.

Knoll, G. F. (2000). *Radiation detection and measurement* (3rd ed.). New York ; Toronto: Wiley.

Knoll, G. F. (2010). *Radiation Detection and Measurement*: John Wiley & Sons.

Kuo, H. P., Knight, P. C., Parker, D. J., Adams, M. J., & Seville, J. P. K. (2004). Discrete element simulations of a high-shear mixer. *Advanced Powder Technology, 15*(3), 297-309.

Kuo, H. P., Knight, P. C., Parker, D. J., & Seville, J. P. K. (2005). Solids circulation and axial dispersion of cohesionless particles in a V-mixer. *Powder Technology, 152*(1-3), 133-140.

Lacey, P. M. C. (1954). Developments in the theory of particle mixing. *Journal of Applied Chemistry, 4*(5), 257-268. doi: 10.1002/jctb.5010040504

Larachi, F., Cassanello, M., Chaouki, J., & Guy, C. (1996). Flow structure of the solids in a 3-D gas-liquid-solid fluidized bed. *Aiche Journal, 42*(9), 2439-2452. doi: 10.1002/aic.690420905

Larachi, F., Chaouki, J., & Kennedy, G. (1995). 3-D Mapping of Solids Flow-Fields in Multiphase Reactors with Rpt. *Aiche Journal, 41*(2), 439-443. doi: 10.1002/aic.690410226

Larachi, F., Grandjean, B. P. A., & Chaouki, J. (2003). Mixing and circulation of solids in spouted beds: particle tracking and Monte Carlo emulation of the gross flow pattern. *Chemical Engineering Science, 58*(8), 1497-1507. doi: 10.1016/S0009-2509(02000676-0

Larachi, F., Kennedy, G., & Chaouki, J. (1994). A Gamma-Ray Detection System for 3-D Particle Tracking in Multiphase Reactors. *Nuclear Instruments & Methods in Physics Research Section a-Accelerators Spectrometers Detectors and Associated Equipment, 338*(2-3), 568-576. doi: 10.1016/0168-9002(94)91343-9

Laurent, B. F. C., Bridgwater, J., & Parker, D. J. (2000). Motion in a particle bed agitated by a single blade. *Aiche Journal, 46*(9), 1723-1734.

Leadbeater, T. W., Parker, D. J., & Gargiuli, J. (2012). Positron imaging systems for studying particulate, granular and multiphase flows. *Particuology, 10*(2), 146-153. doi: 10.1016/j.partic.2011.09.006

Lemieux, M., Bertrand, F., Chaouki, J., & Gosselin, P. (2007). Comparative study of the mixing of free-flowing particles in a V-blender and a bin-blender. *Chemical Engineering Science, 62*(6), 1783-1802.

Li, S. Q., Yan, J. H., Li, R. D., Chi, Y., & Cen, K. F. (2002). Axial transport and residence time of MSW in rotary kilns - Part I. Experimental. *Powder Technology, 126*(3), 217-227. doi: 10.1016/S0032-5910(02)00014-1

Lin, J. S., Chen, M. M., & Chao, B. T. (1985). A novel radioactive particle tracking facility for measurement of solids motion in gas fluidized beds. *Aiche Journal, 31*(3), 465-473. doi: 10.1002/aic.690310314

Link, J. M., Deen, N. G., Kuipers, J. A. M., Fan, X., Ingram, A., Parker, D. J., . . . Seville, J. P. K. (2008). PEPT and discrete particle simulation study of spout-fluid bed regimes. *Aiche Journal, 54*(5), 1189-1202. doi: 10.1002/Aic.11456

Liu, X. Y., Specht, E., Gonzalez, O. G., & Walzel, P. (2006). Analytical solution for the rolling-mode granular motion in rotary kilns. *Chemical Engineering and Processing, 45*(6), 515-521. doi: 10.1016/j.cep.2005.10.009

Longo, S., & Lamberti, A. (2002). Grain shear flow in a rotating drum. *Experiments in Fluids, 32*(3), 313-325. doi: 10.1007/s003480100359

Makse, H. A. (1999). Continuous avalanche segregation of granular mixtures in thin rotating drums. *Physical Review Letters, 83*(16), 3186-3189. doi: 10.1103/PhysRevLett.83.3186

Mankad, S., & Fryer, P. J. (1997). A heterogeneous flow model for the effect of slip and flow velocities on food steriliser design. *Chemical Engineering Science, 52*(12), 1835-1843. doi: 10.1016/S0009-2509(97)00028-6

McCarthy, J. J., Khakhar, D. V., & Ottino, J. M. (2000). Computational studies of granular mixing. *Powder Technology, 109*(1), 72-82.

Meier, S. W., Lueptow, R. M., & Ottino, J. M. (2007). A dynamical systems approach to mixing and segregation of granular materials in tumblers. *Advances in Physics, 56*(5), 757-827. doi: 10.1080/00018730701611677

Mellmann, J. (2001). The transverse motion of solids in rotating cylinders-forms of motion and transition behavior. *Powder Technology, 118*(3), 251-270. doi: 10.1016/S0032-5910(00)00402-2

Mellmann, J., Specht, E., & Liu, X. (2004). Prediction of rolling bed motion in rotating cylinders. *Aiche Journal, 50*(11), 2783-2793. doi: 10.1002/aic.10266

MiDi, G. D. R. (2004). On dense granular flows. *Eur Phys J E Soft Matter, 14*(4), 341-365. doi: 10.1140/epje/i2003-10153-0

Mostoufi, N., & Chaouki, J. (2004). Flow structure of the solids in gas-solid fluidized beds. *Chemical Engineering Science, 59*(20), 4217-4227. doi: 10.1016/j.ces.2004.06.006

Mostoufi, N., Kenned, G., & Chaouki, J. (2003). Decreasing the sampling time interval in radioactive particle tracking. *Canadian Journal of Chemical Engineering, 81*(1), 129-133.

Muzzio, F. J., Robinson, P., Wightman, C., & Brone, D. (1997). Sampling practices in powder blending. *International Journal of Pharmaceutics, 155*(2), 153-178.

Nakagawa, M., Altobelli, S. A., Caprihan, A., Fukushima, E., & Jeong, E. K. (1993). Non-invasive measurements of granular flows by magnetic resonance imaging. *Experiments in Fluids, 16*(1), 54-60. doi: 10.1007/BF00188507

Ng, B. H., Kwan, C. C., Ding, Y. L., Ghadiri, M., Fan, X. F., & Parker, D. J. (2008). Granular flow fields in vertical high shear mixer granulators. *Aiche Journal, 54*(2), 415-426. doi: 10.1002/Aic.11389

Orpe, A. V., & Khakhar, D. (2007). Rheology of surface granular flows. *Journal of Fluid Mechanics, 571*, 1-32.

Orpe, A. V., & Khakhar, D. V. (2001). Scaling relations for granular flow in quasi-two-dimensional rotating cylinders. *Physical Review E - Statistical, Nonlinear, and Soft Matter Physics, 64*(3 I), 313021-3130213. doi: 10.1103/PhysRevE.64.031302

Ottino, J., & Khakhar, D. (2000). Mixing and segregation of granular materials. *Annual Review of Fluid Mechanics, 32*, 55-91.

Parker, D. J., Broadbent, C. J., Fowles, P., Hawkesworth, M. R., & McNeil, P. (1993). Positron emission particle tracking-a technique for studying flow within engineering equipment. *Nuclear Instruments & Methods in Physics Research, Section A (Accelerators, Spectrometers, Detectors and Associated Equipment), A326*(3), 592-607. doi: 10.1016/0168-9002(93)90864-E

Parker, D. J., Dijkstra, A. E., Martin, T. W., & Seville, J. P. K. (1997). Positron emission particle tracking studies of spherical particle motion in rotating drums. *Chemical Engineering Science, 52*(13), 2011-2022. doi: 10.1016/S0009-2509(97)00030-4

Paul, E. L., Atiemo-Obeng, V. A., & Kresta, S. M. (2004). *Handbook of industrial mixing : science and practice*. Hoboken, N.J.: Wiley-Interscience.

Perrault, M., Bertrand, F., & Chaouki, J. (2010). An investigation of magnesium stearate mixing in a V-blender through gamma-ray detection. *Powder Technology, 200*(3), 234-245.

Pugsley, T., Tanfara, H., Malcus, S., Cui, H., Chaouki, J., & Winters, C. (2003). Verification of fluidized bed electrical capacitance tomography measurements with a fibre optic probe. *Chemical Engineering Science, 58*(17), 3923-3934.

Rao, S., Bhatia, S., & Khakhar, D. (1991). Axial transport of granular solids in rotating cylinders. Part 2: Experiments in a non-flow system. *Powder Technology, 67*(2), 153-162.

Rasouli, M., Bertrand, F., & Chaouki, J. (2015). A multiple radioactive particle tracking technique to investigate particulate flows. *Aiche Journal, 61*(2), 384-394. doi: 10.1002/aic.14644

Ridgway, K., & Rupp, R. (1971). Mixing of powder layers on a chute. The effect of particle size and shape. *Powder Technology, 4*(4), 195-202. doi: 10.1016/0032-5910(71)80035-9

Roy, S., Kernoun, A., Al-Dahhan, M. H., & Dudukovic, M. P. (2005). Experimental investigation of the hydrodynamics in a liquid-solid riser. *Aiche Journal, 51*(3), 802-835. doi: 10.1002/Aic.10447

Roy, S., Larachi, F., Al-Dahhan, M. H., & Dudukovic, M. P. (2002). Optimal design of radioactive particle tracking experiments for flow mapping in opaque multiphase reactors. *Appl Radiat Isot, 56*(3), 485-503. doi: 10.1016/s0969-8043(01)00142-7

Santomaso, A. C., Ding, Y. L., Lickiss, J. R., & York, D. W. (2003). Investigation of the granular behaviour in a rotating drum operated over a wide range of rotational speed. *Chemical Engineering Research and Design, 81*(8), 936-945. doi: 10.1205/026387603322482176

Savage, S. B. (1984). The Mechanics of Rapid Granular Flows. In W. H. John & Y. W. Theodore (Eds.), *Advances in applied mechanics* (Vol. Volume 24, pp. 289-366): Elsevier.

Scott, D. M. (2003). Characterizing particle characterization. *Particle and Particle Systems Characterization, 20*(5), 305-310.

Sheritt, R. G., Chaouki, J., Mehrotra, A. K., & Behie, L. A. (2003). Axial dispersion in the three-dimensional mixing of particles in a rotating drum reactor. *Chemical Engineering Science, 58*(2), 401-415. doi: 10.1016/S0009-2509(02)00551-1

Snyder, B. J., & Gyorey, G. L. (1965). Calculating gamma efficiencies in scintillation detectors. *Nucleonics, 23*(2), 80-82.

Suzzi, D., Toschkoff, G., Radl, S., Machold, D., Fraser, S. D., Glasser, B. J., & Khinast, J. G. (2012). DEM simulation of continuous tablet coating: Effects of tablet shape and fill level on inter-tablet coating variability. *Chemical Engineering Science, 69*(1), 107-121. doi: 10.1016/j.ces.2011.10.009

Tobiska, S., & Kleinebudde, P. (2003). Coating uniformity and coating efficiency in a Bohle Lab-Coaterusing oval tablets. *European Journal of Pharmaceutics and Biopharmaceutics, 56*(1), 3-9. doi: 10.1016/S0939-6411(03)00026-2

Tsoulfanidis, N., & Landsberger, S. (2011). *Measurement and Detection of Radiation*: CRC Press.

Van Puyvelde, D. R., Young, B. R., Wilson, M. A., & Schmidt, S. J. (2000). Modelling transverse segregation of particulate solids in a rolling drum. *Chemical Engineering Research and Design, 78*(4), 643-650. doi: 10.1205/026387600527590

Waters, K. E., Rowson, N. A., Fan, X., Parker, D. J., & Cilliers, J. J. (2008). Positron emission particle tracking as a method to map the movement of particles in the pulp and froth phases. *Minerals Engineering, 21*(12-14), 877-882.

Wightman, C., & Muzzio, F. J. (1998a). Mixing of granular material in a drum mixer undergoing rotational and rocking motions I. Uniform particles. *Powder Technology, 98*(2), 113-124. doi: 10.1016/S0032-5910(98)00010-2

Wightman, C., & Muzzio, F. J. (1998b). Mixing of granular material in a drum mixer undergoing rotational and rocking motions II. Segregating particles. *Powder Technology, 98*(2), 125-134. doi: 10.1016/S0032-5910(98)00011-4

Wilson, K. E., & Crossman, E. (1997). The Influence of Tablet Shape and Pan Speed on Intra-tablet Film Coating Uniformity. *Drug Development and Industrial Pharmacy, 23*(12), 1239-1243. doi: 10.3109/03639049709146164

Woodle, G. R., & Munro, J. M. (1993). Particle motion and mixing in a rotary kiln. *Powder Technology, 76*(3), 241-245.

Xu, S. K., Qu, Y. H., Chaouki, J., & Guy, C. (2005). Characterization of homogeneity of bubble flows in bubble columns using RPT and fibre optics. *International Journal of Chemical Reactor Engineering, 3*.

Yamane, K., Nakagawa, M., Altobelli, S., Tanaka, T., & Tsuji, Y. (1998). Steady particulate flows in a horizontal rotating cylinder. *Physics of Fluids (1994-present), 10*(6), 1419-1427.

Yang, R., Zou, R., & Yu, A. (2003). Microdynamic analysis of particle flow in a horizontal rotating drum. *Powder Technology, 130*(1), 138-146.

Yang, Z., Fan, X., Bakalis, S., Parker, D. J., & Fryer, P. J. (2008). A method for characterising solids translational and rotational motions using Multiple-Positron Emission Particle Tracking (Multiple-PEPT). *International Journal of Multiphase Flow, 34*(12), 1152-1160. doi: 10.1016/j.ijmultiphaseflow.2008.06.002

Zhu, H., Zhou, Z., Yang, R., & Yu, A. (2007). Discrete particle simulation of particulate systems: theoretical developments. *Chemical Engineering Science, 62*(13), 3378-3396.